



HR Wallingford

Towards the development of an estuary
regime model

M P Dearnaley
A J Hogg

Report SR 274
July 1991

This report describes work funded by the Department of the Environment under Research Contract PECD 7/6/145, for which the DoE nominated officer was Dr R P Thorogood and by HR Wallingford. It is published on behalf of the Department of the Environment, but any opinions expressed in this report are not necessarily those of the Funding Department. The work was carried out at HR Wallingford by Mr A J Hogg and Dr M P Dearnaley in Mr T N Burt's section in the Tidal Engineering Department under the management of Mr M F C Thorn.

© Crown copyright 1991

Published by permission of the Controller of Her Majesty's Stationery Office, and on behalf of the Department of the Environment.

DEVELOPMENT OF AN ESTUARY REGIME MODEL

Report SR 274

July 1991

ABSTRACT

The work described in this report is part of a larger programme aimed at updating estuary regime processes. The ultimate aim of which is to produce a tool which will enable a prediction to be made of long term estuary behaviour and evolution due to engineering works, climate change, drainage, water abstraction, disposal of pollutants etc.

The best hope for long term modelling probably lies in a different type of model from those which are currently used which is not so spatially precise but better able to represent the factors which govern long term changes.

The regime model developed in this study is based upon the discovery of a friction velocity based stress parameter; the maximum of which appears to be constant over most of the length of an estuary but which varies according to the amount of freshwater flow in the upper tidal reaches.

This basic tidal volume model has been run and compared with field data for the Thames, Parrett, Conwy and Nene Estuaries. As a result the applicability of a regime model to these estuaries has been assessed. The model has been successfully used to predict the depth profile of the Thames, starting with only the tidal range at the mouth, the freshwater flow and the hypothesis of the constancy of maximum stress.



DEVELOPMENT OF AN ESTUARY REGIME MODEL

Report SR 274

July 1991

CONTENTS

	Page
1. INTRODUCTION	1
1.1 Background	1
1.2 Objectives	2
1.3 Programme	2
1.4 Classification of estuaries by physical processes	3
1.5 Report structure	6
2. REGIME MODEL	8
2.1 Equations governing motion in an estuary	8
2.2 Modelling the movement of sediment	19
2.2.1 Bed sediment motion	19
2.2.2 Modelling the movement of sediment	21
2.3 Stability of estuarine channels	22
2.3.1 Application to Thames Estuary	26
2.4 Tidal volume model	28
2.5 Geometric approximation for the cross section	31
2.6 Stress parameter	32
3. MODEL RESULTS	34
3.1 Ideal estuary	34
3.1.1 Results	35
3.2 Thames Estuary	36
3.2.1 Model input data	35
3.2.2 Model cross section	37
3.2.3 Field observations	38
3.2.4 Results	40
3.3 Conwy Estuary	42
3.3.1 Model input data	42
3.3.2 Field observations	43
3.3.3 Results	44
3.4 Parrett Estuary	46
3.4.1 Model input data	46
3.4.2 Field observations	47
3.4.3 Results	48

CONTENTS (CONT'D)

	Page
3.5 River Nene	50
3.5.1 Model input data	50
3.5.2 Field observations	51
3.5.3 Results	52
3.6 Discussion of the case studies	53
4. LONG TERM EVOLUTION OF ESTUARIES	57
4.1 Analytical models	57
4.2 Modelling approach	58
4.3 Attempted modelling procedure	60
5. CONCLUSIONS AND RECOMMENDATIONS FOR FURTHER WORK	67
5.1 Conclusions	67
5.2 Recommendations for further work	68
6. ACKNOWLEDGEMENTS	70
7. REFERENCES	71

TABLES

1. Data specifying the Conwy profile
2. Data specifying the Parrett profile

FIGURES

1. Effect of river flow on maximum stress parameter
2. Stress parameter, velocity and depth through tidal cycle
3. Maximum stress parameter in estuary (magnitude and location)
4. Maximum stress parameter in estuary (magnitude and location)
5. Effect of increasing tidal range on stress parameter
6. Cross sections through Thames Estuary
7. Thames - Maximum observed stress parameter (spring tides)
8. Thames - Maximum observed stress parameter (neap tides)
9. Mean tide level width along Thames
10. Phase difference along Thames
11. Longitudinal profile of Thames
12. Tidal curves for Thames Estuary
13. Tidal curves for Thames Estuary
14. Thames - comparison of model results with observations
15. Thames - comparison of model results with observations
16. Maximum stress parameter for increasing river flow
17. Maximum stress parameter for different tidal ranges
18. Longitudinal profile and channel widths for Conwy Estuary
19. Maximum stress parameter

CONTENTS (CONT'D)

FIGURES (Cont'd)

20. Conwy - comparison of model results with observations
21. Conwy - comparison of model results with observations
22. Maximum stress parameter for increasing river flow
23. Maximum stress parameter for different tidal ranges
24. Longitudinal profile and mean tidal width for River Parrett
25. Parrett - Maximum and minimum stress parameter
26. Tidal curves for River Parrett
27. Tidal curves for River Parrett
28. Parrett - comparison of model results with observations
29. Parrett - comparison of model results with observations
30. Parrett - comparison of model results with observations
31. Comparison of velocity results overlaid with total water depth
32. Maximum stress parameter for different tidal ranges and river flow
33. Longitudinal profile and mean tidal width for River Nene
34. Spring tidal curves and phase differences for River Nene
35. Stress parameter for River Nene
36. Nene - comparison of model results with observations
37. Nene - comparison of model results with observations
38. Maximum stress parameter for increasing river flow
39. Maximum stress parameter for different tidal ranges
40. Magnitude of terms in the momentum equation (Conwy and Parrett)
41. Magnitude of terms in the momentum equation (Nene and Thames)
42. Stage I model prediction results
43. Stage II model prediction results
44. Stage III model prediction results

1. INTRODUCTION

1.1 Background

The work described in this report is part of a larger programme aimed at updating understanding of estuary regime processes. The ultimate aim is to produce a tool which will enable the prediction to be made of long term estuary behaviour and evolution due to engineering works, climate change, drainage, water abstraction, disposal of pollutants etc.

Major engineering works such as the reclamation of intertidal flats, can have far-reaching effects which may include changes to the established pattern of banks and channels, sedimentation in existing navigation channels, and patterns of dispersion from estuary outfalls. De-stabilisation of sediment deposits may undermine existing structures founded on them, and an increase in channel sedimentation may threaten the commercial viability of port and shipping businesses.

The work has attempted to provide information on the factors which determine the size and shape of an estuary together with knowledge of the criteria which will enable a judgement to be made on whether a given estuary is in regime or whether it is still undergoing evolutionary change.

The best hope for long term modelling probably lies in a different type of model from those which are currently used which is not so spatially precise but better able to represent the factors which govern long term changes.

The regime model developed in this study is based upon the discovery of a friction velocity based stress

parameter; the maximum of which appears to be constant over most of the length of an estuary but which varies according to the amount of freshwater river flow in the upper tidal reaches.

1.2 Objectives

The primary objective of the research into estuary regime is to provide engineers with an improved method of predicting the long term evolutionary effects of significant engineering changes in estuaries. This objective is to be met by:-

- (i) Reviewing existing available data on estuaries and selecting a number for in- depth analysis.
- (ii) Attempting a classification of estuaries by physical processes.
- (iii) Attempting to formulate the physical processes involved and model their interaction using microcomputer programmes.

1.3 Programme

A brief outline for the programme of this research is given below:-

- (a) Review of estuary regime theory including sediment transport processes
- (b) Identification of the main factors influencing the regime state
- (c) Attempt to produce a system for the classification of estuaries by physical processes

- (d) Review of the application of mathematical models to estuary regime
- (e) Review of existing available data on estuaries and selection of a number for in depth analysis
- (f) Formulation of a simple micro computer based regime model
- (g) Comparison of regime model with field observations from selected estuaries
- (h) Attempt to use regime model to predict long term evolution of an estuary profile.

Items (a)-(c) and (d) have been reported previously in References 1 and 2 respectively.

1.4 Classification of estuaries by physical processes

A review of the literature has revealed many proposed systems for the classification and characterisation of estuaries and the list below gives some indication of the range of parameters used in this exercise;-

- (i) salinity structure
- (ii) width and depth
- (iii) domination of either river or tide
- (iv) tidal range (high, low or intermediate)
- (v) topography or geomorphology.

Of those listed, salinity structure and topography have traditionally been the most widely used.

Classification by salinity structure is based on the degree of mixing of fresh and salt water. Thus the distinctions are drawn among the following:

- (i) highly stratified or salt wedge
- (ii) partially mixed
- (iii) well mixed or vertically homogeneous.

Classification by topography has been described by Dyer (Ref 3) and others.

Hansen and Rattray (Ref 4) reported on new dimensions in estuary classification. As a result of theoretical studies, a new two-parameter system of estuarine classification was proposed, based on circulation and stratification changes which were associated with variations in salinity and including the relevant estuary dynamics.

Previous work by the same authors (Ref 5) demonstrated that the development of stratification and gravitational convection in estuaries was dependent on two dimensionless parameters. The significance of these parameters, involving both stratification and circulation, for the determination of the partition of the salt flux in relation to discharge, convection (gravitational) and diffusion was clearly shown to be relevant.

The authors concluded that, subject to certain reservations, the classification in terms of stratification and circulation of estuaries was valid. From plots of stratification against circulation for a range of estuaries, seven types of estuary were identified.

Prandle (Ref 6) reported on the salinity regimes and the vertical structure of residual flows in narrow

tidal estuaries. This work demonstrated that the degree of stratification was related to the product of two parameters; one of these was dependent on velocity structure and the other on the ratio of the residual velocity to the amplitude of the tidal velocity.

The classification of well mixed bays and estuaries has been described by Aubrey (Ref 7) in the consideration of hydrodynamic controls on sediment transport. The classification was in terms of flood or ebb tide flow dominance in the context of tidal forcing.

In the consideration of mathematical models applied to estuaries, with particular reference to cohesive sediment transport, Rodger and Odd (Ref 8) have defined three different estuary types:

- (i) Canalised, being "a body of water narrow with respect to length which moves under the influence of external tidal forces and fluvial flows".
- (ii) Outfall of a river, defined as "a meeting place of freshwater and saltwater which gives rise to a variety of important phenomena such as stratification and gravitational circulation".
- (iii) Deep estuary, "is one in which mean depths are in excess of about 10m and the tidal range to mean depth ratio is less than about 0.4".

Some of the systems referred to above classify estuaries (ie assign them to a particular group on the basis of quantitative data) or characterise estuaries by describing their distinctive features in a qualitative manner. In almost all cases the

classification is done using a limited number of the processes or parameters involved. Broadly speaking there are four main headings associated with the physical properties of estuaries:

- (i) geometrical properties
- (ii) fluid properties
- (iii) sediment properties
- (iv) tidal effects

Within each of these main headings there are between six and twelve other variables.

Dennis (Ref 1) outlines an approach for classifying estuaries by physical processes by considering the possible effect of each variable and trying to identify their relative importance with respect to the regime state. To this end, each of the processes involved was 'quantified' by assigning to each of them what was generally accepted as being the appropriate fundamental equation. The next stage of the work will be to consider individual estuaries with a view to quantifying the processes referred to, using field data. The object of this exercise would be to build up a data base for each estuary as part of a knowledge based (expert) system which it is hoped will enable each estuary to be identified by a 'fingerprint'. As a major part of this work a judgement will need to be made on the relative importance of the processes contributing to the regime state.

1.5 Report structure

The basic theory behind the regime model is presented in Chapter 2. This includes discussion of the approximations that are made to develop the one dimensional tidal volume model, of the geometric approximation for the cross section and of the

derivation of the bottom stress parameter. In Chapter 3 model results are presented and discussed for five cases; an ideal estuary and one dimensional representations of the Thames, Conwy, Parrett and Nene Estuaries. In Chapter 4 the development of an analytical model to predict the long term evolution of an estuary is presented. Conclusions and recommendations for further work are given in Chapter 5.

2. REGIME MODEL

2.1 Equations governing motion in an estuary

While the dynamics of an estuary include many important three dimensional effects, arising from factors such as flow reversal and the diffusion of suspended material, it is possible to develop one dimensional equations which provide a framework in which the dynamics can be simply considered and which provide a 'first approximation' of the effects observed. The derivation of these equations are shown below to highlight the approximations made and to detail the physical processes.

Since the flow is predominately horizontal, a Cartesian coordinate system is adopted with the x-y plane horizontal and the z-plane vertical. The x-direction is parallel with the channel direction, while the y-direction is perpendicular to this. The full continuity and momentum equations expressing the conservation of mass and momentum are;

$$\frac{\partial \rho}{\partial t} + \nabla \cdot (\rho \underline{u}) = 0$$

$$\frac{\partial \underline{u}}{\partial t} + \underline{u} \cdot \nabla \underline{u} = -\frac{1}{\rho} \nabla p + \frac{1}{\rho} \nabla \cdot \underline{\underline{\sigma}} + \underline{F}$$

where

$\rho(\underline{x}, t)$	=	density
$\underline{u}(\underline{x}, t)$	=	velocity
$p(\underline{x}, t)$	=	pressure
$\underline{\underline{\sigma}}(\underline{x}, t)$	=	Newtonian stress, associated with viscosity
\underline{F}	=	body force

In this situation, the body force term includes gravitational and coriolis acceleration.

$$\underline{F} = \underline{g} + 2\underline{\Omega} \times \underline{u}$$

First of all, make the assumption of incompressibility. This simplifies the mass continuity equation:

$$\frac{D\rho}{Dt} = 0 \quad \text{hence } \nabla \cdot \underline{u} = 0$$

The flow situation is turbulent and so the velocity and pressure fields have to be 'time smoothed', by considering a basic evolving field, with random fluctuations about it, ie denote the velocity and pressure fields as:

$$\underline{u} + \underline{u}' \text{ and } p + p'$$

Then the governing equations expressing the conservation of mass and momentum read:

$$\nabla \cdot \underline{u} = 0$$

$$\begin{aligned} \frac{\partial \underline{u}}{\partial t} + \underline{u} \nabla \cdot \underline{u} &= -\frac{1}{\rho} \nabla \rho + \frac{1}{\rho} \nabla \cdot \underline{\underline{\sigma}} - \underline{u}' \cdot \nabla \underline{u}' + \underline{F} \\ &= -\frac{1}{\rho} \nabla p + \frac{1}{\rho} \nabla \cdot (\underline{\underline{\sigma}} + \underline{\underline{\tau}}) + \underline{F} \end{aligned}$$

where $\underline{\underline{\tau}} = \text{Reynolds stress, due to turbulent fluctuations} = -\rho \underline{u}' \underline{u}'$

The Boussinesq approximation is made which ignores the density fluctuation in the inertial terms and considers it only in the gravitational term.

The 'hydrostatic balance' approximation is also made: vertical accelerations of fluid particles are much smaller than the gravitational acceleration. There is said to exist a hydrostatic balance between the

vertical pressure gradient and the gravitational acceleration and all vertical velocities are negligible in the vertical momentum equation. The non-dimensional measure for this is $\frac{w^2}{gH} \ll 1$, together with $\frac{w}{gT} \ll 1$ (ie low frequency motion, where T is the time scale of the motion).

Finally, the Newtonian stress is negligible in comparison to the Reynolds stress and can be ignored.

$$|\underline{\tau}| \gg |\underline{\sigma}|$$

And the only significant components of the Reynolds stress tensor are those expressing vertical shear.

$$\text{ie } \frac{\partial}{\partial z} \tau_{xz} \gg \frac{\partial}{\partial y} \tau_{xy}$$

$$\frac{\partial}{\partial z} \tau_{yz} \gg \frac{\partial}{\partial x} \tau_{yx}$$

henceforth, denote $\tau_{yz} \equiv \tau_y$, $\tau_{xz} \equiv \tau_x$

$$0 = -\frac{1}{\rho} \frac{\partial \rho}{\partial z} - g$$

$$\frac{\partial u}{\partial t} + u \frac{\partial u}{\partial x} + v \frac{\partial u}{\partial y} + w \frac{\partial u}{\partial z} - \Omega v = -\frac{1}{\rho} \frac{\partial p}{\partial x} + \frac{1}{\rho} \frac{\partial}{\partial z} \tau_x$$

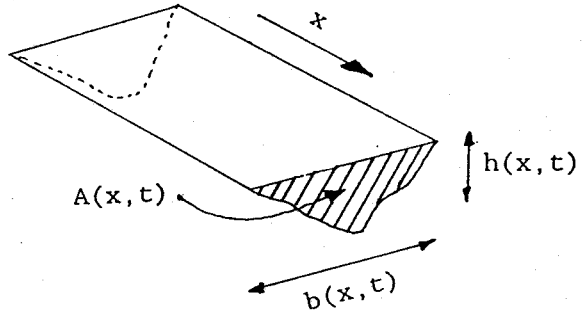
$$\frac{\partial v}{\partial t} + u \frac{\partial v}{\partial x} + v \frac{\partial v}{\partial y} + w \frac{\partial v}{\partial z} + \Omega u = -\frac{1}{\rho} \frac{\partial p}{\partial y} + \frac{1}{\rho} \frac{\partial}{\partial z} \tau_y$$

Where $\Omega = 2\omega \sin \Phi$ (the coriolis parameter)

and $\omega =$ angular velocity of earth, $\Phi =$ latitude

To simplify this problem we consider the equations averaged over a channel cross section and concentrate on the evolution of the variables along the channel. This reduces the system to one dimension where variables are functions only of the downstream distance, x. It is usual to regard the channel as 'straight', compensating for bends and 3-dimensional circulation by the inclusion of an appropriate friction factor.

Consider then, averaging over a cross-sectional area $A(x,t)$:



where $b(x,t)$ is the width of the cross section, $h(x,t)$ is the depth and $\eta(x,t)$ is the free surface elevation.

Taking the continuity equation $\nabla \cdot \underline{u} = 0$ integrated over depth

$$\int_{-h}^{\eta} (u_x + v_y) dz = - \int_{-h}^{\eta} w_z dz = -w(\eta) + w(-h)$$

but the bottom boundary condition is $u(-h) = 0$,
 $v(-h) = 0$, $w(-h) = - \frac{\partial h}{\partial y}$.

$$\text{and } \int_{-h}^{\eta} u_x dz = \frac{\partial}{\partial x} \int_{-h}^{\eta} u dz - u(\eta) \frac{\partial \eta}{\partial x} - u(-h) \frac{\partial h}{\partial x}$$

$$\int_{-h}^{\eta} v_y dz = \frac{\partial}{\partial y} \int_{-h}^{\eta} v dz - v(\eta) \frac{\partial \eta}{\partial y} - v(-h) \frac{\partial h}{\partial y}$$

$$\begin{aligned} \text{At surface, } w(\eta) &= \frac{\partial \eta}{\partial t} + \frac{\partial \eta}{\partial x} \frac{\partial x}{\partial t} + \frac{\partial \eta}{\partial y} \frac{\partial y}{\partial t} \\ &= \frac{\partial \eta}{\partial t} + u(\eta) \frac{\partial \eta}{\partial x} + v(\eta) \frac{\partial \eta}{\partial y} \end{aligned}$$

$$\text{Hence } \frac{\partial}{\partial x} \int_{-h}^{\eta} u dz + \frac{\partial}{\partial y} \int_{-h}^{\eta} v dz + \frac{\partial}{\partial t} (\eta+h) = 0$$

Now define average quantities:

$$U = \frac{1}{\eta+h} \int_{-h}^{\eta} u dz, \quad V = \frac{1}{\eta+h} \int_{-h}^{\eta} v dz$$

$$\text{So } \frac{\partial}{\partial x} ((\eta+h)U) + \frac{\partial}{\partial y} ((\eta+h)V) + \frac{\partial}{\partial t} (\eta+h) = 0$$

Integrating across channel width from $y = 0$ to $y = B$, noting that

$$V = 0 \text{ at } y = 0, B.$$

$$\int_0^B \frac{\partial}{\partial x} ((\eta+h)U) dy + \int_0^B \frac{\partial}{\partial y} ((\eta+h)V) dy + \int_0^B \frac{\partial(\eta+h)}{\partial t} dy$$

$$\frac{\partial}{\partial x} \int_0^B (\eta+h) u dy - [(\eta+h)u \frac{\partial B}{\partial x}]_0^B + [(\eta+h)V]_0^B + \frac{\partial}{\partial t} \int_0^B (\eta+h) dy$$

$$- [(\eta+h) \frac{\partial B}{\partial t}]_0^B = 0$$

apply the boundary conditions, giving

$$\frac{\partial}{\partial x} \int_0^B (\eta+h) u dy + \frac{\partial}{\partial t} \int_0^B (\eta+h) dy = 0$$

$$\text{Now } \frac{\partial}{\partial t} \int_0^B (\eta+h) dy = \frac{\partial}{\partial t} A$$

$$\text{and } \int_0^B (\eta+h) u dy = \int_0^B u dA = A\bar{u} = Q$$

$$\text{Hence, } \frac{\partial Q}{\partial x} + \frac{\partial A}{\partial t} = 0$$

Consider the dynamic equations and depth integrate;

$$\int_{-h}^{\eta} \frac{\partial u}{\partial t} dz = \frac{\partial}{\partial t} \left(\int_{-h}^{\eta} u dz \right) - \frac{\partial \eta}{\partial t} u(\eta) - \frac{\partial h}{\partial t} u(-h)$$

(similarly for $\frac{\partial v}{\partial t}$)

$$\int_{-h}^{\eta} \frac{\partial}{\partial x} (uu) dz = \frac{\partial}{\partial x} \left(\int_{-h}^{\eta} u^2 dz \right) - \frac{\partial \eta}{\partial x} u^2(-\eta) - \frac{\partial h}{\partial x} u^2(-h)$$

(similarly for $\frac{\partial}{\partial y} (uv)$)

$$p - p_1 = - \int_{\eta}^z \rho g dz \quad p_1 = \text{pressure at surface}$$

$$\int_{-h}^{\eta} \frac{\partial p}{\partial x} dz = \int_{-h}^{\eta} \left(\int_z^{\eta} g \frac{\partial \rho}{\partial x} dz + g \rho \frac{\partial \eta}{\partial x} \right) dz$$

Then, if $\frac{\partial \rho}{\partial x}$ is independent of depth

$$\int_{-h}^{\eta} \frac{\partial \rho}{\partial x} dz = \frac{1}{2} g(\eta+h)^2 \frac{\partial \rho}{\partial x} + g\rho(\eta+h) \frac{\partial \eta}{\partial x}$$

(similarly for $\frac{\partial \rho}{\partial y}$)

$$\int_{-h}^{\eta} \frac{\partial}{\partial z} \tau_x dz = \tau_x(\eta) - \tau_x(-h)$$

where the first term on the right hand side is the shear stress at surface (due to wind) and the second term is the shear stress at bed (due to bottom friction). It has been argued that $|\tau_x(\eta)| \ll |\tau_x(-h)|$ (Ref 9), so surface stresses may be ignored.

Now consider the integral $\int_{-h}^{\eta} u^2 dz$ and make the substitution

$$\int_{-h}^{\eta} u^2 dz = \frac{\beta}{(\eta+h)} \left[\int_{-h}^{\eta} u dz \right]^2$$

$\beta \geq 1$ since

$$0 \leq \int_{-h}^{\eta} \left(u - \frac{1}{\eta+h} \int_{-h}^{\eta} u dz \right)^2 dz = \int_{-h}^{\eta} u^2 dz - \frac{1}{\eta+h} \left[\int_{-h}^{\eta} u dz \right]^2$$

$$\text{hence } \int_{-h}^{\eta} u^2 dz \geq \frac{1}{\eta+h} \left[\int_{-h}^{\eta} u dz \right]^2$$

β is termed the momentum correction co-efficient and accounts for the variation in velocity throughout the depth. Henceforth, set $\beta = 1$ (where max $\beta = 1.05$ in real flows (Ref 10)).

Reconsidering the dynamic equations together with the continuity equation.

$$\text{so } \frac{\partial u}{\partial x} + \frac{\partial v}{\partial y} + \frac{\partial w}{\partial z} = 0$$

$$\frac{\partial u}{\partial t} + u \frac{\partial u}{\partial x} + v \frac{\partial u}{\partial y} + w \frac{\partial u}{\partial z} + u \left(\frac{\partial u}{\partial x} + \frac{\partial v}{\partial y} + \frac{\partial w}{\partial z} \right) - \Omega v = -\frac{1}{\rho} \frac{\partial p}{\partial x} + \frac{1}{\rho} \frac{\partial \tau_x}{\partial z}$$

$$\frac{\partial v}{\partial t} + u \frac{\partial v}{\partial x} + v \frac{\partial v}{\partial y} + w \frac{\partial v}{\partial z} + v \left(\frac{\partial u}{\partial x} + \frac{\partial v}{\partial y} + \frac{\partial w}{\partial z} \right) + \Omega u = \frac{1}{\rho} \frac{\partial p}{\partial y} + \frac{1}{\rho} \frac{\partial \tau_y}{\partial z}$$

Then, depth intergrating

$$\begin{aligned} & \frac{\partial}{\partial t} \int_{-h}^{\eta} u dz - \frac{\partial \eta}{\partial t} u(\eta) - \frac{\partial h}{\partial t} u(-h) \\ & + \frac{\partial}{\partial x} \int_{-h}^{\eta} u^2 dz - \frac{\partial \eta}{\partial x} u^2(\eta) - \frac{\partial \eta}{\partial x} u^2(-h) \\ & + \frac{\partial}{\partial y} \int_{-h}^{\eta} u v dz - \frac{\partial \eta}{\partial y} u(\eta) v(\eta) - \frac{\partial \eta}{\partial y} u(-h) v(-h) \\ & + [wu]_{-h}^{\eta} \\ & - \Omega \int_{-h}^{\eta} v dz = \frac{1}{2} (\eta + h)^2 g \frac{\partial \rho}{\partial x} + g \rho (\eta+h) \frac{\partial \eta}{\partial x} - \tau_x(-h) \end{aligned}$$

$$\begin{aligned} \text{and } & \frac{\partial}{\partial t} \int_{-h}^{\eta} v dz - \frac{\partial \eta}{\partial t} v(\eta) - \frac{\partial h}{\partial t} v(-h) \\ & + \frac{\partial}{\partial x} \int_{-h}^{\eta} u v dz - \frac{\partial \eta}{\partial x} v(\eta) u(\eta) - \frac{\partial \eta}{\partial x} u(-h) v(-h) \\ & + \frac{\partial}{\partial y} \int_{-h}^{\eta} v^2 dz - \frac{\partial \eta}{\partial y} v^2(\eta) - \frac{\partial \eta}{\partial y} v^2(-h) \\ & + [wv]_{-h}^{\eta} \\ & + \Omega \int_{-h}^{\eta} u dz = \frac{1}{2} (\eta+h)^2 g \frac{\partial \rho}{\partial y} + g \rho (\eta+h) \frac{\partial \eta}{\partial y} - \tau_y(-h) \end{aligned}$$

Now write Total Depth $H = h + \eta$

Depth averaged velocities $UH = \int_{-h}^{\eta} u dz$, where $U \equiv U(x, t)$,

$VH = \int_{-h}^{\eta} v dz$, where $V \equiv V(x, t)$.

and recall that $w(\eta) = \frac{\partial \eta}{\partial t} + u(\eta) \frac{\partial \eta}{\partial x} + v(\eta) \frac{\partial \eta}{\partial y}$

$$w(-h) = \frac{\partial h}{\partial t} - u(-h) \frac{\partial h}{\partial x} - v(-h) \frac{\partial h}{\partial y}$$

So the momentum equations read

$$\frac{\partial}{\partial t}(HU) + \frac{\partial}{\partial x}(HU^2) + \frac{\partial}{\partial y}(HUV) - \Omega HV = \frac{1}{2}Hg^2 \frac{\partial \rho}{\partial y} + g\rho \frac{\partial \eta}{\partial y} - \tau_x(-h)$$

$$\frac{\partial}{\partial t}(HV) + \frac{\partial}{\partial x}(HUV) + \frac{\partial}{\partial y}(HV^2) + \Omega H\eta = \frac{1}{2}Hg^2 \frac{\partial \rho}{\partial y} + g\rho \frac{\partial \rho}{\partial y} - \tau_y(-h)$$

However the depth integrated continuity equation in this form gives

$$\frac{\partial H}{\partial t} + \frac{\partial}{\partial x}(HU) + \frac{\partial}{\partial y}(HV) = 0$$

So substituting for $\frac{\partial H}{\partial t}$ and dividing by H gives:

$$\frac{\partial U}{\partial t} + \frac{U\partial U}{\partial x} + \frac{V\partial V}{\partial y} - \Omega V = \frac{1}{2} \frac{gH}{\rho} \frac{\partial \rho}{\partial x} + g\rho \frac{\partial \eta}{\partial x} - \frac{\tau_x(-h)}{H}$$

$$\frac{\partial V}{\partial t} + \frac{U\partial V}{\partial x} + \frac{V\partial V}{\partial y} + \Omega U = \frac{1}{2} \frac{gH}{\rho} \frac{\partial \rho}{\partial y} + g\rho \frac{\partial \eta}{\partial y} - \frac{\tau_y(-h)}{H}$$

If we now consider flow in the axial direction only, such as is predominantly the case in rivers, set $V=0$, then

$$\frac{\partial U}{\partial t} + \frac{U\partial U}{\partial x} = \frac{1}{2} \frac{gH}{\rho} \frac{\partial \rho}{\partial x} + g\rho \frac{\partial \eta}{\partial x} - \frac{\tau_x(-h)}{H}$$

$$\text{and } \Omega U = \frac{1}{2} \frac{gH}{\rho} \frac{\partial \rho}{\partial y} + g\rho \frac{\partial \eta}{\partial y} - \frac{\tau_y(-h)}{H}$$

So there is a cross channel pressure gradient due to the Coriolis effect. If the river/estuary is sufficiently narrow this contribution to the pressure is negligible.

$$\begin{aligned} P_{\text{coriolis}} &= O(\Omega U \rho B) \\ P_{\text{hydraulic}} &= O(\rho g H) \end{aligned}$$

For typical Thames data:

$$\frac{P_{\text{coriolis}}}{P_{\text{hydraulic}}} = 0 \left(\frac{\Omega U B}{gH} \right) \sim 0 \left(\frac{10^{-4} \cdot 1 \cdot 10^3}{10 \cdot 10} \right) = 0(10^{-3})$$

Hence the model equations for depth averaged velocity, along the axial direction are:

$$\frac{\partial U}{\partial t} + U \frac{\partial U}{\partial x} = \frac{1}{2} \frac{gH}{\rho} \frac{\partial \rho}{\partial x} + g \frac{\partial \eta}{\partial x} - \frac{\tau_x(-h)}{H}$$

$$\text{and } \frac{\partial}{\partial x} ((h+\eta)U) + \frac{\partial \eta}{\partial t} = 0$$

where

$$U = \frac{1}{\eta+h} \int_{-h}^{\eta} u dz \quad \begin{array}{l} \eta = \text{free surface elevation} \\ -h = \text{bed} \\ \eta+h = H \end{array}$$

ρ = density, $\tau_x(-h)$ = bottom stress

The following assumptions have been made in this derivation:

- (i) Newtonian stresses associated with viscosity \ll Reynolds stresses associated with turbulent velocity fluctuations.

$$\text{ie } |\underline{\sigma}| \ll |\underline{\tau}|$$

- (ii) The Bousinesq approximation that density fluctuations are only included in gravitational term and ignored in the inertial terms.

- (iii) Hydrostatic balance: the vertical momentum equation is dominated by the balance of the gravitational acceleration by the vertical pressure gradient

$$\frac{W^2}{gH} \ll 1, \quad \frac{W}{gT} \ll 1$$

- (iv) Neglect surface stress due to wind.

$$|\tau_x(\eta)| \ll |\tau_x(-h)|$$

- (v) Set momentum correction coefficient, β , equal to unity.

$$\beta = \frac{\int_{-h}^{\eta} u^2 dz}{\frac{1}{\eta+h} \left[\int_{-h}^{\eta} u dz \right]^2} \quad (\beta_{\max} = 1.05, \text{ (Ref 10)})$$

- (vi) For axial flow, set $V=0$

- (vii) Ignore the pressure gradient set up across flow, due to the coriolis effect:

$$\left| \frac{P_{\text{coriolis}}}{P_{\text{hydrostatic}}} \right| \ll 1 \text{ ie } \frac{\Omega U B}{gH}$$

- (viii) Longitudinal density gradient does not vary with depth.

$$\frac{\partial \rho}{\partial x} \text{ independent of depth}$$

It is possible to recast these governing equations in terms of variables Q and A , discharge and cross sectional area respectively, rather than in terms of the velocity and depth of flow. Amein and Chu (Ref 11) argue that it is advantageous to do this, especially when dealing with irregular channels. They claim that the discharge is a much smoother function of (x,t) than the velocity. Between adjacent sections, the area and average velocity might both vary significantly, whereas the discharge, the product of the two, varies more smoothly.

$$\text{Discharge } Q = \int_0^B \int_{-h}^{\eta} u dz dy = A \bar{u}$$

The governing equations are averaged over the width giving:

$$\frac{\partial Q}{\partial x} + \frac{\partial A}{\partial t} = 0$$

$$\frac{1}{A} \frac{\partial Q}{\partial t} + \frac{1}{A} \frac{\partial}{\partial x} \left(\frac{Q^2}{A} \right) = \frac{1}{2} \frac{gH}{\rho} \frac{\partial \rho}{\partial x} + \frac{g \partial \eta}{\partial x} - \frac{\tau_x(-h)}{H}$$

2.2 Modelling the movement of sediment

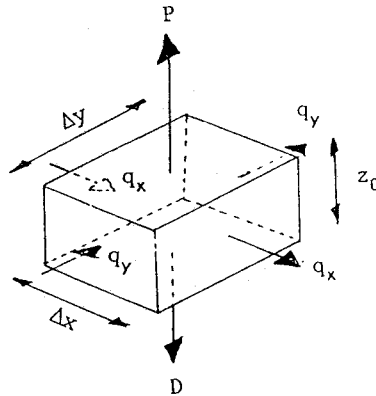
To complete the set of equations describing the dynamics of the estuary, it is necessary to describe the sediment movement. As usual, a distinction may be made between 'bed sediment' and suspended sediment. The former refers to sediment loads in which the grains roll along the bed, with occasional entrainment into the main flow. The latter refers to material which is permanently in suspension, due to the turbulence of the flow. The distinction between the two is clear enough when different materials with

widely different grain sizes are under consideration (for example a silt laden river flowing over a bed of gravel/coarse sand). However, if the two loads are of a similar nature (for example a silt laden river flowing over its own silt), the distinction becomes rather arbitrary. Nevertheless from the point of view of wishing to describe the dynamics, it is useful to maintain this difference.

2.2.1 Bed sediment motion

Changes in estuary bed levels may be related to sediment transport rates by means of a 'mass continuity' relation, which balances the net rate of sediment transport into a region with the increase of bed level.

Consider a control volume:



where q_x = longitudinal sediment flux,
 q_y = transverse sediment flux,
 z_0 = depth of sediment,
 P = rate of suspension of sediment from bed,
and D = rate of deposition of sediment to bed.

Flow of sediment into box $\Delta y \Delta z_0$ in time Δt :

$$\begin{aligned}
 &= (q_x(x) - q_x(x + \Delta x)) \Delta y \Delta t + (q_y(y) - q_y(y + \Delta y)) \Delta x \Delta t \\
 &= - \frac{\partial q_x}{\partial x} \Delta x \Delta y \Delta t - \frac{\partial q_y}{\partial y} \Delta x \Delta y \Delta t
 \end{aligned}$$

Balanced by suspension/deposition/increase of depth in time Δt :

$$= \rho_s \frac{\partial z_0}{\partial y} \Delta x \Delta y \Delta t (1-m) - P \Delta x \Delta y \Delta t + D \Delta x \Delta y \Delta t$$

m = porosity, $0 \leq m \leq 1$, $m = 0$ is non porous, $m = 1$ is pure constituent fluid.

$$\frac{\partial q_x}{\partial x} + \frac{\partial q_y}{\partial y} + \rho_s (1-m) \frac{\partial z_0}{\partial t} - P+D = 0$$

For a river in steady, equilibrium conditions, the rate of deposition equals the rate of suspension and so there exists a balance between the incoming sediment flux and the increase of sediment depth. If it were possible to formulate 'erosive and depositive' fluxes as functions of the velocity field, position and time within a tidal environment, then this continuity equation would permit the calculation of sediment depth. However, the precise form of these parameters is unknown and the equation remains an 'overriding' principle.

2.2.2 Suspended sediment motion

Many deposits consist of fine grained sand (60-300 microns) which is easily entrained from the bed by turbulent flow. Since the particles have a relatively low mass, they are kept in suspension by the turbulent eddies. This form of sediment transport may comprise 75-95% of the total sediment load (Ref 9). When formulating a mass continuity equation for these fine particles, it is necessary to include the diffusion induced by the turbulence, since this motion is of a similar magnitude as the motion induced by advection with the velocity field.

The diffusion equation:

$$\frac{\partial c}{\partial t} + \underline{u} \cdot \nabla c = \nabla \cdot (\underline{\xi} \cdot \nabla c)$$

where $\underline{\xi}$ = eddy diffusivity tensor

c = concentration of sediment

and $\underline{u} = \bar{\underline{u}} - \underline{u}_f$

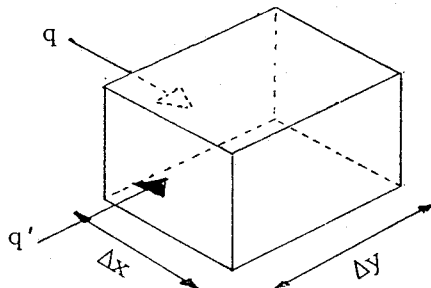
(average velocity field - fall velocity of sediment).

This equation may be depth integrated, with appropriate boundary conditions, to form an equation of the same general form as that for the bed load, but with a diffusion term included.

2.3 Stability of estuarine channels

The stability of any particular channel depends upon the sediment type to be found at the channel bed, the transporting ability of tidal streams and the supply of sediment from external sources. Consider the sediment equations for mass continuity, integrated over the channel cross section and with time. The condition for stability is that no change occurs to the channel profile. This may be expressed as follows:

Difference of sediment flux into and out of control volume $\Delta x \Delta y$.



In time t :

$$[q(x,t)-q(x+\Delta x,t)]\Delta y\Delta t+[q'(y,t)-q'(y+\Delta y,t)]\Delta x\Delta t = -[c(t)-c(t+\Delta t)]\Delta x\Delta y\Delta t$$

$$\Rightarrow \frac{\partial q}{\partial x} + \frac{\partial q'}{\partial y} + \frac{\partial c}{\partial t} = 0$$

where q = total sediment flux in x-direction
and q' = total sediment flux in y-direction
(both q and q' are independent of time).

Hence, integrating over width y and time interval $[t_1, t_2]$:

$$\int_{t_1}^{t_2} \frac{\partial q}{\partial x} dt + \int_{t_1}^{t_2} [q'] dt + \Delta C_t = 0 \text{ for equilibrium}$$

where the first term is the flux per unit width, the second term is the lateral inflow and the third term is the change in concentration per unit area.

The choice of the time interval with this 'averaging' is critical. It must be long enough such that all major variations of parameters affecting sediment transport are averaged out. These parameters include factors such as tidal conditions, freshwater inflows and meteorological conditions. To account for the tidal conditions, there is a need to average over a spring-neap cycle. However freshwater inflows and meteorological conditions may vary over a much longer timescale. So although the above equation for an equilibrium profile elegantly expresses the required conditions for channel equilibrium, it is doubtful

whether it can be applied under the required circumstances to permit averaging to take place. However, it is possible to consider the equation in a hypothetical situation where the tidal conditions and freshwater inflows are constant. Then the time period required for averaging is just one tidal cycle and the stability criteria reduces to:

$$\frac{\partial}{\partial x} [[Q]] = 0$$

where [[]] denotes a tidal average.

This equation is satisfied if the sediment flux is constant along the estuary, indicating that the bed shear stress never exceeds the critical value required to initiate sediment movement. Alternatively, as argued by McDowell and O'Connor (Ref 9), it is satisfied if the sediment flux is proportional to the tidal velocity and the estuary conforms to 'ideal conditions' :-

- (i) constant depth along estuary length
- (ii) width decreases exponentially from estuary mouth
- (iii) constant phase lag of tidal velocity behind water surface elevation
- (iv) small tidal range compared with channel depth.

(see later case studies for the validity of these assumptions, Sections 3.1-3.5).

The solution presented reads:

water elevation, $\eta = A_0 \cos(\sigma t - kx)$

velocity,
$$u = -\frac{A_o g}{C_o} \sin\phi \sin(\sigma t - kx - \phi)$$

width,
$$B = B_o \exp(-kx \cot\phi)$$

with mean tidal depth, H , $C_o^2 = gH$. and $C_o = \sigma/k$

The following is a verification that this solution satisfies the governing equations.

continuity equation:
$$\frac{\partial Q}{\partial x} + \frac{B \partial \eta}{\partial t} = 0$$

where $Q = (H + \eta)Bu$

So,

$$\begin{aligned} \frac{\partial Q}{\partial x} &= (H + \eta) B_o \exp(-kx \cot\phi) \frac{A_o g k}{C_o} \sin\phi \cos(\sigma t - kx - \phi) \\ &\quad + (H + \eta) B_o \exp(-kx \cot\phi) k \cot\phi \frac{A_o g}{C_o} \sin\phi \sin(\sigma t - kx - \phi) \\ &\quad - (B_o \exp(-kx \cot\phi) \cdot \frac{A_o g}{C_o} \sin\phi \sin(\sigma t - kx - \phi) A_o k \sin(\sigma t - kx)) \\ &= (H + \eta) B k \frac{A_o g}{C_o} (\sin\phi \cos(\sigma t - kx - \phi) + \cos\phi \sin(\sigma t - kx - \phi)) \\ &\quad + B u \frac{\partial \eta}{\partial x} \\ &= (H + \eta) \frac{B g A_o k}{C_o} \sin(\sigma t - kx) + B u \frac{\partial \eta}{\partial x} \\ &= \left[-\frac{(H + \eta)g}{C_o^2} + \frac{u}{\frac{\partial \eta}{\partial t}} \frac{\partial \eta}{\partial x} \right] B \frac{\partial \eta}{\partial t} \end{aligned}$$

Now $H \gg \eta$, so $\frac{(H+\eta)g}{C_o^2} \approx \frac{Hg}{C_o^2} = 1$

as $C_o^2 = Hg$ for surface waves on 'deep' waters

Looking at the order of magnitude of these terms

$$\text{and } O\left(\frac{\partial \eta}{\partial t}\right) = O\left(\frac{uk}{\sigma}\right) = O\left(\frac{u}{C_o}\right) = O\left(\frac{\eta g}{C_o^2}\right) = O\left(\frac{\eta}{H}\right) \ll 1$$

So to first order the continuity equation is satisfied by the proposed solution. Now consider the momentum equation:

$$\frac{\partial u}{\partial t} + u \frac{\partial u}{\partial x} = -g \frac{\partial \eta}{\partial x} + \text{friction term}$$

Comparing order of magnitude of each term:

$$\left(\frac{\partial u}{\partial t}\right) \sim \left(\frac{\sigma \eta g}{C_o}\right), \quad \left(u \frac{\partial u}{\partial x}\right) \sim \left(\frac{\eta^2 g^2 k}{C_o^2}\right),$$

$$\left(g \frac{\partial \eta}{\partial x}\right) \sim (\eta g k), \quad \sigma = k C_o \quad \text{so} \quad \left(\frac{\partial \eta}{\partial x}\right) \sim \left(\frac{\partial u}{\partial t}\right)$$

$$\text{and } \left(\frac{u \partial u}{\partial x} / \frac{\partial u}{\partial t}\right) \sim \left(\frac{\eta g}{C_o^2}\right) \sim \left(\frac{\eta}{H}\right) \ll 1$$

So in this approximation, we neglect the convective term.

$$\frac{\partial u}{\partial t} = - \frac{\sigma A_o}{C_o} \sin\phi \cos(\sigma t - kx - \phi)$$

$$g \frac{\partial \eta}{\partial x} = - k A_o g \sin(\sigma t - kx)$$

If linearised friction term = fu, where f is a constant then:

$$-k A_o g \sin\phi \cos(\sigma t - kx - \phi) = k A_o g \sin(\sigma t - kx) + f \sin\phi \sin(\sigma t - kx - \phi)$$

$$k A_o g \sin(\sigma t - kx - \phi) \cos\phi = f \sin\phi \sin(\sigma t - kx - \phi)$$

and $f = \cot\phi k A_o g = \text{constant as required.}$

Hence, if the friction constant is of this form, the solution satisfies the modelling hydrodynamic equations.

2.3.1 Application to Thames Estuary

The observation in the Thames is that at the estuary mouth, the velocity and water elevation are 3 hours 45 minutes out of phase. The tidal range at the entrance is 5.5m and the depth of the estuary, assumed constant is 7.93m.

So:

$$A_o = \frac{5.5}{2} = 2.75\text{m}$$

$$C_o = (gH)^{\frac{1}{2}} = 8.82 \text{ m/s}$$

Phase lag 3.75 hours = $\frac{3.75}{12} \cdot 360^\circ = 113^\circ$ phase lag
so $\phi = 23^\circ$

$$k = \frac{2\pi/T}{C} = \frac{2\pi}{8.82 \cdot 3600 \cdot 12}$$

$x = 0$ at Southend

$$\text{So } U_{\max} = \frac{A_o g}{C_o} \sin\phi = 1.2 \text{ m/s}$$

$$\text{and if } B = B_o e^{2\alpha x}, \alpha = \frac{-k \cot\phi}{2} = 1.94 \times 10^{-5} \text{ m}^{-1}$$

compared with the observed values $\alpha = 2.06 \times 10^{-5} \text{ m}^{-1}$
and $u_{\max} = 1.0 \text{ m/s}$. Thus the model renders reasonably accurate data, even though it solves a linearised set of equations as well as making the other simplifying assumptions, elucidated above. For the Thames, downstream of London Bridge it appears that the assumptions are reasonable.

Further note, the behaviour of the model in the limits of large and small friction effects.

(i) $f \rightarrow 0$, so $\phi \rightarrow \pi/2$, $B \rightarrow B_o$ across width.

The velocity and surface elevation are in phase with this limit, as expected, and the channel width is constant across the estuary length.

(ii) $f \rightarrow \infty$, so $\phi \rightarrow 0$, $B \rightarrow 0$, $u \rightarrow 0$.

Frictional effects dominate, so although there is surface elevation propagation along the

estuary length, the friction effects prevent the establishment of a non zero velocity field. Thus, the width of the channel diminishes to zero upstream after an infinitesimal distance.

The above suggests that there is a balance between the friction and the estuary shape, causing the tidal propagation upstream.

The application of this method to other estuaries is feasible, but only if sufficiently detailed data is available to allow the calculation of the phase lag between the surface elevation and the flow velocity, especially because $\cot\phi$ is considered:

Making the Taylor expansion:

$$\cot(\phi + \delta\phi) = \cot\phi + \delta\phi \operatorname{cosec}^2\phi + O(\delta\phi^2)$$

With velocity readings every 15 minutes it is possible to determine u_{\max} to within ± 15 minutes

$$\text{Phase error } \delta\phi = \frac{15}{12.60} \cdot 2\pi = \frac{\pi}{24}$$

$$\text{So at } \phi = 22^\circ, \quad \frac{\delta\phi}{\sin^2\phi} = 0.93$$

$$\text{Which is } \frac{0.93}{\cot\phi} \times 100\% \sim 35\% \text{ error}$$

2.4 Tidal Volume model

In order to simulate the fluctuations in depth and velocity due to the tide, it is necessary to run some kind of tidal model. The model adopted for use in this study is a simple calculation involving the

manipulation of tidal volumes. It satisfies the continuity equation, but takes no account of the velocity field alterations caused by dissipative forces.

$$\bar{u}(x,t) = \frac{\left[\frac{\partial}{\partial t} \int_0^x A_T dx + Q \right]}{A}$$

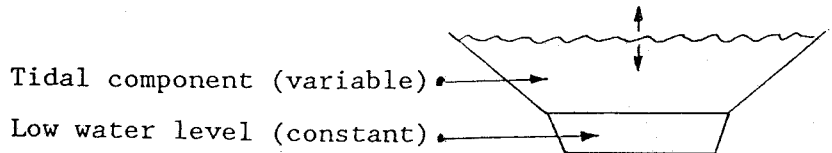
where Q = river flow (m^3/s), constant

$A(x,t)$ = cross sectional area

$A_T(x,t)$ = tidal cross sectional area

$\bar{u}(x,t)$ = average velocity

The cross sectional area $A(x,t)$ is pictured as being composed of a time independent low water contribution, together with a time dependent tidal component such that:



The data required for input to the model is:

- (i) profile data at prescribed downstream distances. This specifies the cross section in simple geometric terms making it possible to calculate cross sectional area as a function of water depth.
- (ii) tidal elevations at these downstream locations for an entire tidal cycle.
- (iii) the freshwater river flux.

The advantages of this simple model are:

- (i) that the resulting solution for the velocity field is potentially an exact solution for the dynamical system. Consider the continuity and dynamic equations:

$$\frac{\partial Q}{\partial x} + \frac{B d \eta}{\partial t} = 0 \text{ and } \frac{\partial u}{\partial t} + u \frac{\partial u}{\partial x} = -g \frac{\partial \eta}{\partial x} - \frac{\tau_x}{H}$$

These are in effect two equations for two unknowns, velocity $u(x,t)$ and tidal elevation $\eta(x,t)$. If the prescribed tidal elevations are viewed as a solution of the system, then integration of the continuity equation yields the velocity field.

- (ii) It is not necessary that all elevations are measured with respect to the same datum, or indeed that the mean tidal level is constant along the estuary.

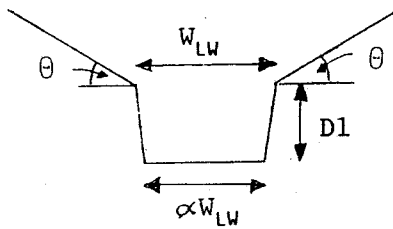
The disadvantages of the simple model are :

- (i) The system is purely one dimensional and so no account may be taken of secondary circulation.
- (ii) The sections were at distances, typically 0(3km), and so it is assumed that these sections are typical of the intervening reaches.
- (iii) The use of a geometrical representation of the cross section, although simplifying calculations, at times does not present an accurate portrayal it.

2.5 Geometric approximation for the cross section

In this study three types of cross section are used, a triangular cross section, a trapezoidal cross section and a trapezoidal cross section with associated mud or sand banks.

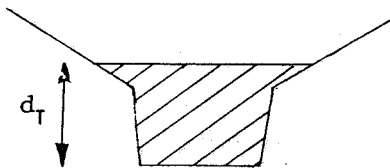
For the case of a trapezoidal channel section with 'mud flats':



$$\tan\theta = m$$

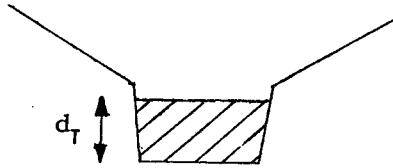
$$A_{LW} = \frac{d_{LW}}{2} (W_{LW} + W_B)$$

Case $d_T > D1$



$$A = (d_T - D1) \left[\frac{1}{2} \left[W_B + \frac{D1}{d_{LW}} (W_{LW} - W_B) \right] + \frac{(d_T - D)}{m} \right] + \frac{D1}{2} \left[2W_B + \frac{D1}{d_{LW}} (W_{LW} - W_B) \right]$$

Case $d_T \leq D1$



$$A = d_T \cdot \frac{1}{2} \left[2W_B + \frac{d_T}{d_{LW}} (W_{LW} - W_B) \right]$$

This may be reduced to a pure trapezoidal cross section, if $(d_T)_{\max} < D1$ and further reduces to a triangular cross section if $W_B = 0$ and $(d_T)_{\max} < D1$. The data required to specify each section is thus, bottom width, W_B , low water width, W_{LW} , low water depth, d_{LW} , channel depth, $D1$ and mud flats gradient, m .

2.6 Stress parameter

The Chezy formula for velocity is a semi empirical formula based on dimensional analysis (Ref 12):

$$\text{depth average velocity } \bar{u} = c (RS_f)^{1/2}$$

$$\text{and shear stress } \tau_o = \rho g RS_f$$

where R is the Hydraulic radius and S_f is the 'friction slope'. However, observation suggested that the Chezy co-efficient varied as $R^{1/6}$, in rivers and large channels. This led to the Manning formula:

$$\bar{u} = \frac{1}{n} S^{1/2} R^{2/3}$$

where n is a characteristic of the surface material (for smooth mud $n \approx 0.025 \text{ s/m}^{1/3}$). A shear velocity, u^* , is now defined:

$$u^* = (\tau_o / \rho)^{1/2} = (gRS_f)^{1/2}$$

The shear velocity has dimensions of velocity, but can not be equated directly with any real physical velocity. Instead it gives an indication of bottom shear stress and has been used in the formulation of various sediment transport equations. Consider:

$$\frac{u^*}{u} = \frac{(gRS_f)^{1/2}}{\frac{1}{n} S_f^{1/2} R^{2/3}} = n \frac{g^{1/2}}{R^{1/6}}$$

$$\frac{\bar{u}}{R^{1/6}} = \frac{1}{n\sqrt{g}} u^*$$

So studying this parameter is equivalent to studying the shear velocity, which in turn is equivalent to studying $\sqrt{\tau_o}$, the shear stress exerted by the fluid. For shallow, wide channels (width, w and depth, d):

$$A=wd, P=2d+w \text{ with } w \gg d$$

where P = the wetted perimeter.

$$R = \frac{wd}{2d+w} = d(1 + \frac{2d}{w})^{-1} \approx d(1 - \frac{2d}{w} + 0 [(\frac{d}{w})^2])$$

$$\text{So } R \approx d$$

Hence, study the parameter

$$\frac{\bar{u}}{d^{1/6}}$$

3. MODEL RESULTS

In this chapter the results of five case studies using the model described in Section 2.4 and representations of estuary cross section described in Section 2.5 are presented. The first case is an idealised estuary then results of modelling the Thames, Conwy, Parrett and Nene estuaries are presented.

3.1 Ideal estuary

As a prototype case study an idealised estuary is considered. The idealisations are made with respect to the estuary geometry and the propagation of the water elevation up the estuary. The estuary is modelled as a triangular cross section (see Section 2.5.1), with low water depth and cross section specified by exponential functions.

$$\begin{aligned}d &= 2.\exp(0.0275x) \\A &= 10.\exp(0.0622x) \\w &= 10.\exp(0.0347x)\end{aligned}$$

where $x=0$ at tidal limit and $0 < x < 40\text{km}$.

The tidal elevation from the mean tide level is given by:

$$\eta(x,t) = \frac{x}{10} \sin \left(\frac{2\pi t}{12} - \phi(x) \frac{2\pi}{12} \right)$$

the tidal period is taken to be 12 hours and the phase given by:

$$\phi(x) = \left(1 - \frac{x}{40} \right)$$

$$\Rightarrow \eta(x,t) = \frac{x}{10} \sin \left(\frac{2\pi t}{12} - \frac{2\pi}{12} \left(1 - \frac{x}{40} \right) \right)$$

$$\text{cf. } \eta(x,t) = R(x) \sin(\omega t - kx)$$

where $k = \frac{\omega}{c}$ and c = wave speed.

So this corresponds to a surface wave of speed 40 km/h, propagating upstream (the negative x direction).

3.1.1 Results

It can be seen from Figure 1 that the maximum stress parameter that occurs through the tidal cycle for a given downstream distance tends to a constant value downstream, near the estuary mouth. In this region, the tidal flux exceeds the river flux and so increasing the river flux has only a limited influence. This observation motivates the idea of studying the stress parameter along estuaries and testing its constancy. Note that as the river flow increases, so the upstream end of the estuary becomes increasingly dominated by it.

The stress parameter, velocity and depth are shown at various times through the tidal cycle in Figure 2. The similarity between the stress parameter and velocity is easily seen. This is because there is little dependency on depth, if the depth is doubled and the velocity remains the same, the stress parameter is only reduced by 11%. The constancy of the stress parameter along the length of the estuary can be seen for the $t=9$ curve. This corresponds to peak flood conditions.

Figure 3a shows the maximum stress parameter that occurs within the estuary for a given river flow. Figure 3b shows the location within the estuary at which the maximum stress occurs. The observation is that there exists a critical river flow, q_c , at which the location of the peak stress parameter switches from the estuary mouth ($q < q_c$) to being located at the tidal limit ($q > q_c$). This change coincides with a change of sign of the peak stress, indicating the direction of flow becomes seaward when the change

occurs. It can also be seen that there is a change of gradient, resulting from the change of location of the stress.

As expected this change is 'total', there are no intervening positions of peak stress as confirmed in Figure 4 showing the same graphs for a smaller range of river flows.

The procedure has been repeated for a number of tidal ranges (linearly scaled). The results are presented in Figure 5. The tidal ranges used somewhat exaggerate the differences between springs and neaps. However the observation is that increasing the tidal range leads to a different constant 'stress parameter envelope' downstream.

3.2 Thames Estuary

The Thames estuary is studied between its imposed tidal limit at Teddington Weir and its mouth at Southend. This comprises a 100km long tidally influenced reach, over which many studies have been carried out. The Thames is regarded as, in some senses, an 'ideal estuary' as it evolves in a regular manner and exhibits a dynamic morphological equilibrium.

3.2.1 Model input data

The data used for the model of the Thames was compiled from two sources (Ref 13 and 14). Reference 13 gives velocity, depth, salinity and suspended sediment concentrations at 13 sections along the estuary measured concurrently throughout an entire tidal cycle. It comprises four different field surveys; spring and neap tides with high and low freshwater flows. Furthermore it presents tidal curves and an analysis of the bed material. Readings at each of the

stations were taken at half hour intervals. This data set, therefore, permits the stress parameter to be calculated during the tidal cycle. The tidal curves were used to simulate the elevation of the free surface.

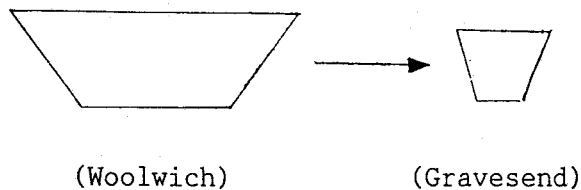
Reference 14 gives details of the mean tide level (MTL) cross sectional area and MTL width; these are used in conjunction with the tidal data to run the tidal volume model. Also an approximate channel depth is presented. It is difficult to use the notion of channel depth, as it will vary across the cross section; at some locations the variation is quite rapid.

3.2.2 Model cross sections

The mean tide level cross section area and width are specified, but not the actual cross sectional profile. It is possible to enter a digitised image of the actual cross-section profiles, but this is somewhat unnecessary as such a level of accuracy is not sought. Instead motivated by the cross sections shown in Reference 14 (see Fig 6 a trapezoidal representation of the cross section is used (see Section 2.5).

The evolution of the trapezium shape is governed by the function:

$$\alpha = \alpha(x)$$



A functional form of $\alpha(x)$ is used, such that α decreases along the estuary.

$$\alpha(x) = 0.5 \left((X_L - x)/X_L \right)^{1/2}$$

where X_L = length of estuary. This produces reasonable correspondence between the observed approximate depth and the calculated depth D . It is possible to include mud/sand banks on either side of the low water channel (see Section 2.5). While this allows the model to be 'tuned', it was found to be unnecessary with the Thames, which was modelled by the generic trapezium alone and produced reasonable results.

3.2.3 Field observations

The maximum and minimum stress parameters for the 12 different sections are shown in Figures 7 and 8 for spring and neap tides during periods of high ($\approx 93 \text{ m}^3/\text{s}$) and low ($\approx 14 \text{ m}^3/\text{s}$) river flow. The observation is that in each case the maximum stress parameter remains approximately constant.

Furthermore, this constant is similar for the two spring tide cases (Fig 7) and the two neap tide cases (Fig 8) giving the following values:

$$\begin{aligned} S_{\text{neap,highflow}} &\approx 0.7 \\ S_{\text{neap,lowflow}} &\approx 0.7 \\ S_{\text{spring,highflow}} &\approx 0.95 \\ S_{\text{spring,lowflow}} &\approx 0.85 \end{aligned}$$

It can be seen (Fig 9) that there is a strong linear relationship between the logarithm of the MTL width and the distance downstream, giving:

$$\text{Width}_{\text{MTL}} = w_0 \exp(-\alpha x), \text{ with } \alpha = 0.0405 \text{ km}^{-1}$$

This compares with a value of 0.0412km^{-1} determined by McDowell and O'Connor (Ref 9).

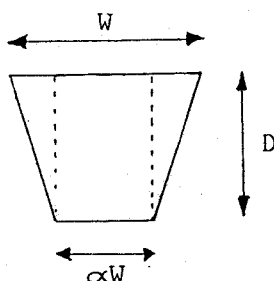
Similarly there is a strong linear relationship between the phase and the distance downstream (Fig 10), giving:

$$\text{Phase } \phi = 2.362 - 0.0264x$$

where ϕ is in hours and x is in km.

The longitudinal profile of the Thames estuary is shown in Figure 11. Note that the channel depth shown is the maximum depth not the averaged depth. It can be seen that the amplitude of the maximum surface oscillation (high water to low water on spring tides) is considerably less than the channel depth except at the tidal limit.

A notion of average depth across the profile may be introduced:



$$\text{Average depth} = (1-\alpha) \frac{D}{2} + \alpha D = \frac{(1+\alpha)}{2} D$$

(here $0 \leq \alpha \leq \frac{1}{2}$, so average depth is in the range:

$$\frac{D}{2} \rightarrow \frac{3D}{4}$$

note - in the calculation of the stress parameter,

$$s = \frac{\bar{u}}{d^{1/6}}$$

d = channel depth
if average depth used $\bar{d} = \frac{(1+\alpha)d}{2}$

$$\text{and } \bar{d}^{1.6} = \left(\frac{1+\alpha}{2}\right)^{1.6} d^{1.6}$$

hence $S_{\text{ay depth}} = \left(\frac{2}{1+\alpha}\right)^{1.6} S_{\text{ch depth}}$

and $1.05 \leq \left(\frac{2}{1+\alpha}\right)^{1.6} \leq 1.12$ corresponding to a 5-12% increase of stress parameter. (At this stage the channel depth is used, although this may be corrected at a later stage to average depth).

For comparison with observations the choice of which depth to use depends upon the location of the observer across the channel width. If it is assumed that observations are taken in mid channel, then it is appropriate to use the maximum channel depth.

Comparison of the observed tidal curves with the appropriate sinusoidal approximation are shown in Figures 12 and 13. The sinusoidal approximations are made by matching the tidal range and time of maximum elevation to the observed curves.

For the downstream sections (Fig 13) the sinusoidal approximation is reasonably accurate, but this is not the case upstream. By the time the surface disturbance has propagated to these upstream locations, there are considerable distortions from the sinusoidal, resulting typically in a shorter flood than ebb tide period. Hence there is a need to employ the actual tidal curves when running the tidal volume model.

3.2.4 Results

Figures 14 and 15 show the predicted and observed velocity and shear stress parameter at selected downstream locations. It can be seen that in general there is good agreement between the predicted and the

observed values. At each section, the general shape of the predicted curves follows that of the observed. There are, however, some differences between the two, especially at the upstream locations (see Fig 14). Here at peak ebb, the velocities and stresses predicted by the model exceed those observed. This over prediction occurs for the first 2-3 sections, whereas thereafter the agreement is much better. At downstream sections, there is a slight tendency to underpredict the velocity and stress, this slight difference may be due to the difference between average and channel depth and the uncertainty of which to use for the stress calculation. (The previous calculations of Section 3.2.3 would permit a 5-12% increase of the stress parameter). There is much scope for tuning with this model, by adjusting the cross sectional profile, which would yield closer correspondence between predicted and calculated if required.

Figure 16 shows the maximum stress parameter along the estuary for different river flows in the range (0-133.3m³/s). The maximum value of the stress parameter is constant along the estuary length (ignoring the first 3 sections which are dominated by river flow) and the constant value it attains is independent of the fresh water flow. This bears out the observation of the value of the maximum stress parameter depending upon tidal range only (Figs 7 and 8). At downstream locations, independence of freshwater flow results from the tidal flux far exceeding the fresh water flux, whereas at upstream locations, the two are comparable.

For completeness, graphs are shown in Figure 17 giving the dependence of the maximum stress parameter along the entire length of the estuary upon river flow and tidal range (which is linearly scaled). These

demonstrate the same bifurcation as observed with the idealised case.

3.3 Conwy Estuary

The Conwy estuary is studied between the Deganwy Narrows, where it flows out into Conwy Bay and the Tan-lan road bridge; the tidal limit, located 20km upstream of the estuary's mouth. The estuary has a large amplitude tide compared with its low water depth and so consequently there are considerable mud and sand banks at low water. The estuary is considerably constrained in its shape within the downstream reaches, by an engineering and geological imposition. Crossing between Llandudno and Conwy, there are the bridges and their associated causeways, while the estuary mouth is constrained geologically at the Deganwy Narrows. It is expected, therefore, that this estuary should form an interesting case study, exemplifying the interaction of a number of physical processes.

3.3.1 Model input data

Although HR has conducted a number of studies on the Conwy estuary these have concentrated upon the region downstream of the bridges, considering the effects of improvement schemes. Hence it was necessary to use a series of data sources in order to study the estuary from its tidal limit (Refs 15-20).

Since the data was compiled from so many sources, there was a need to standardise and rescale as appropriate. The only source giving continuous through the tide depth and velocity data at upstream locations was Reference 16 and as this case studied a spring tide with an average river flow of $27.1 \text{ m}^3/\text{s}$, this was used for the tidal volume model.

The cross sectional profile of the estuary was taken to be trapezoidal with mud/sand banks on either side (see Section 2.5.3). The actual data used for the profiles is presented in Table 1.

3.3.2 Field observations

The depth profile and channel widths along the estuary length are shown in Figure 18. This illustrates the effect of the constrictions on the flow at the bridges and the Deganwy Narrows. There is a considerable increase of depth in these two regions caused by the width restriction. The flow velocity is also considerably increased in these regions and there is some indication of bed armouring. If this is the case then it is unlikely that the Conwy will fit into any 'regime' ideas.

Detailed spring tide curves are available for the downstream reaches of the Conwy, but not for the upstream reaches. While it is possible to assess the tidal range of these upstream locations, it is difficult both to assess the phase relation between them and the downstream tidal disturbance, and the celerity of the tidal disturbance. The data was generated by appropriate scaling of the downstream disturbance and by introduction of an appropriate phase factor. Further, it was assumed that there was no tidal oscillation at the tidal limit. It appears that there is no tidal resonance along the Conwy estuary; the tidal amplitudes decay along the entire length (see Fig 18a). As with the Thames, the actual tidal elevations rather than a series of sinusoidal curves were used.

It is difficult to draw conclusions from only 4 data points there is some evidence in Figure 19 of the

constancy of the maximum stress parameter along the estuary length giving a value of $S_{\max} \approx 0.75$. With the existence of such a pronounced low water channel it is particularly critical that the velocity and depth measurements are taken there, as this is where they reach their maxima.

3.3.3 Results

Observations of velocity and depth through the tidal cycle exist at four locations along the channel. These are compared with the predictions from the model in Figures 20 and 21. Apart from providing a general representation of the variation of velocity and stress through the tidal cycle, the agreement is not at all good. The particular areas of difference are discussed below.

Location 2 (Fig 20a), here there is a large difference between predicted and observed magnitudes of flow velocity and bottom stress. This could be slightly improved upon by imposing a tidal range at the tidal limit, implying the model would account for a larger volume throughflow and hence greater velocities. However, the observed velocities at this location do not seem to follow a simple tidal cycle, they peak at 12:30 and then again at 19:30 indicating that the flow here is possibly dominated by secondary circulation and so this could dominate the velocity readings. Secondary circulation is not included in the model.

Location 3 (Fig 20b), although there is broad agreement with the magnitude of the velocities and stress, the 'phase' relationship is incorrect; the peaks of velocity and stress do not occur at the same time during the tidal cycle for the observed and predicted results. A possible reason for this is that

the tidal curve is 'distorted' further upstream so that the ebb becomes longer than the flood. The model simply assumes a linear scaling of the shape of the downstream tidal curve, where the two are comparable.

Locations 7 and 8 (Fig 21), once again there is broad agreement between the observed and predicted results, although the magnitude of the predicted results is approximately 25% greater than the observed. Possibly the difference arises from the measurement of the observed data in positions away from the low water channel where the largest velocities are to be found.

In addition to the possible reasons detailed above which could reconcile the predicted and observed data, there are other factors such as errors in the modelling of the estuary profile, or the inapplicability of the generic cross section.

The graph of the maximum stress parameter along the length of the estuary is shown in Figure 22 for river flows in the range (0-150m³/s). This indicates somewhat different results to those of the Thames and the 'ideal' estuary. There is no indication that for the downstream locations there is a constant maximum stress parameter. Increasing the river flow does appear to have some influence upon the maximum stress parameter observed at a particular location (presumably because the river flux \approx tidal flux). These two observations are in conflict with the results for the previous two case studies.

If the maximum stress occurring along the entire estuary is considered (Fig 23) as a function of river flow for various different tidal ranges, the same type of result as for the earlier cases is attained. The location of the maximum stress moves upstream as the

river flow increases. For the flow rate used (27.lm³) the peak stress is always located at the estuary mouth regardless of the tidal strength.

3.4 Parrett Estuary

The Parrett estuary is studied between Stert Point, where it joins with the Severn estuary, and its tidal limits at Oath Loch on the River Parrett and New Bridge on the river Tone. The Tone is a major tributary which is far enough downstream to be influenced by the tidal oscillations. The Parrett estuary is very 'energetic'; the tidal range far exceeds the low water depth (at Stert Point, the low water depth was less than 1m whereas at high water the depth can be as much as 11.7m); the flood is very much shorter than the ebb and at times a 'tidal bore' exists. The river seems to be free of 'man made' or geological restrictions, with the possible exception of the stretches through Bridgwater and Stert Point. At low water there is a definite low water channel which wanders across the river and which, at times, is braided.

3.4.1 Model input data

Several studies have been carried out on the Parrett, including a 'through the tide' series of observations at seven different locations. The data used for modelling was taken from References 21-24, the appropriate ordnance survey 1:25000 maps and surveyed cross sections from Wessex Water Authority.

The data sets were fairly detailed, but the tidal curves were not given along the estuary length. Hence it was difficult to accurately assess the speed of propagation upstream of the tidal disturbance. Furthermore there was a need to patch together the

observed data at the locations near the tidal limit with the observations downstream. A freshwater flow of $12.5\text{m}^3/\text{s}$ was used.

The cross sectional profile of the estuary was taken to be trapezoidal with mud/sand banks on either side (see Section 2.5.3). The actual data used for the profiles is presented in Table 2.

3.4.2 Field Observations

The depth profile along the estuary length are shown in Figure 24a. This demonstrates that the tidal range along the Parrett far exceeds the low water depth. Also there are some locations, notably at 15km and 18km where the river is virtually dry at low water. Note that there appears to be an error with the observations at 15 km.

The mean tidal width along the estuary is shown in Figure 24b. There is a good correlation between $\log(\text{width})$ and downstream distance with:

$$w = w_0 \exp(\alpha x), \quad \text{with } \alpha = 0.101\text{km}^{-1}$$
$$\text{and } w_0 = \exp(2.262) = 9.60$$

Figure 25 shows the maximum and minimum stress parameters along the estuary. There is some discrepancy between the downstream locations (below Bridge) and those upstream, with upstream values being approximately half those downstream. This may be due to having taken the observations on different occasions with different conditions. Alternatively it may indicate that the tidal influence (which is probably dominant in the Parrett) is considerably diminished at these locations. The maximum stress observed on the flood (negative values) is

considerably greater than that occurring on the ebb. This reflects the energetic nature of the tide and the existence of the tidal bore. It is possible, although not entirely convincing, to claim that there exists a constant maximum stress parameter along the estuary length and a possible value is indicated on the graph. There are some surprising data observations at Pims and Marchants where the observed stress on the flood is smaller than expected. It is possible that the observations here were not taken in the fast moving stream which would of course be highly significant, especially with such an energetic tide.

A series of tidal curves, at various sections upstream are shown together with a sinusoidal approximation in Figures 26 and 27. The approximation is based upon matching the phase at highwater and prescribing the tidal range. The graphs indicate the asymmetric nature of the tidal oscillation within the Parrett. The flood is much shorter than the ebb. The asymmetry becomes more pronounced further upstream as the curves become more distorted from the sinusoidal approximation.

3.4.3 Results

Comparison of the observed velocity and stress throughout the tidal cycle, at various downstream locations are shown in Figures 27 - 30. This permits assessment as to whether the model produces reasonable results or whether a more accurate (and complicated) modelling procedure is required. The model predicts velocities and stresses which follow the general behaviour of the observations. There are, however, a number of points that should be noted:

During the low water period there is a tendency to overestimate the flow rate (by as much as a factor of 4).

Coincident with flow reversal, the predicted and observed velocities often conflict in direction as well as magnitude. This discrepancy reflects the sensitivity of the modelling procedure upon the tidal curves prescribed at each section. Any error will have an effect on the sections downstream, when the tidal volume is calculated. This is particularly significant for the River

Parrett as the tide propagates upstream so fast and hence it is critical to assess the phase difference between adjoining sections. Errors in the phase difference leads to the prediction of an erroneous increase of downstream velocity just prior to flow reversal (at locations 7, 8 and 12).

In some instances there is accurate prediction of flow velocity for some or all of the tidal cycle (locations 6, 8 and 11).

Graphs showing the superposition of tidal elevation upon flow velocity, (Fig 31) show that in general the model produces reasonable results, excepting the increase just prior to flow reversal. The short flood induces high upstream velocities, whereas the velocities associated with the longer ebb are slightly smaller.

The graph of maximum stress parameter along the entire estuary length, against river flow, for increasing tidal range is shown in Figure 32. The graph shows the same change of gradient when the river flow dominates the tidal effects, but the bifurcation is not accompanied by the location of the maximum stress parameter moving upstream. Instead, the location of the maximum stress parameter is always to be found at the same position, 18km downstream (Fig 32), which corresponds to the region of extremely shallow water at low tide. As discussed above, it is doubtful

whether the model is reproducing realistic effects with these parameters, as it models a high river flow through a shallow water depth, the low water depth is not modelled to increase with river flow. Nevertheless the graph does indicate the existence of a bifurcation point (change of gradient of curves) when the maximum stress parameter moves from being tidally to river dominated.

3.5 River Nene

The River Nene is studied along its tidal which extends for 40km from its mouth, to its imposed tidal limit at the Dog in a Doublet sluices. The Nene is a narrow channel with a tidal range which varies from 7m at the mouth to 2.5m at the tidal limit. The channel appears to be free from any geological or artificial constraints which limit its evolution (with the exception of flow through Wisbech, at 22km downstream). A dynamic equilibrium is thought to exist with regard to the sediment movement, as it appears to be free from any long term morphological variation. The tidal range is of the same order of magnitude as the low water depth (typically tidal range $\approx 2 \times \text{LW depth}$) and so it is expected that the Nene's hydrodynamic behaviour should be well reproduced by the modelling procedure.

3.5.1 Model input data

HR comprehensively surveyed the Nene in 1964 and 1965 (Refs 25 and 26). Reference 25 contains through the tide observations of flow velocity and water depth at 4 stations during a spring and neap tide. Also it gives details of cross sections across the channel at 13 points along the channel length. These cross sections were observed to be approximately trapezoidal in nature and so this this was used as the generic

shape along the estuary length (see also Section 2.5.2). Tidal curves were not specified at any section and so the observed water depths were used, together with linear interpolation to give the data for the sections where observations were not taken. Clearly this includes an approximation which does not truly represent the propagation of the tidal disturbance along the estuary length. A freshwater river flow of $2\text{m}^3/\text{s}$ was used,

3.5.2 Field observations

The depth profile along the estuary is shown in Figure 33. The low water depth is of the same order of magnitude as the tidal range. Hence the river is to be contrasted with the Parrett; it does not become shallow at low water. The observed neaps tidal range is about half of the spring range. The tidal data was linearly interpolated; the observed data is at (38.1, 31.8, 22.1 and 12.6 km).

Considering the mean tide width and performing regression on the nine downstream widths, it is found that the width is exponentially dependent upon downstream distance with

$$w = w_0 \exp(\alpha x), \text{ with } \alpha = 0.0504\text{km}^{-1}$$

and $w_0 = 11.66\text{m}$

Figure 34 shows the spring tide elevation at 4 locations along the Nene. These observations show what is presumably an error at 13:30 for Wisbech; this has been corrected to smooth the curve. It can be seen that a sinusoidal approximation to the tidal curve is not appropriate for any location on the Nene.

The phase difference along the estuary is considered by plotting the time difference of HW to that at the estuary mouth, against downstream distance. For both spring and neap tides, the gradient of the best fit line is $-3.45(\pm 0.02)$ mins/km. However, this result is not necessarily conclusive as there are only 4 data points and it is not necessarily true that a linear trend should occur. (If the tidal propagation is $= R(x)\exp(i(wt-kx))$ then, there should be a linear trend.

The stress parameter is plotted in Figure 35a for a complete tidal cycle. In Figures 35b and c the maximum and minimum stress parameter is plotted for spring and neap tides. The graphs for spring and neap tides do not offer 'obvious' verification of a constant stress parameter, but they are suggestive of it.

3.5.3 Results

Bar charts comparing the observed and predicted velocity and stress are shown in Figures 36 and 37. Very close agreement is found between observed and predicted values both in magnitude and phase. The only errors occur at flow reversal where for the upstream observations (H9 and H6) the model is slightly out of phase predicting flows in the wrong direction. This probably results from the linear interpolation of the tidal curves upstream; it is possible that the distortion of the tidal curves is not linear. Nevertheless, in general the agreement is excellent.

The maximum stress parameter against downstream distance for increasing river flow is shown in Figure 38. This graph is highly suggestive that the maximum stress parameter remains constant along the

river length, and that increasing river flow has only marginal influence upon the downstream maximum stresses, these are tidally dominated). This graph, in the light of the good agreement between the model's predictions and observed data, justifies the proposition that the maximum stress parameter is constant along the estuary length. There is an exception to this generality at $\approx 28\text{km}$, where the maximum stress exceeds the constant value.

The Nene shows the same bifurcation when considering the dependence of the maximum stress parameter upon river flow for increasing tidal strength (Fig 39). As before, when the river flow has reached a sufficiently high value, the maximum stress at the head of the estuary exceeds that observed along its length. However, the specific nature of the bifurcation is somewhat different, whereas before the gradient of the curve increased with increasing tidal scale, here the opposite is found.

3.6 Discussion of the case studies

The case studies were chosen to form a representative sample of the estuaries within the UK. The Thames and the Nene are of different length scales, but have tidal ranges which are of the same order as the water depths. The Parrett is an 'energetic' estuary, where the tidal range greatly exceeds the low water depth (resulting from resonance in the Severn). The Conwy is an estuary dominated by geological and engineering restrictions, which greatly influence the estuary's shape and hydrodynamics.

It is observed that the simple integration of the continuity equation produces accurate results for the Thames and Nene, but is prone to error with the

Parrett and Conwy. The Nene and Thames evolve regularly downstream and have fairly regular tidal curves. Thus the degree of accuracy required for the modelling data is not as high as for the other two case studies. The Parrett, with an irregular tidal cycle and the Conwy with a highly irregular evolution of cross section along the estuary, require more detail in setting up a model.

Before the question of which of these case studies could be described as 'in regime' may be answered, a number of notions need to be introduced. First of all, the description 'in regime'; this may be taken to imply a dynamic morphological equilibrium over a timescale which averages out the fluctuations of the tidal conditions. The idea is that the net sediment movement at all locations over the averaging timescale is zero and so the estuary maintains its longitudinal and transverse profiles. The time period needs to include not only the tidal period, but also the timescale of spring/neap fluctuations as well as any seasonal and 'freak' events. It is somewhat doubtful whether any particular estuary ever fully attains this equilibrium, but rather it approaches equilibrium in an asymptotic sense. Also, coupled with the idea of the approach to equilibrium is the notion of morphological timescale. This is the time period over which significant adjustments to the river profile occur. It is immensely difficult to even estimate the order of magnitude of this timescale, but possibly it is of the order of 50 years.

Considering then which of the studied estuaries is 'in regime'; the Conwy is influenced by the construction of the road and rail bridges and the causeway, which leads to a deep channel underneath them. Here there is armouring at the channel bed and so it seems

unlikely that a dynamic equilibrium exists. Also since it is possible that these obstructions were built within the morphological timescale, adjustment is still occurring. The other case studies do show some indication of sustaining an equilibrium, especially as they seem to evolve in a regular manner. For example, there appears to be an exponential dependence of the channel width with the downstream distance and this concurs with what is accepted as an 'ideal' estuary (Ref 9, p114). Hence we may tentatively say that these estuaries are 'in regime'.

The dynamic equilibrium governing the estuaries is

$$\frac{u}{g} \frac{\partial u}{\partial t} + \frac{u}{g} \frac{\partial u}{\partial x} = - \frac{\partial H}{\partial x} - \frac{u|u|}{c^2 R}$$

using the Chezy frictional term and neglecting the longitudinal variation of density and the Coriolis term. We may then assess the magnitude of each term during a tidal cycle (Figures 40 and 41 follow Fig 28 of Ref 9). The conclusions from Reference 9 are borne out in the case studies considered here. It was found that the term involving the fluctuation of the free surface elevation dominates, while the other terms are of similar orders of magnitude, possibly excepting the non-linear convective acceleration which is at times smaller than the others. Hence it is not possible to describe the hydrodynamics by simply balancing two physical processes. Instead all the processes contribute to the dynamics, thus it is difficult to classify estuaries by dominant physical processes, although linearisation is feasible at times, easing the solution of modelling equations. Furthermore, it is necessary to consider the rate of dissipation of energy when considering axial dynamics, while density

gradients (resulting from freshwater flow) may determine the dynamical behaviour through the stream depth. Finally it should be noted that for any particular estuary, the relative magnitude of the terms is not fixed along the estuary length.

4. LONG TERM EVOLUTION OF ESTUARIES

4.1 Analytical models

Many authors have sought to find analytical solutions to the momentum and continuity equations for shallow water flow. These are solved within a simple prescribed topograph, such as exponentially increasing width with constant depth or linearly increasing width and depth. Furthermore various authors have been able to impose appropriate upstream boundary conditions to model the effects of imposing tidal limits. These analytical solutions are useful in that they give insight into the behaviour of the tidal disturbance as it propagates upstream.

However, the problem they solve is somewhat different in emphasis from the problem under study here. These analytical solutions start with a prescribed topographic boundary and boundary conditions for the tidal disturbance and then solve the velocity and tidal elevation fields. The problem we would like to solve is that given a river of prescribed behaviour, interacting with a tide of a prescribed behaviour, what is the equilibrium (or stability) profile of the estuary so formed. Hence the value of the analytic solutions is that they highlight the appropriate approximations to be made and present appropriate techniques.

Hunt (1964) (Ref 27) considers tidal oscillations in estuaries with friction. He uses the linearised equations with a linearised friction co-efficient, which is valid provided that the non-periodic river flow is negligible compared to the periodic flow.

For the Thames, this is true up to London Bridge, at least. Modelling the Thames as an exponentially diverging channel of constant depth Hunt was able to match the predicted and observed velocity fields. The conclusion of his analytical modelling is that

- (i) The principal effect of the friction factor is to introduce a phase change of high water along the estuary length, while the phase difference between peak elevation and peak current remains fixed.
- (ii) The propagation of the tidal disturbance can not be regarded as a progressive wave of speed $(gH)^{\frac{1}{2}}$ in an estuary of any cross section other than one of constant cross section.

With the Thames, it turns out that the speed of propagation of the high water is numerically virtually equal to $(gH)^{\frac{1}{2}}$. Hunt interprets this as fortuitous and misleading as the origin of this velocity is quite different. Instead, he regards the disturbance as a standing wave of variable phase. Hunt does note, however, that this linearised theory is not applicable in the shallow regions upstream of London Bridge.

4.2 Modelling approach

While it is possible to develop numerical modelling schemes which fully account for all the interacting physical processes, as well as allowing prescribed bathymetry and fluctuations of natural conditions (eg. tides and freshwater flow) these models are exceptionally intensive on computational resources and even then run at speeds of the order of one sixth real time. Thus it is not feasible to use these models to

make predictions over time periods of the order of decades (also these schemes may be subject to instability/chaos over this period). Hence an approach is required which predicts possible profiles corresponding to an estuary 'in regime', although it may not be possible to indicate the timescale with which this profile is attained (morphological timescale).

In the first instance any modelling attempt is to be in essence one dimensional. This reduces the problem to the study of one dimensional hydrodynamics, but reduces the predictive scope of the model. Only the influence of certain types of engineering work can be considered. These include changing the tidal limit, by means of a weir etc, but not the effect of a jetty (for example). The jetty (or other similar) induces a two dimensional effect on the flow, which has an influence in the short term, best predicted by a complex numerical model and which also has a long term influence on the 'equilibrium profile'. This however falls outside the scope of this modelling approach.

The object of this modelling approach, therefore, is to develop and test various criteria which may be used to govern the evolution of the estuary's shape. Ideally the modelling technique should be able to address the question of what is the equilibrium profile of the estuary resulting from the intersection of a river with prescribed conditions with a prescribed tidal range at the river's junction with the sea. The model should be able to account for the distortion of the tidal disturbance along the estuary's length, although this increases the complexity of the problem.

The Thames has been studied and modelled in many studies. In some ways this estuary is an easy case

to study, not only due to the availability and multitude of the data sources, but also because it appears to evolve regularly. Furthermore, the observations of the case study suggest that its tidal disturbance maintains its sinusoidal time dependence. Thus the tidal disturbance may be specified as

$$\eta(x,t) = R(x) e^{i(\omega t - \phi(x))}$$

where $\phi(x)$ is the phase difference and $R(x)$ is the tidal range. Thus in the first instance the modelling approach is to be tested with the Thames estuary.

4.3 Attempted modelling procedure

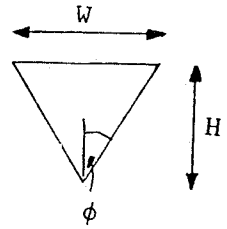
The Thames estuary was modelled to predict its profile given only data about its tidal elevations and characteristics at its tidal limit. The Thames was chosen to be modelled in preference to the other estuaries studied in Chapter 3, since it shows more regular behaviour, its tidal range is much smaller than the mean tide depth; its width evolves exponentially downstream; and the tidal disturbance remains sinusoidal in time along the estuary length (it is not distorted). Thus it forms what is potentially the simplest case to model as its behaviour is simple to predict.

The models proceeded along steps of increasing complexity and lack of initial data. In the first instance, the tidal behaviour and cross section was prescribed along the estuary length and the model was just to predict the low water depths. The criteria used for this prediction was the constancy of the stress parameter along the estuary. The cross section

used was of a triangular generic type with the bottom angle prescribed (see Section 2.5).

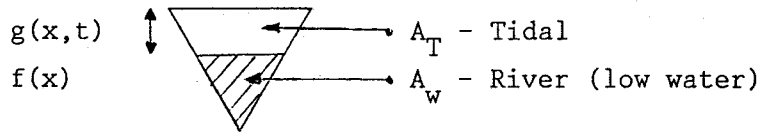
$$\tan\phi = \frac{w}{2H}$$

and $\phi = \phi(x)$



where x is the downstream distance

Details of calculation



$$\text{Area} = A_T + A_{LW}$$

$$A_{LW} = f^2 \tan\phi \quad A = (f+g)^2 \tan\phi$$

$$\text{So, } A_T = (g^2 + 2fg) \tan\phi$$

$$\frac{\partial A}{\partial t} = \frac{\partial A_T}{\partial t} = 2 \frac{\partial g}{\partial t} (f+g) \tan\phi$$

$$\text{Continuity equation: } \frac{\partial Q}{\partial x} + \frac{\partial A}{\partial t} = 0$$

$$\text{So } \bar{A}u = - \int_0^x \frac{\partial A_T}{\partial t} dx + Q_{\text{river}}$$

$$\Rightarrow u(x,t) = \frac{(- \int_0^x \frac{\partial A_T}{\partial t} dx + Q_{\text{river}})}{(f+g)^2 \tan\phi}$$

so stress parameter is given ;

$$S = \frac{\bar{u}}{d^{1.486}} = \frac{(- \int_0^x 2 \frac{\partial g}{\partial t} (f+g) \tan\phi dx + Q_{\text{river}})}{(f+g)^{1.972} \tan\phi}$$

Hence in this first stage with

$\phi(x)$, $g(x,t)$ and Q_{river} specified, use the criteria

$$0 \leq S_{\text{max}} \leq S(x,t) = S_{\text{critical}} \text{ (constant)}$$

This then specifies the low water depth $f(x)$

The results are shown on a graph of Thames longitudinal profile (Fig 42). It is clear that very good agreement is produced between the actual and calculated depths. This is not a startling result in any sense as it follows directly from the observation that the stress parameter is constant along the estuary length. The computational procedure has just performed the calculations 'in reverse', demonstrating that the constancy of stress parameter is an appropriate criteria for determining the estuary profile.

The second stage of the modelling procedure is to avoid having to specify the cross section type along the estuary length. This indicates the need, as suggested earlier, to develop another criterion perhaps related to stream power, stream energy or width evolution. The only method which yielded reasonable results was to propose an exponentially increasing width downstream, with prescribed exponential parameters.

$$w = w_0 \exp(\alpha x)$$

$$\text{and } \tan \theta = w/2H, \quad \theta(x) = \tan^{-1}(w_0 \exp(\alpha x)/2H(x))$$

The agreement between the actual and predicted is still reasonable, although at locations where the width deviates from the exponential, the predicted

depth also shows some deviation. Nevertheless the predicted form generally follows that of the observed (see Fig 43). As to be expected the predicted width closely follows that of the observed, this simply follows from the observed exponential fit.

As a final stage it was wished to remove the necessity to specify the tidal behaviour at all points along the estuary and for all times through a tidal cycle. Instead the tide behaviour is specified at the estuary mouth. For the Thames this is considerably simplified since the tidal curves are virtually sinusoidal and remain so along the estuary length. For other estuaries it is possible, at least in principle, to calculate the tidal disturbance at upstream positions along the estuary. Furthermore with the Thames, neglecting the first few upstream locations near the tidal limit, it is true to a first level of approximation that the tidal range is constant along the estuary length. This somewhat simplifies the modelling approach. Finally with the Thames, the tidal disturbance behaves as if it were a progressive wave travelling upstream in deep, frictionless water. According to Hunt (Ref 27), this is fortuitous and misleading for he claims the disturbance is best modelled as a standing wave, within a constant depth channel of exponentially increasing width. However, it would seem to arise naturally from the analysis.

Consider, then, modelling the Thames with the following linearised equations following Hunt, (Ref:27):

Depth	$h = h_0$
Width	$b = b_0 \exp(2ax)$
Continuity	$\frac{\partial \eta}{\partial t} = -\frac{1}{b} \frac{\partial}{\partial x} (hbu)$
Momentum	$\frac{\partial u}{\partial t} = -g \frac{\partial \eta}{\partial x} - fu$

where

η = free surface elevation

u = flow velocity

f = friction coefficient (linearised)

x = distance upstream

These equations lead to the following pairs of solutions:

$$\eta = A \exp(a+\alpha)x \cos(\beta x - \sigma t)$$

$$u_1 = A\sigma \frac{\cos\phi}{h\beta} \exp(-(a+\alpha)x) \cos(\beta x - \sigma t - \phi)$$

and $\eta_2 = B \exp(-(a-\alpha)x) \cos(\beta x + \sigma t)$

$$u_2 = \frac{B\sigma \cos\Psi}{h\beta} \exp(-(a-\alpha)x) \cos(\beta x + \sigma t + \Psi)$$

where

$$\alpha^2 - \beta^2 + \frac{\sigma^2}{gh} = a^2$$

$$2\alpha\beta - \sigma f/gh = 0$$

$$\beta \tan\theta = \alpha - a, \quad \beta \tan\Psi = \alpha + a$$

Solving for β :

$$\frac{\sigma^2 f^2}{4\beta^2} - \beta^2 + \left(\frac{\sigma^2}{gh} - a^2\right) = 0$$

$$\beta^4 - \left(\frac{\sigma^2}{gh} - a^2\right)\beta^2 - \sigma^2 f^2/4 = 0$$

$$\text{So } \beta^2 = \frac{\left(\frac{\sigma^2}{gh} - a^2\right) \pm \left(\left(\frac{\sigma^2}{gh} - a^2\right)^2 + \sigma^2 f\right)^{1/2}}{2}$$

It transpires for the Thames that $\beta \sim \frac{\sigma}{(gh)^{1/2}}$

This follows from the observation that the tidal range is virtually constant along the estuary. Hence write:

$$\alpha = a + \epsilon \quad \text{where } \left| \frac{\epsilon}{a} \right| \ll 1$$

$$\text{ie } \eta = \beta \exp(\epsilon x) \cos(\beta x + \sigma t)$$

$$\text{Then } (\alpha + \epsilon)^2 - \beta^2 + \frac{\sigma^2}{gh} = a^2$$

$$2\epsilon a + \epsilon^2 - \beta^2 + \frac{\sigma^2}{gh} = 0$$

$$\text{So to zeroth order, } \beta^2 = \frac{\sigma^2}{gh}$$

$$\text{ie } \beta = \frac{\sigma}{(gh)^{1/2}}$$

So the observation that the tidal disturbance can be modelled as a progressive wave travelling upstream on deep, frictionless water, arises from the constancy of the tidal range. This link is not stated by Hunt.

Hence, for modelling the Thames, the tidal disturbance is treated as a progressive wave with speed $(gh)^{1/2}$.

Two results are shown, one with a constant range along the estuary, the other with a diminished range at the upstream end. With both, the agreement between the observed and the calculated is reasonable, suggesting there is some merit in the approximations made. From an initial study of where the 'tidal range diminishes', it would seem to coincide with those reaches where the kinetic energy of the river flow is of the same order of magnitude as the tidal flows.

These two quantities were studied by considering $\frac{Q^2_{\text{river}}}{A_{\text{LW}}}$ and $\frac{Q^2_{\text{tidal}}}{A_{\text{T}}}$. For most of the Thames estuary

the tidal volume flux far exceeds the river flux and so likewise with the kinetic energies. In these upstream reaches, however, the two are comparable and it is plausible at least that this should cause a decrease of the tidal range.

5. CONCLUSIONS AND RECOMMENDATIONS FOR FURTHER WORK

This study has sought to investigate and simulate the behaviour of estuaries using a simple numerical procedure, with the aim of finding physical parameters which seem to govern the long term evolution of the estuary and hence determine its regime profile.

At its fundamental level, an estuary is a region where there is an interaction between freshwater flow and the tidal rise and fall of a body of saline water. Its extent is from a landward tidal limit, where the free surface oscillations do not affect the water flow, to a seaward boundary beyond which the effect of tidal flow and sediment movement on the estuary are negligible. McDowell and O'Connor (Ref 9) argue that the study of an estuary must include the whole system and the full range of dynamical influences.

Ideally one would like to be able to develop a morphological model which could predict the regime profile assumed by the estuary in an equilibrium state. The secondary problem of considering the influence of major engineering works would then also fall under the bounds of this model, but it would predict over morphological timescales (which are presumably of the order of decades).

5.1 Conclusions

- (i) This study has demonstrated that there is some merit in the postulate that the maximum stress parameter is constant along an estuary's length, although this is best demonstrated for

the Thames, which is in some senses an 'ideal' estuary.

- (ii) The mean tidal width tends to increase exponentially with downstream distance.
- (iii) Increased river flow tends only to influence the upstream dynamics.
- (iv) The three criteria above have been used in reverse to predict the estuary's profile and this was successfully accomplished for the Thames which exhibits a number of simplifying features.
- (v) The study has demonstrated that the continuity equation can be integrated in a simple way to generate the velocity field.
- (vi) The way forward is to proceed via a morphological model, the development of which requires a thorough study of estuary morphology to investigate the evolution of parameters governing the development of the equilibrium profile.

5.2 Recommendations for further work

There are a number of issues raised in the case studies which have not yet been fully explored.

- (i) The balance of kinetic energy of the river flow with that due to the tidal. Do the relative sizes of these energies relate directly to the upstream propagation of the tidal disturbance? Is the kinetic energy of an estuary 'in regime' minimised or correlated to any particular variable?

- (ii) The principle of minimum dissipation (or minimum stream power). Does this have any role in the long term evolution of an estuary?

- (iii) The location and definition of the tidal limit, for an unrestrained estuary. Is the tidal limit defined as where there is no flow reversal, or no free surface oscillation on the timescale of a tidal cycle? Is the location of this tidal limit determined by the slope of the estuary, or an energy balance of some sort?

- (iv) Classification of estuaries; given that the terms of the dynamic equation, governing estuary velocity fields are of a similar order of magnitude, it suggests that none may be neglected. However, at the same time, it appears that some estuaries are dominated by river flow. What then is the role of classification?

- (v) Sediment type; the studies have pointed to a shear velocity parameter which appears to be constant along estuaries and even to some degree between different estuaries. Correlation between sediment type and the shear velocity parameter needs to be investigated.

- (vi) There is a need to develop another parameter for governing the evolution of the estuary's morphology.

6. ACKNOWLEDGEMENTS

The authors acknowledge the help of Mr John Dennis from the Department of Civil Engineering, Building and Cartography, Oxford Polytechnic, for many useful discussions and comments throughout the course of this study.

7. REFERENCES

1. Dennis J M. Estuary regime and associated processes, HR Wallingford, Wallingford, England. Report No IT 323, October 1988.
2. Dennis J M. Estuary regime: A collocation of mathematical models, HR Wallingford, Wallingford, England. Report No IT 326, January 1990.
3. Dyer K R. Coastal and estuarine sediment dynamics, John Wiley and Sons, 1988, 342pp.
4. Hansen D V, and Rattray M. New dimensions in estuary classification, *Limnology and Oceanography*, Volume 9 No 3 July 1966, pp319-326.
5. Hansen D V, and Rattray M. Gravitational circulation in straits and estuaries, *Journal of Marine Research*, Volume 23, No 2, 1965, pp104-122.
6. Prandle D. On salinity regimes and the vertical structure of residual flows in narrow tidal estuaries, *Estuarine, Coastal and Shelf Science*, Volume 20, No 5, May 1985, pp615-635.
7. Aubrey D G. Hydrodynamic controls on sediment transport in well mixed bays and estuaries, In Kreeke V Van de (Ed), *Physics of shallow estuaries and bays*, Volume 16, Section 6, pp245-258.

8. Rodger J G and Odd N V M. A mathematical model of mud transport in deep partially-mixed canalised estuaries, HR Wallingford, Wallingford, England, Report No SR 37, March 1985.
9. McDowel D M, and O'Connor B A. Hydraulic behaviour of estuaries, The Macmillan Press Ltd, 1977, 292pp.
10. Henderson F M. Open channel flow. Macmillian Publishing Co, 1966, 522pp.
11. Amein M and Chu H L. Implicit Numerical Modelling of unsteady flow. Journal of the Hydraulic Division, Volume 101, No 6, pp717, 1975.
12. French R H. Open Channel Hydraulics. McGraw Mill Book Company, 1985, 706pp.
13. HR Wallingford, Thames flood protection investigation, field survey data, Wallingford, England, Report No's EX 543-555, February 1971.
14. Inglis, Sir C C, and Allen F H. Regimen of the Thames estuary: currents, salinities and river flow, Proc. Inst. Civil Eng., Volume 7, pp827-878, 1957.
15. HR Wallingford. A5 Trunk road improvement, Wallingford England, Report No EX 561, May 1974.
16. HR Wallingford. Estuarine transmission of heavy metals, Wallingford, England, Report No SR 15, January 1985.
17. HR Wallingford. Conwy estuary crossing, Wallingford, England, Report No EX 1251, May 1985.

18. HR Wallingford. A55 North Wales coast road, Wallingford, England, Report No EX 2219, October 1990.
19. HR Wallingford. A55 North Wales coast road, Wallingford, England, Report No EX 869, April 1979.
20. Ordnance Survey. Maps SH77/87, SH66/76, Crown copyright, Southampton, England, 1977 and 1980.
21. HR Wallingford. River Parrett tidal barrier - summary of hydraulic investigations, Wallingford, England, Report No xx, May 1979. ✓
22. HR Wallingford. River Parrett dredging study, Wallingford, England, Report No EX1428, April 1986. ✓
23. HR Wallingford. River Parrett basin improvement study - spring and neap tide survey, Wallingford, England, Report No xx, 19yy.
24. HR Wallingford. River Parrett tidal barrage, Wallingford, England, Report NO zz, October 1977. ✓
25. HR Wallingford. The effects of proposed extraction of water on siltation in the Nene estuary, Wallingford, England, Report No EX 307, Volumes 1 and 2, February 1966.
26. HR Wallingford. River Nene improvement scheme - initial appraisal of the effects of moving the tidal limit, Wallingford, England, Report No EX 1387, December 1985.
27. Hunt J N. Hydraulic behaviour of estuaries, Geophys. Jnl. Astron. Society, May 1964.

TABLES.

TABLE 1 : Data specifying the Conwy profile

Section	Upstream Distance (km)	Depth of LW Channel (m)	LW Width (m)	Ratio Factor	Gradient	Average Range (m)	Springs Range (m)
Tan-lan	19.75	4.00	50.00	0.50	0.0000	0.00	0.00
Dolgarrog Bridge	14.75	4.80	75.00	0.46	0.9600	2.40	2.83
Tal-y-cafn-Bridge	9.25	2.40	75.00	0.40	0.1800	4.70	5.55
Cymryd	4.13	2.00	225.00	0.31	0.0154	5.00	5.90
Benearth Point	3.03	2.86	150.00	0.28	0.0044	5.14	6.07
Mussel Satation	2.05	8.57	212.50	0.24	0.0085	5.43	6.43
Conwy Quay	1.73	6.68	125.00	0.29	0.0101	5.32	6.29
Deganwy Pier	0.83	2.42	275.00	0.99	0.0112	5.58	6.62
Deganwy Narrows	0.00	8.00	137.50	0.25	0.0686	6.00	7.08

Used to produce the following data

Section	Downstream Distance (km)	LW Width (m)	Bottom Width (m)	Gradient	Depth of LW Channel (m)	LW Depth (m)
Tan-lan	0.00	50.00	25.00	0.0000	4.00	4.00
Dolgarrog Bridge	5.00	75.00	34.36	0.9600	4.80	4.37
Tal-y-cafn Bridge	10.50	75.00	29.87	0.1880	2.40	1.55
Cymryd	15.63	225.00	70.32	0.0154	2.00	1.10
Benearth Point	16.73	150.00	42.72	0.0044	2.86	1.93
Mussel Satation	17.70	212.50	50.00	0.0085	8.57	7.57
Conwy Quay	18.03	125.00	36.79	0.0101	6.68	5.71
Deganwy Pier	18.93	275.00	271.25	0.0112	2.42	1.38
Deganwy Narrow	19.75	137.50	33.75	0.0686	8.00	6.92

TABLE 2

Section	D/S Distance (km)	HW Width (m)	LW Width (m)	Gradient Neaps		Springs	
				LW (m)	HW (m)	LW (m)	HW (m)
Tidal Limits	-2.3	14.14	14.14	5.00			
New Bridge +4 for Atheley/Tone	1.8	14.14	14.14	5.00			
Oath Lock +2.5 for Stathe/Parrett	0	14.14	14.14	5.00	0.7	1.3	0.6
Section D Athelney	2.5	17.68	17.68	5.00	0.6	1.3	0.7
Section C Stathe	7.5	22.98	22.98	5.00	0.9	2.6	1.7
Section A Pipe Bridge	15	40.66	40.66	5.00	1.0	2.0	1.0
Section 1 Bridge	18	70.71	35.36	0.19	0.0	1.9	1.9
Section 2 Pims	22	141.42	44.19	0.10	0.8	3.7	2.9
Section 3 Cottages	24.1	194.45	70.71	0.09	1.7	5.7	4.0
Section 4 Marchant	27.5	247.49	44.19	0.06	1.9	6.3	4.4
Section 5 Barge	31.35	450.78	79.55	0.04	2.5	7.0	4.5
Section 6 Black Rock	33.8	601.04	265.17	0.05	3.0	7.2	4.2
Section 7 Stert					0.0	11.7	11.7

FIGURES.

Maximum stress parameter for various river flows

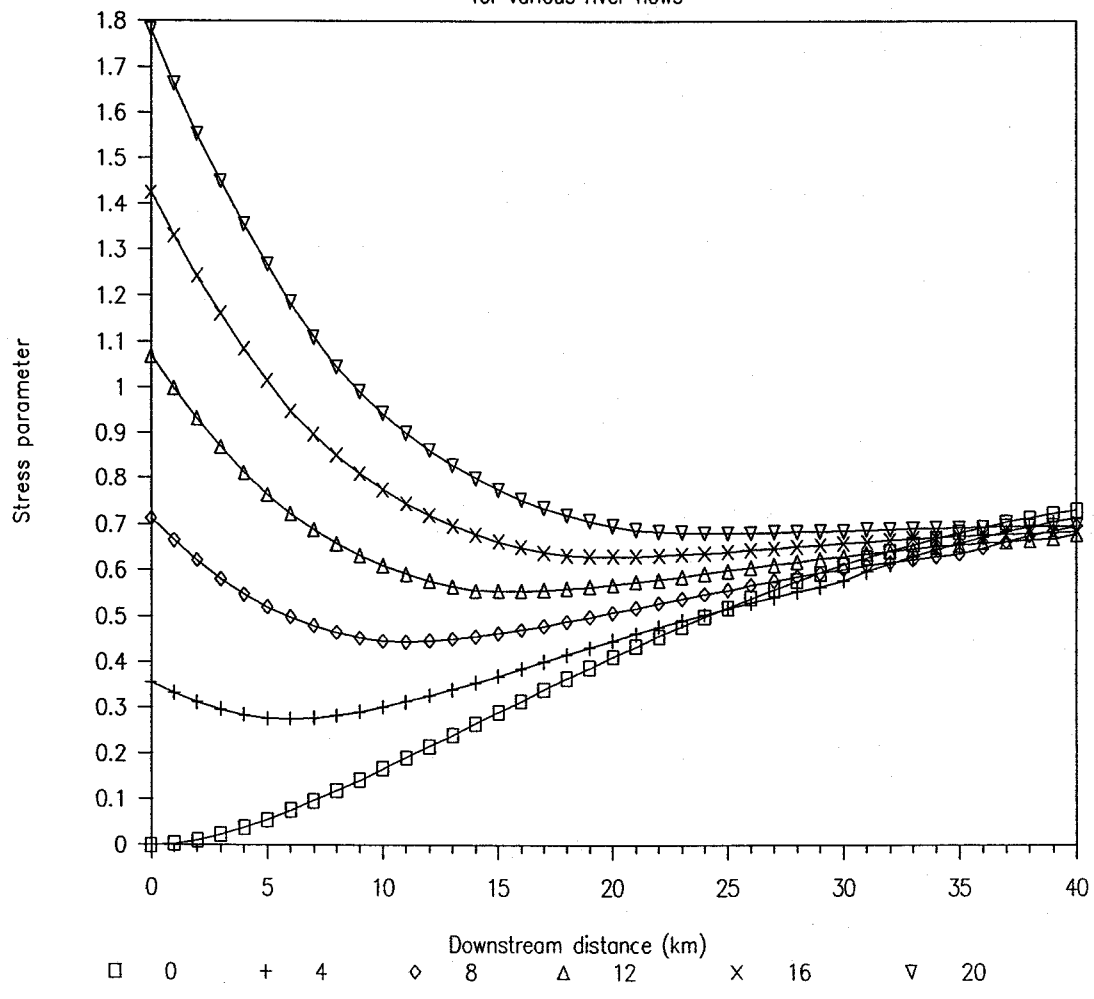


Fig 1 Effect of river flow on maximum stress parameter

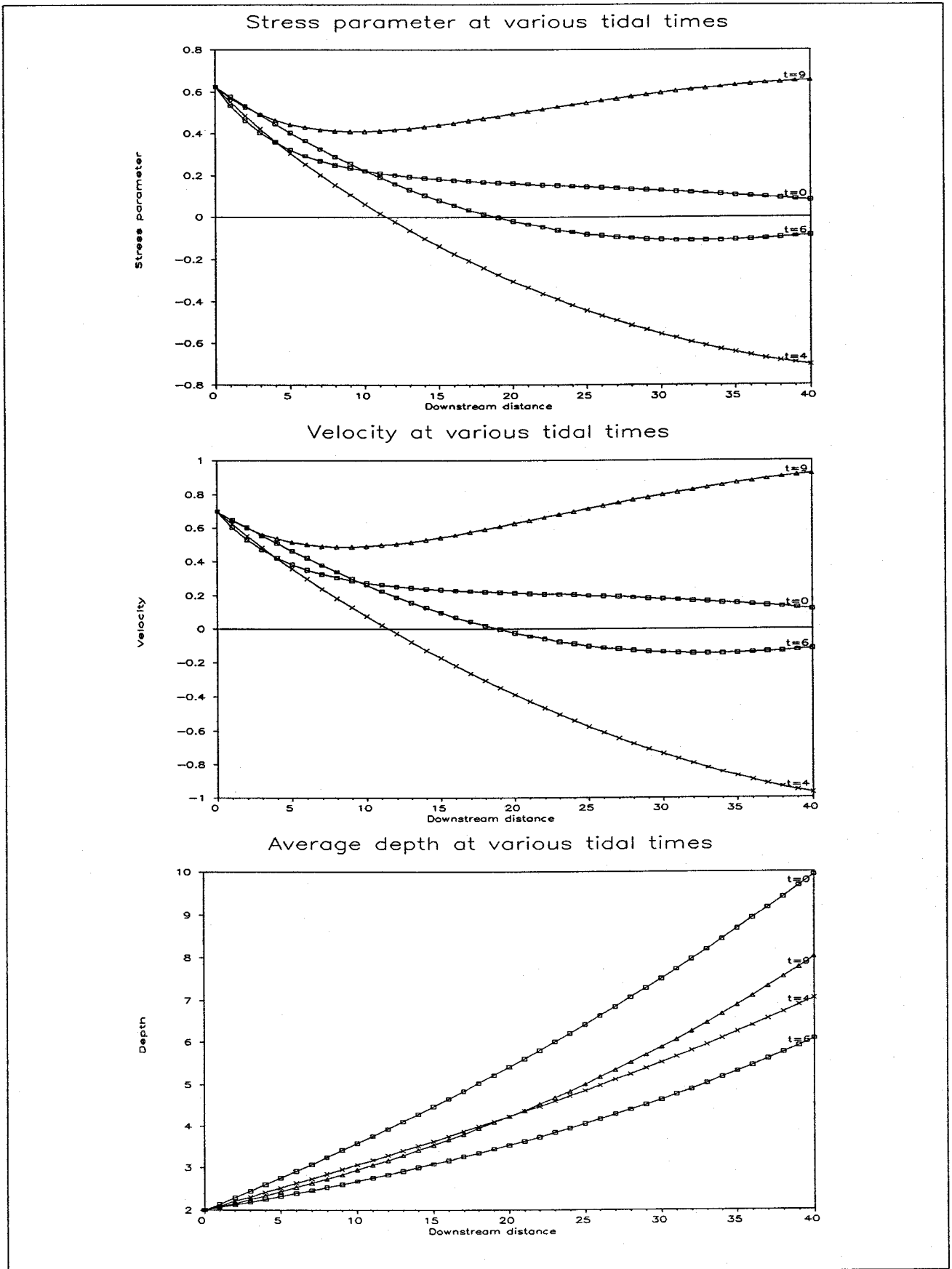
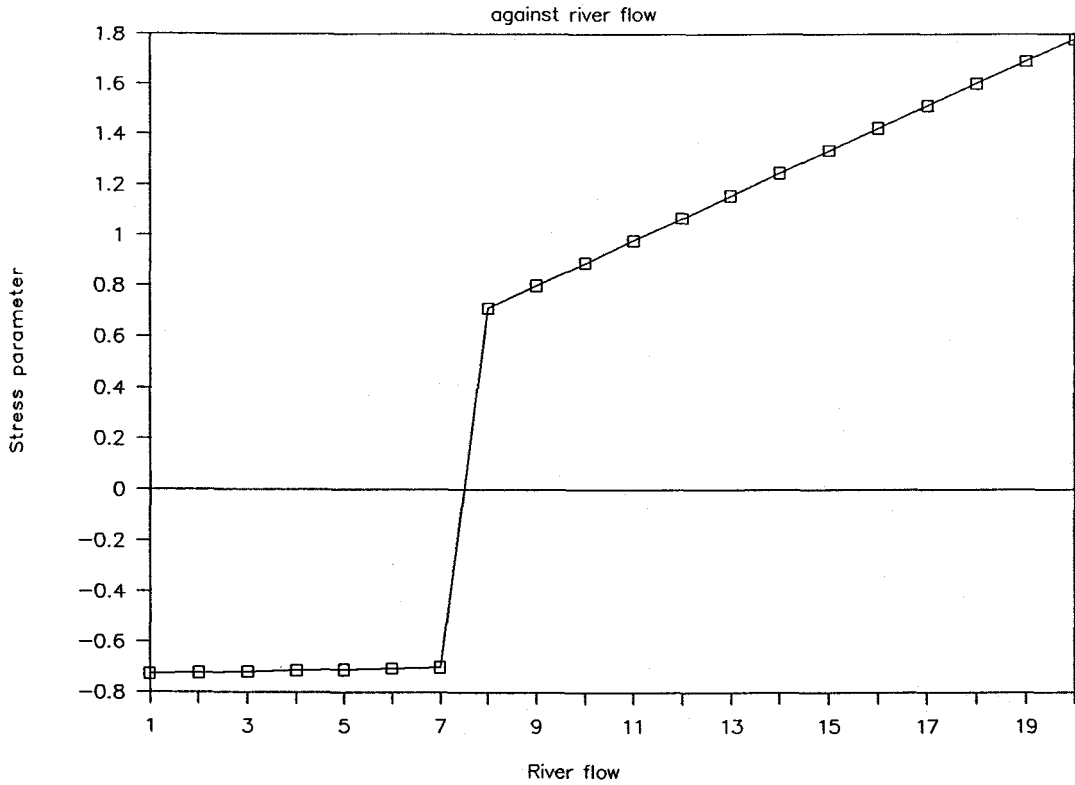


Fig 2 Stress parameter, velocity and depth through tidal cycle

Maximum stress parameter in estuary



Location of maximum stress parameter

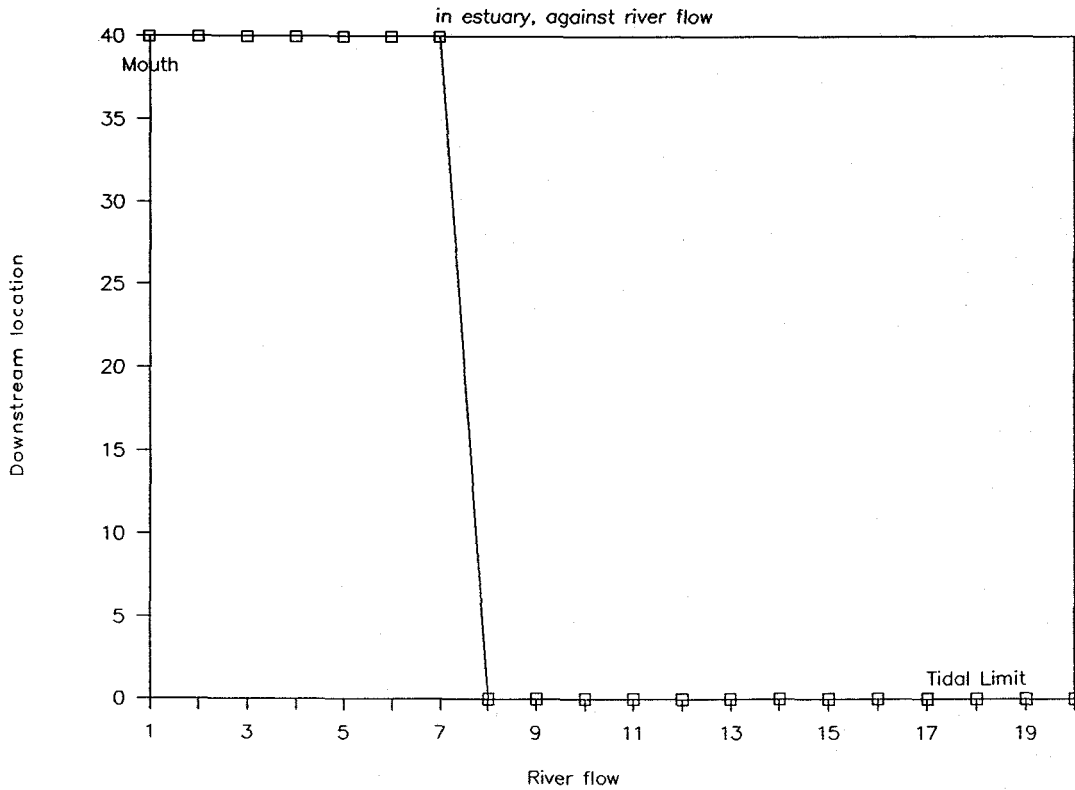


Fig 3 Maximum stress parameter in estuary (magnitude and location)

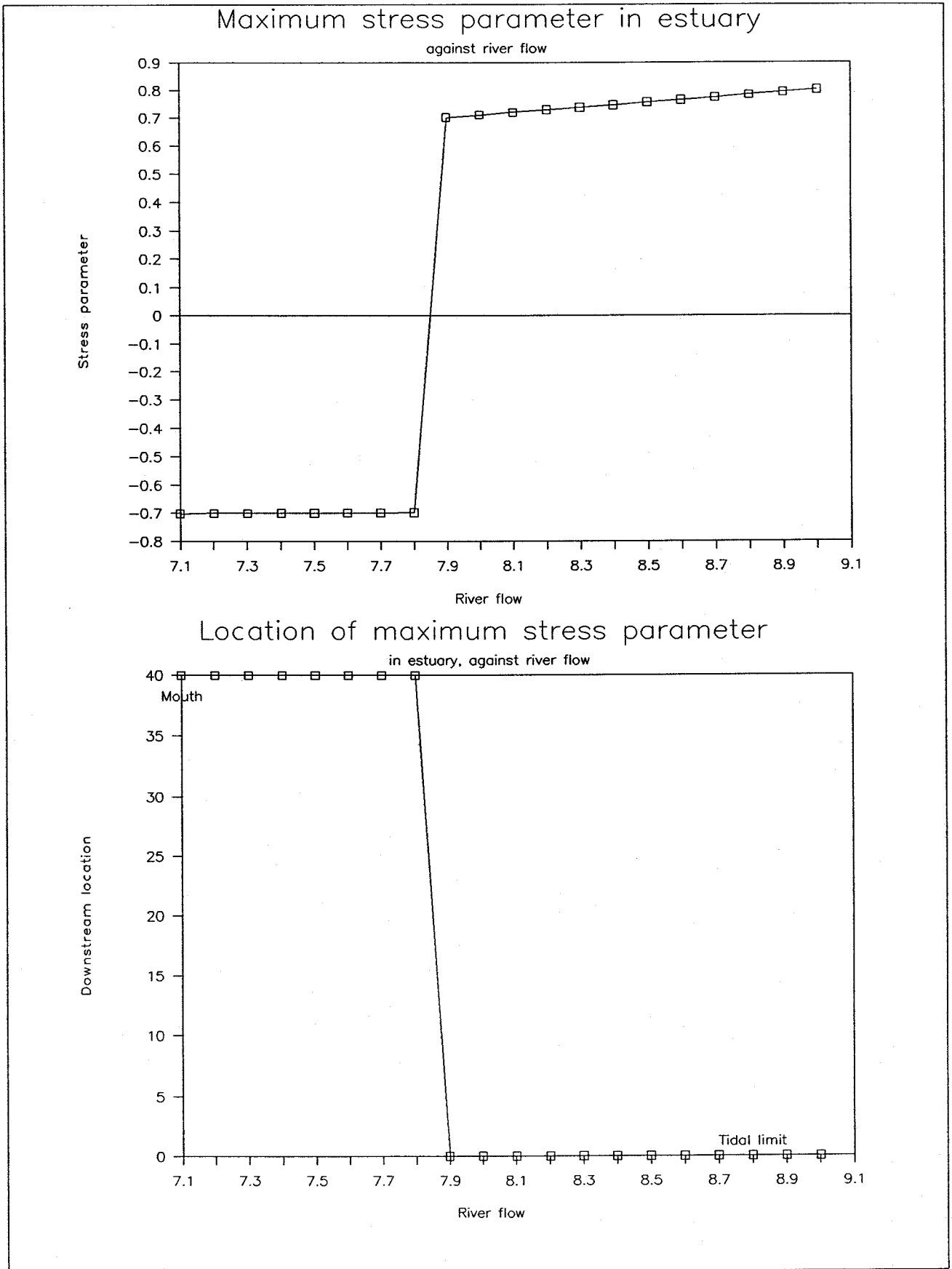


Fig 4 Maximum stress parameter in estuary (magnitude and location)

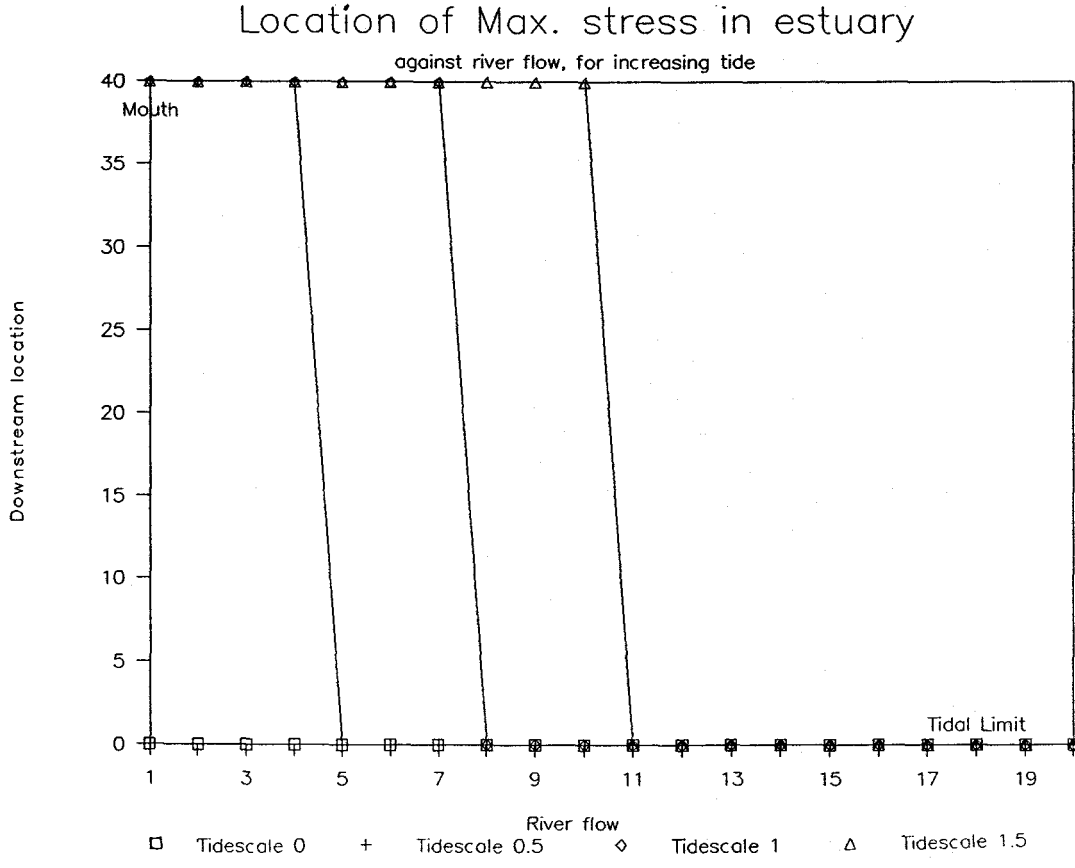
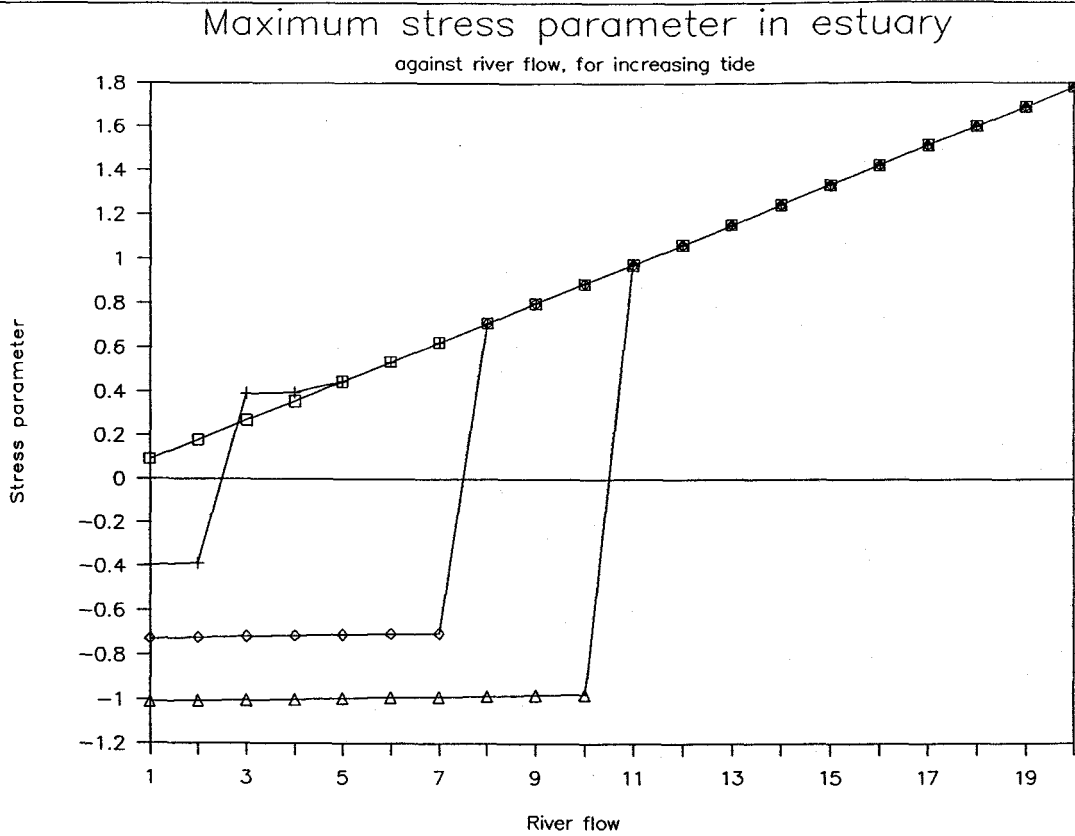


Fig 5 Effect of increasing tidal range on maximum stress parameter in estuary

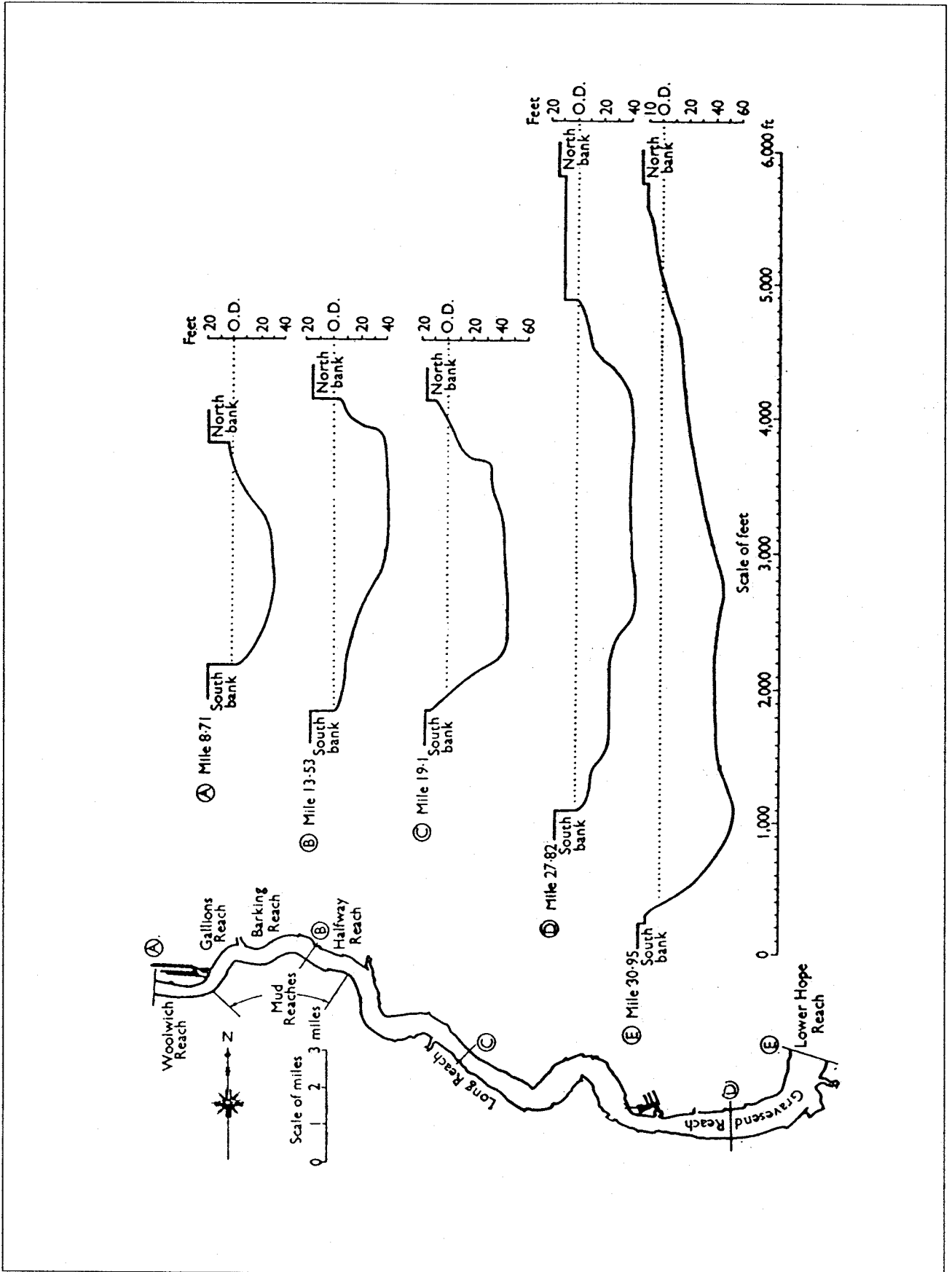
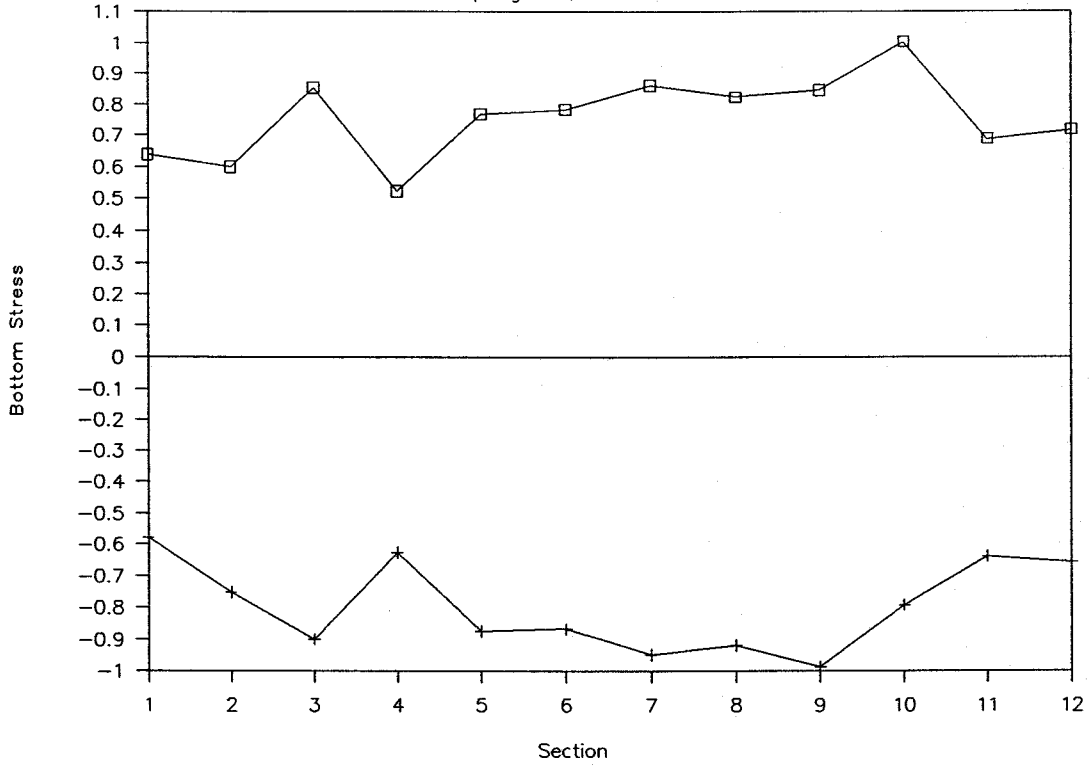


Fig 6 Cross sections through Thames Estuary (from Inglis and Allen, 1957)

Max & min bottom stress parameter

for Spring Tide, with Low Flow



Maximum & Minimum stress parameter for

Spring Tide with High flow

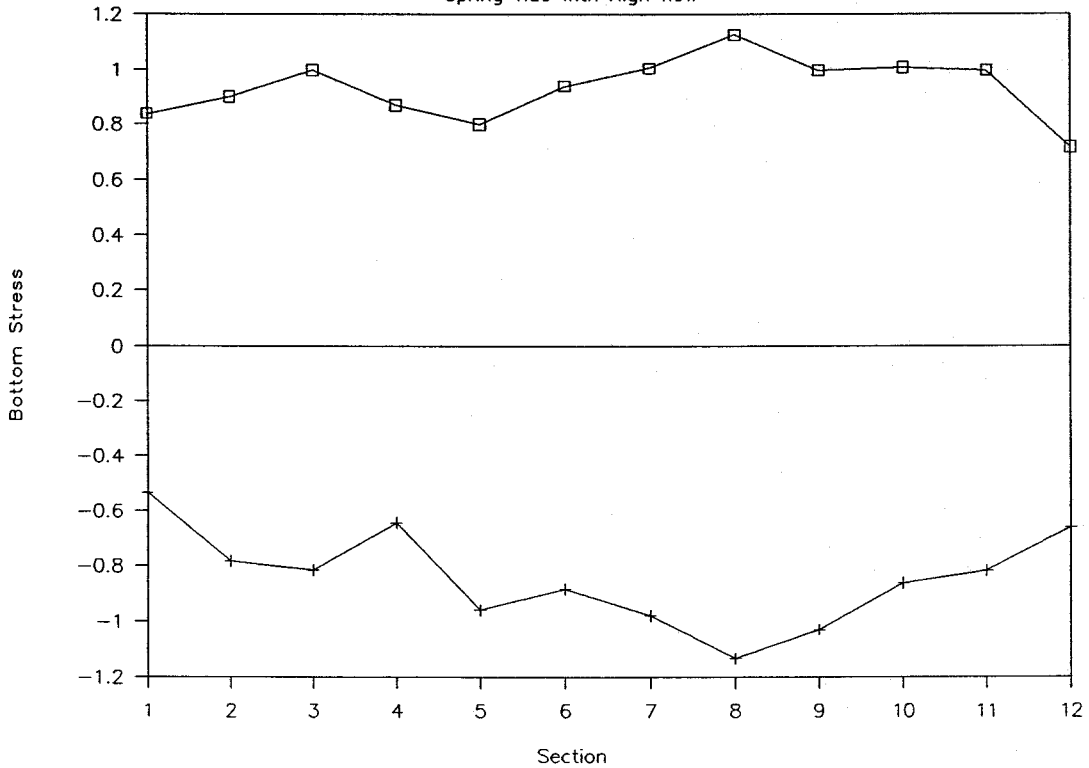


Fig 7 Thames – Maximum observed stress parameter for spring tides

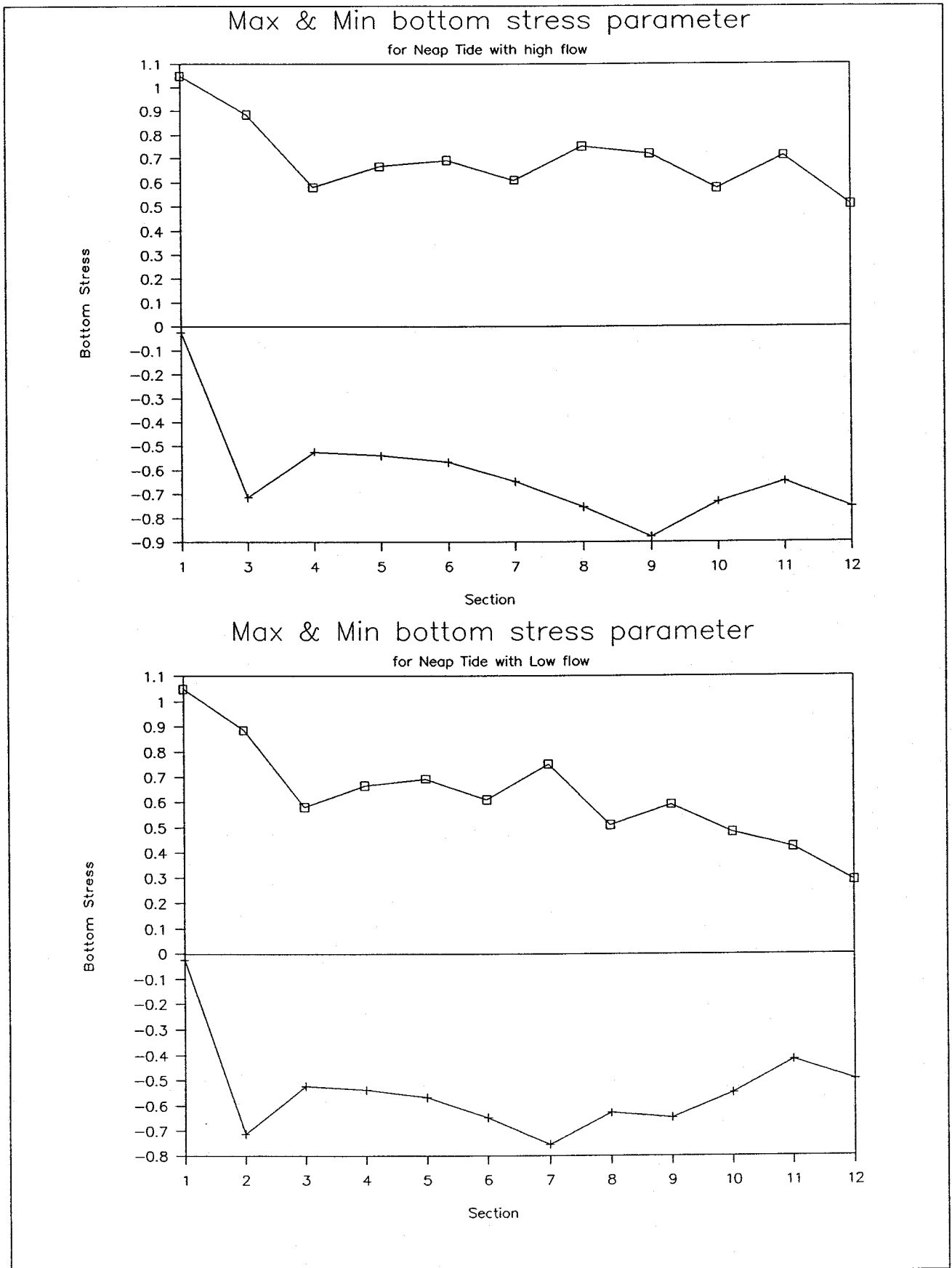


Fig 8 Thames – Maximum observed stress parameter for neap tides

Mean tide level width along the Thames

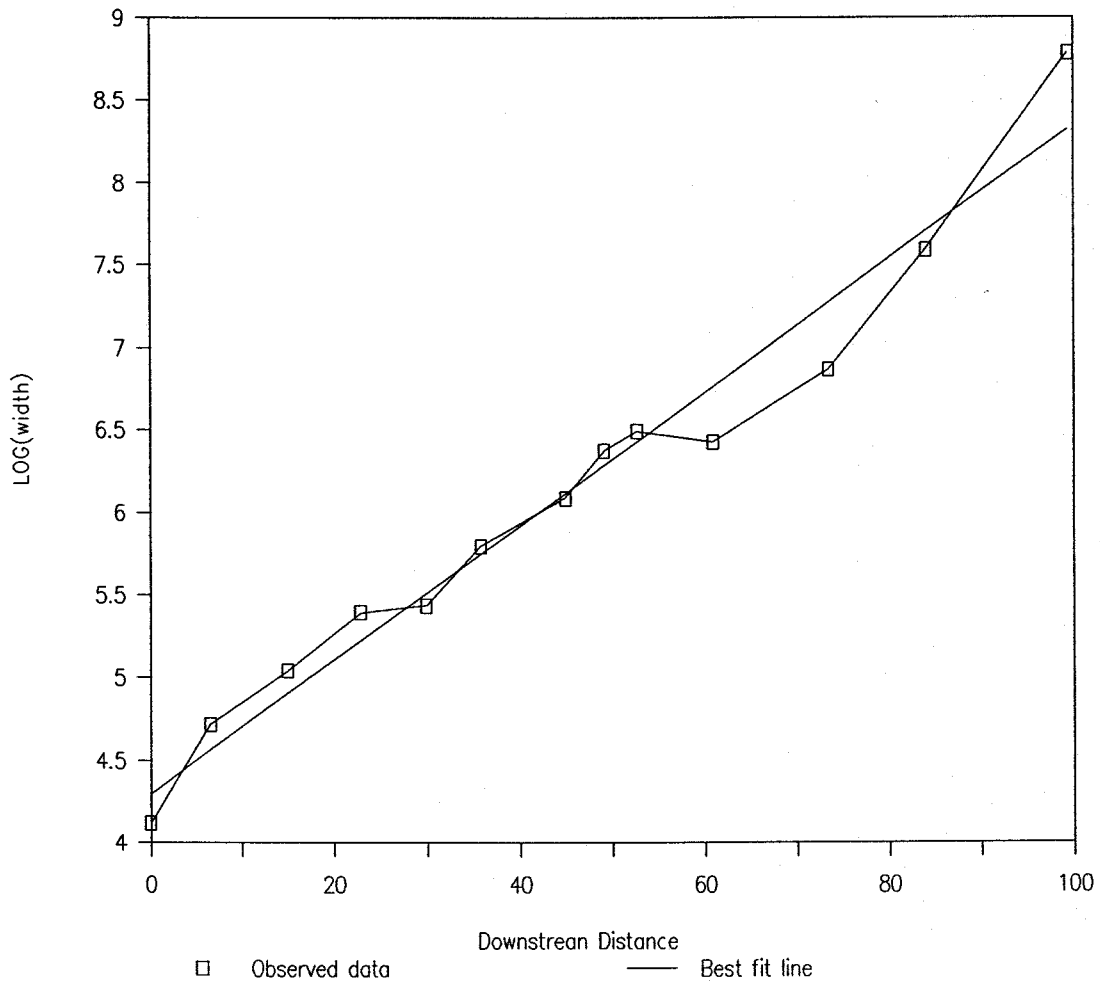


Fig 9 Mean tide level width along Thames

Phase difference along the Thames

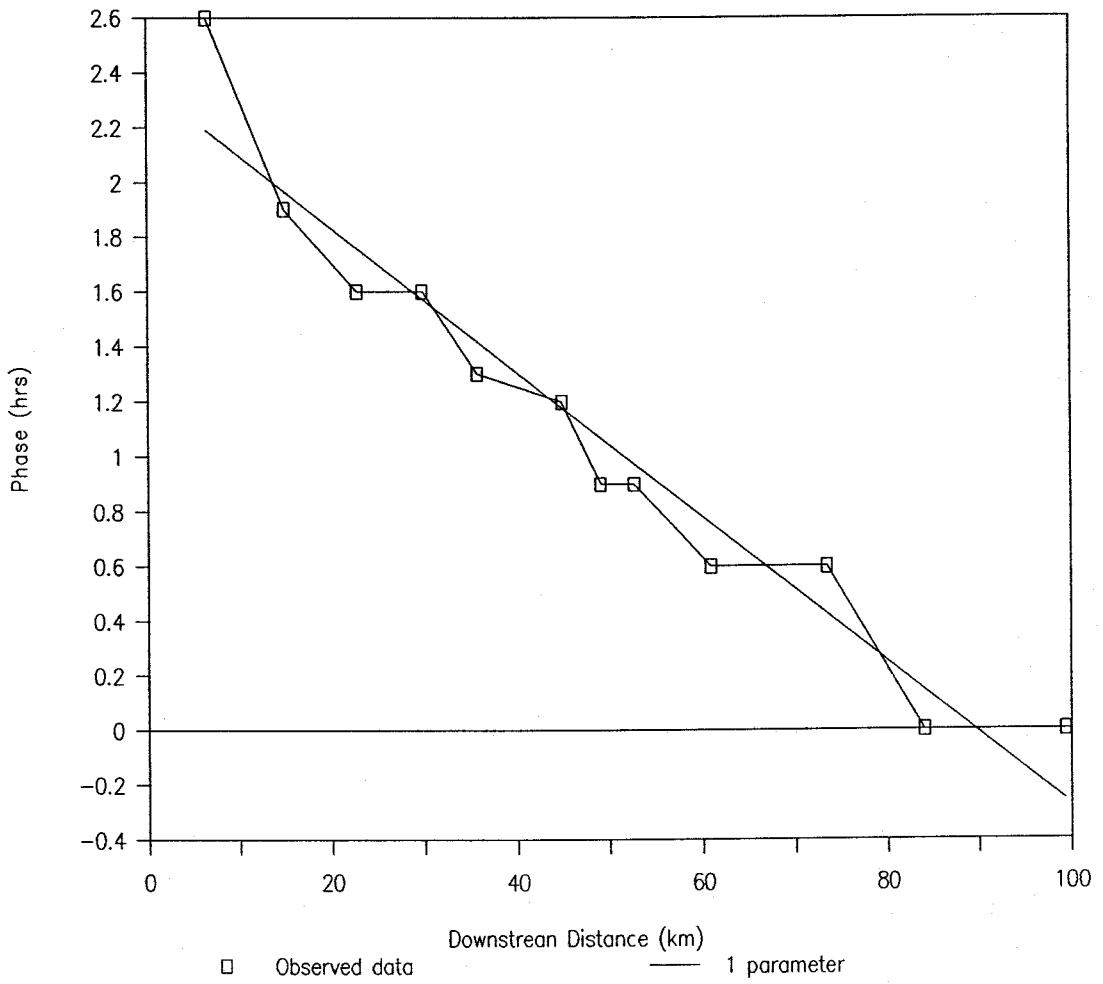


Fig 10 Phase difference along Thames

Longitudinal Profile of River Thames

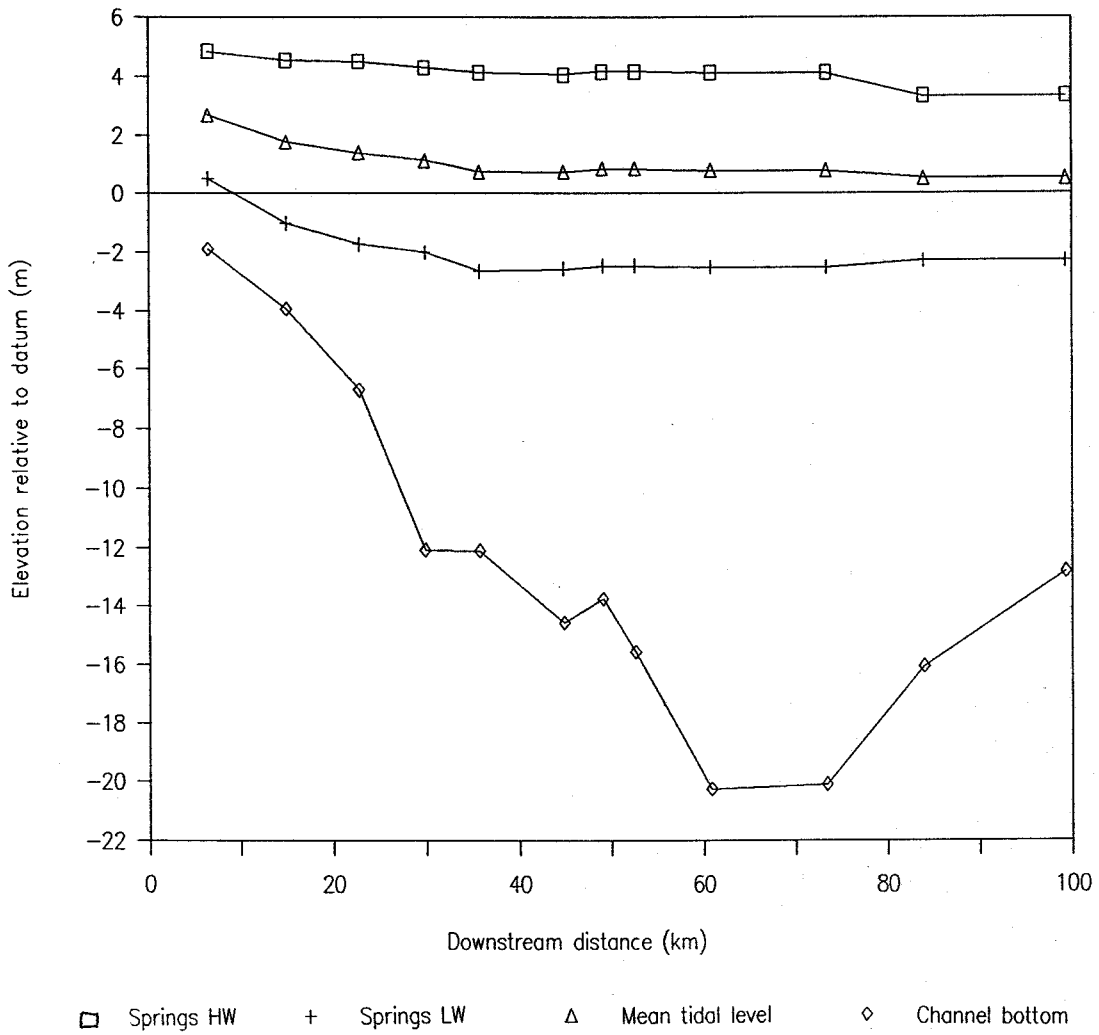
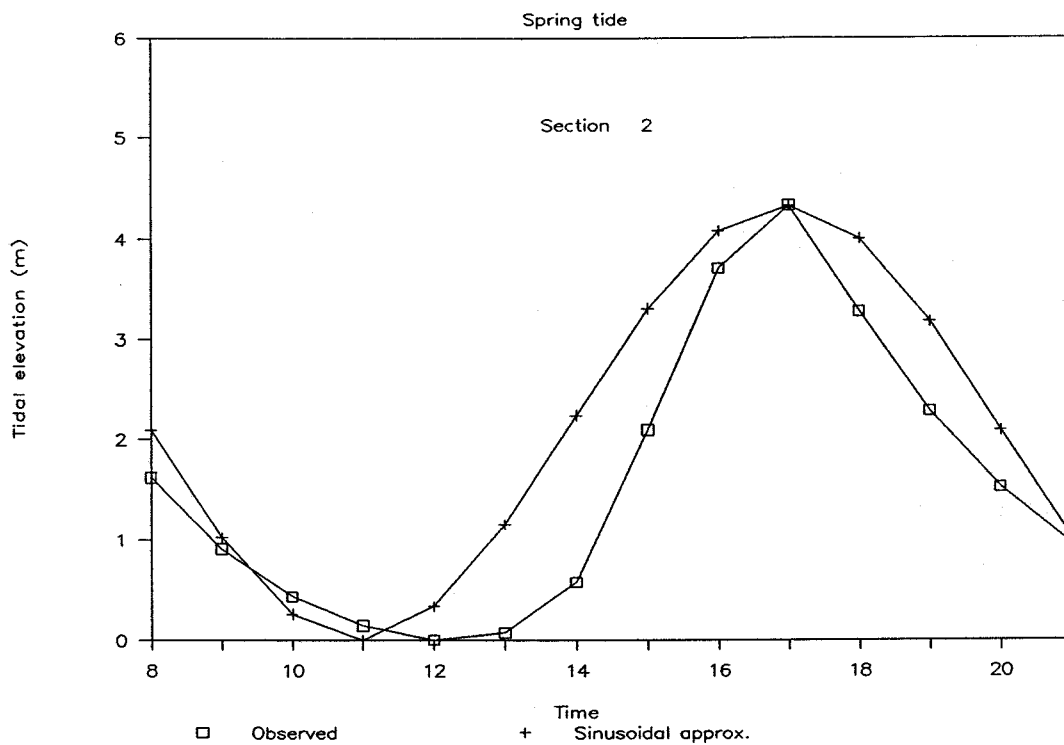


Fig 11 Longitudinal profile of Thames

Tidal data for River Thames



Tidal data for River Thames

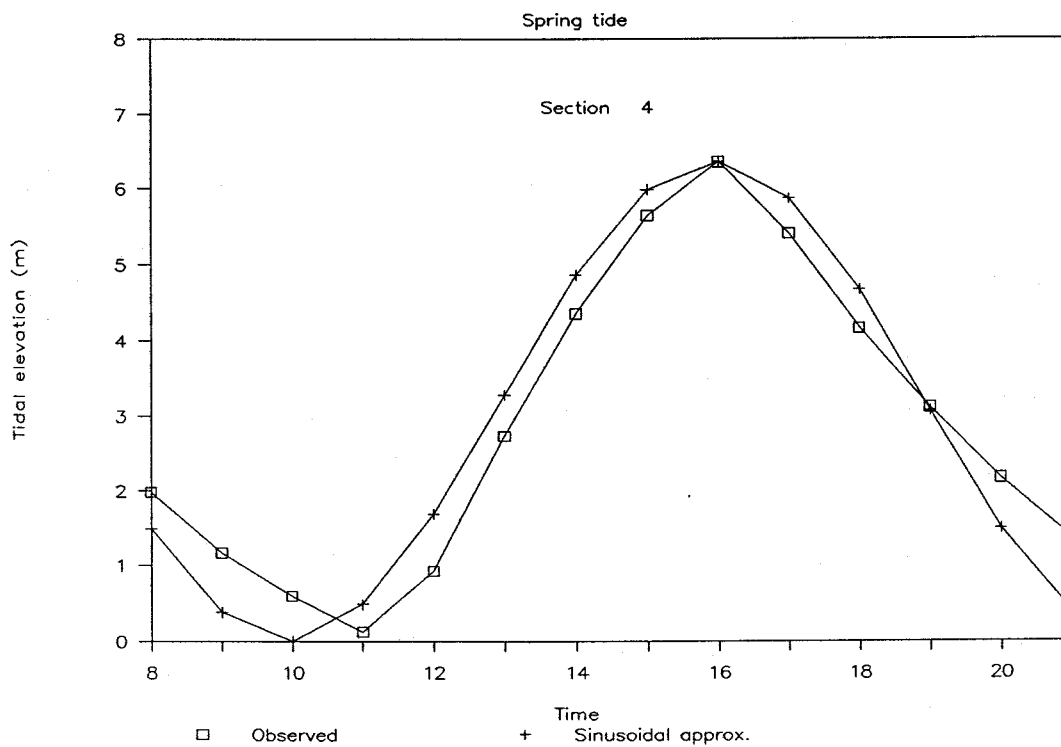
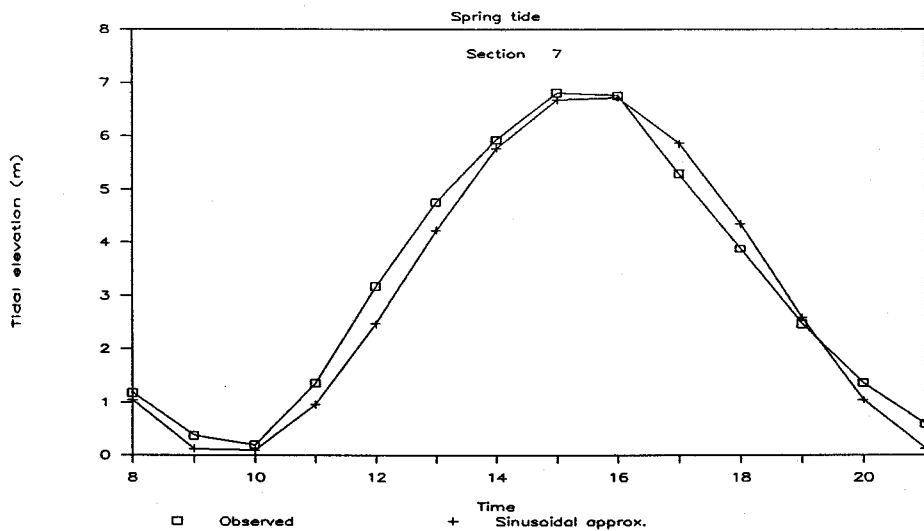
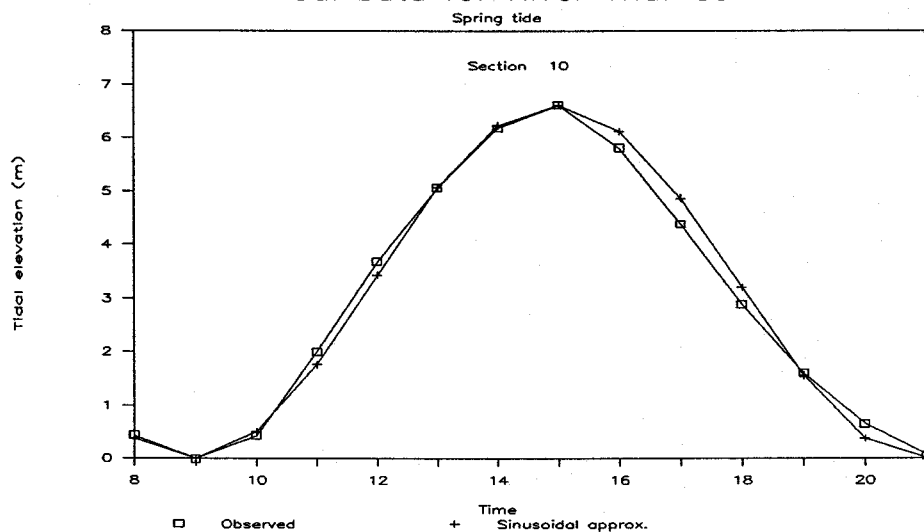


Fig 12 Tidal curves for Thames Estuary

Tidal data for River Thames



Tidal data for River Thames



Tidal data for River Thames

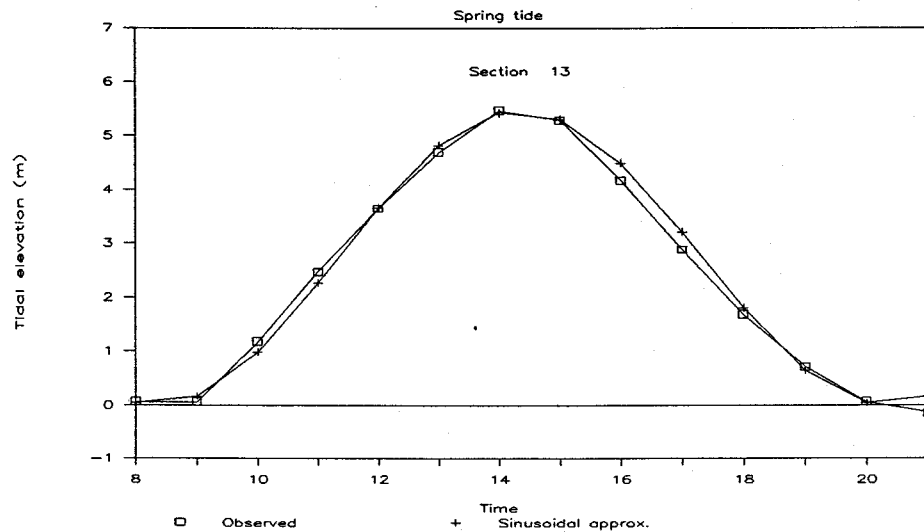


Fig 13 Tidal curves for Thames Estuary

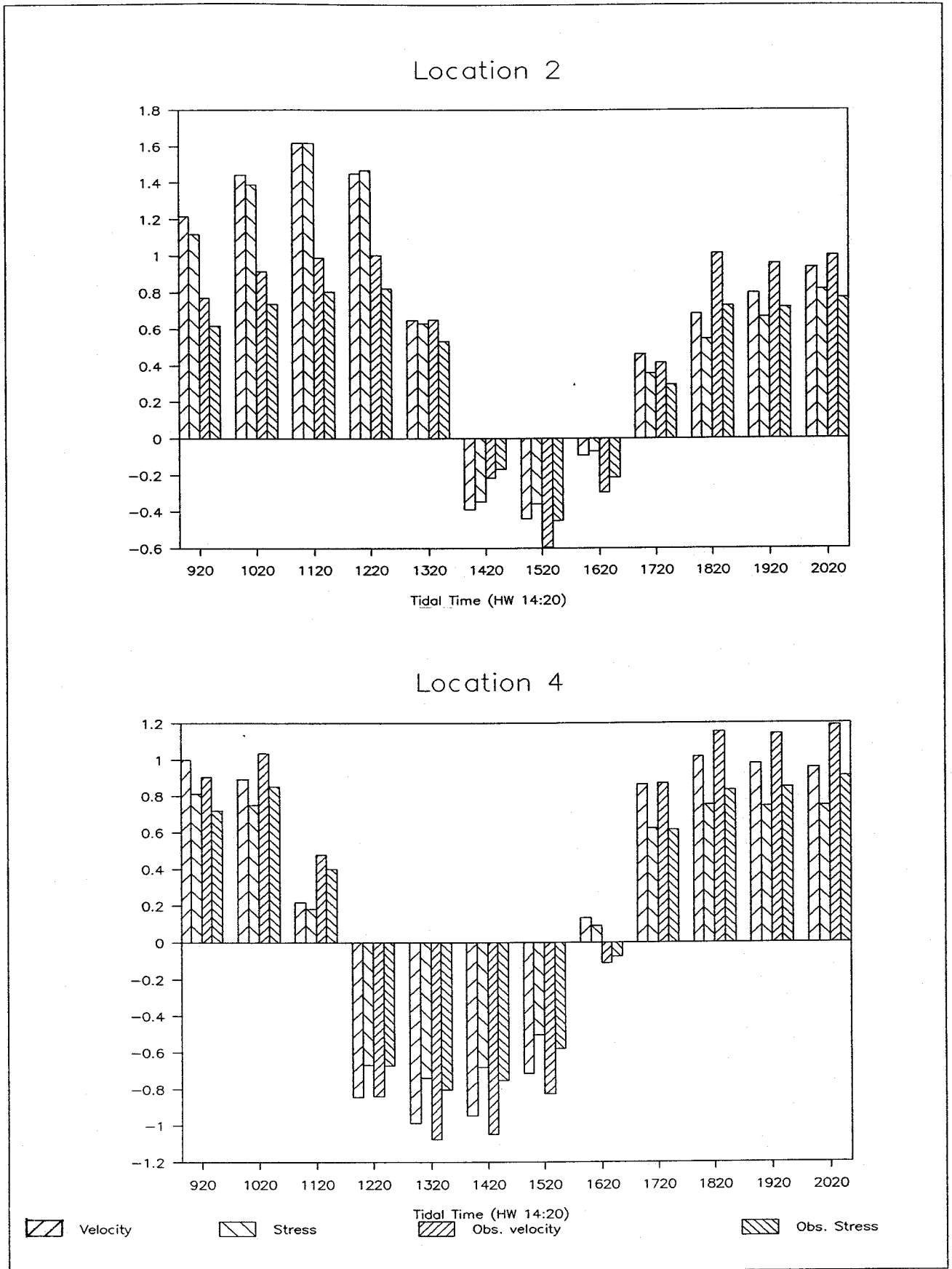
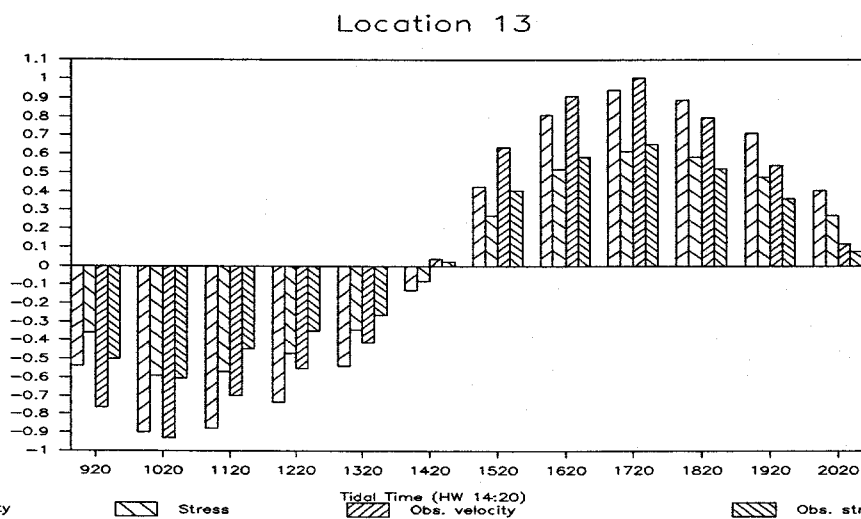
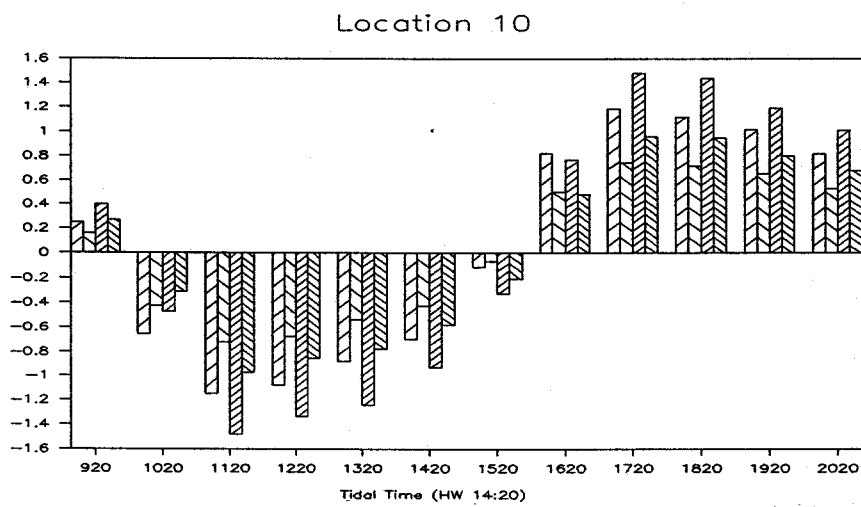
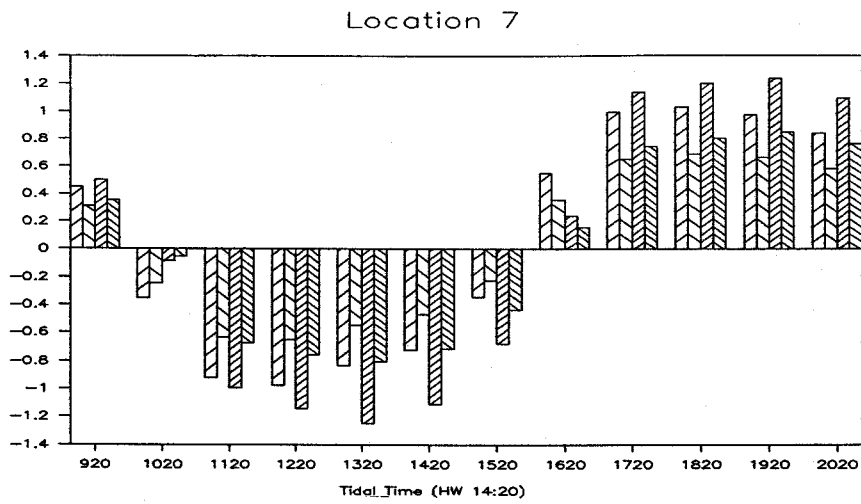


Fig 14 Thames – comparison of model results with observations

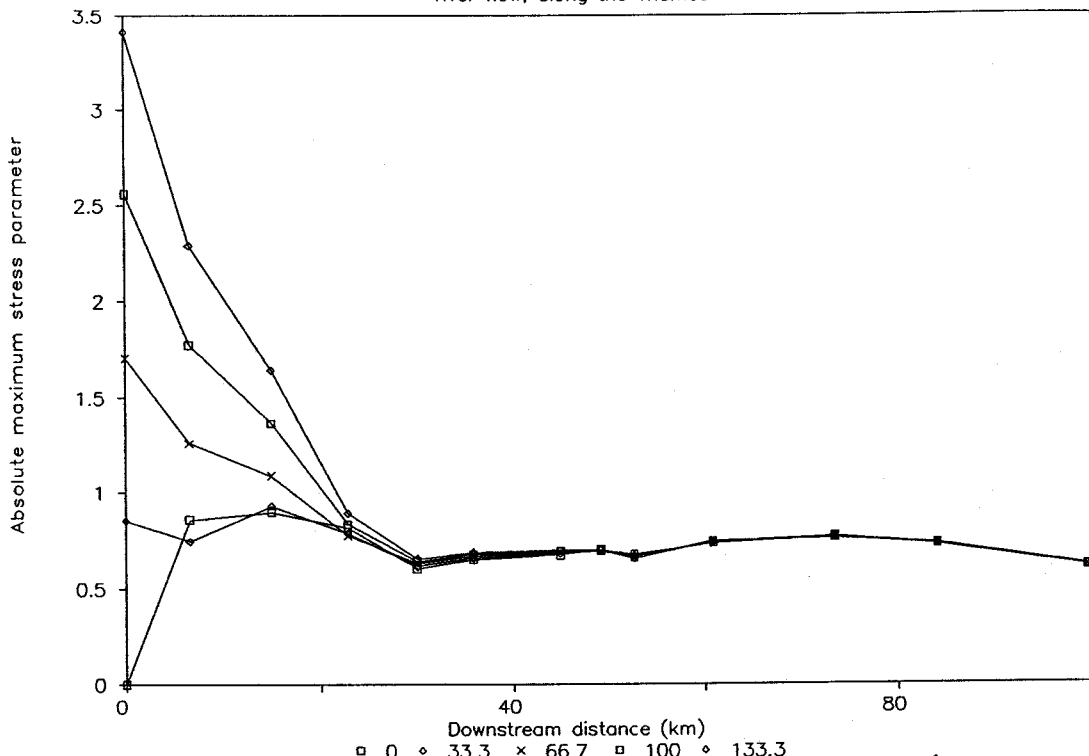


Velocity
 Stress
 Obs. velocity
 Obs. stress

Fig 15 Thames – comparison of model results with observations

Maximum stress parameter for increasing

river flow, along the Thames



Maximum stress parameter for increasing

river flow, along the Thames

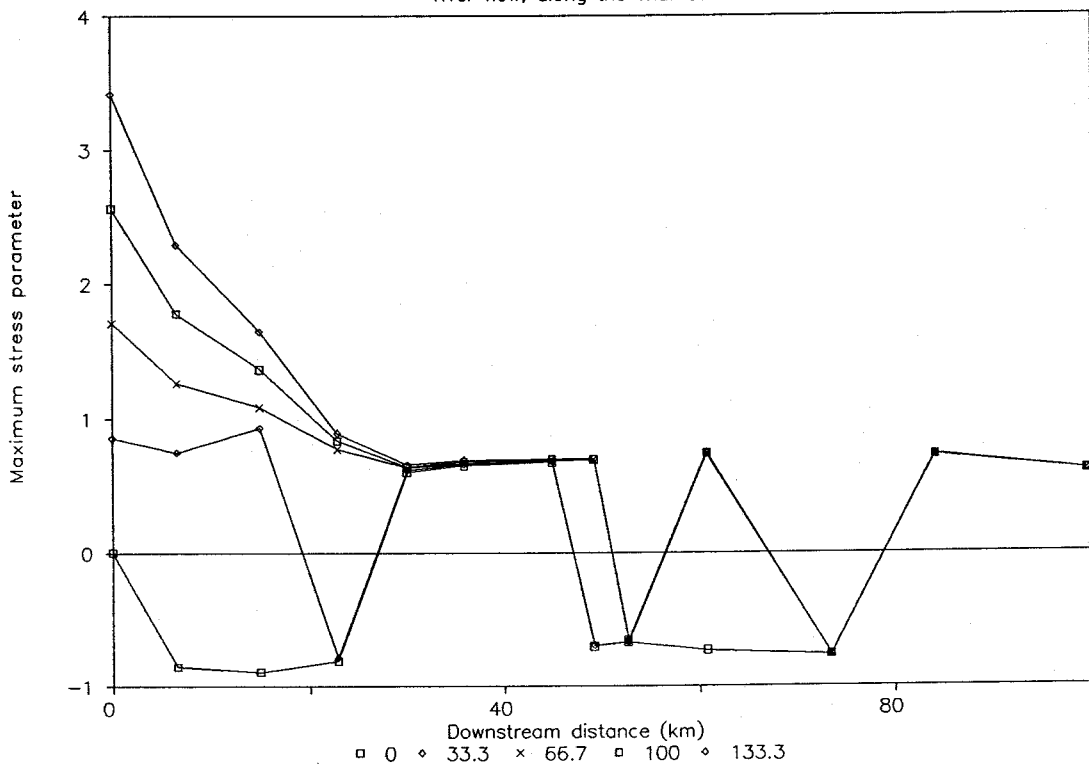
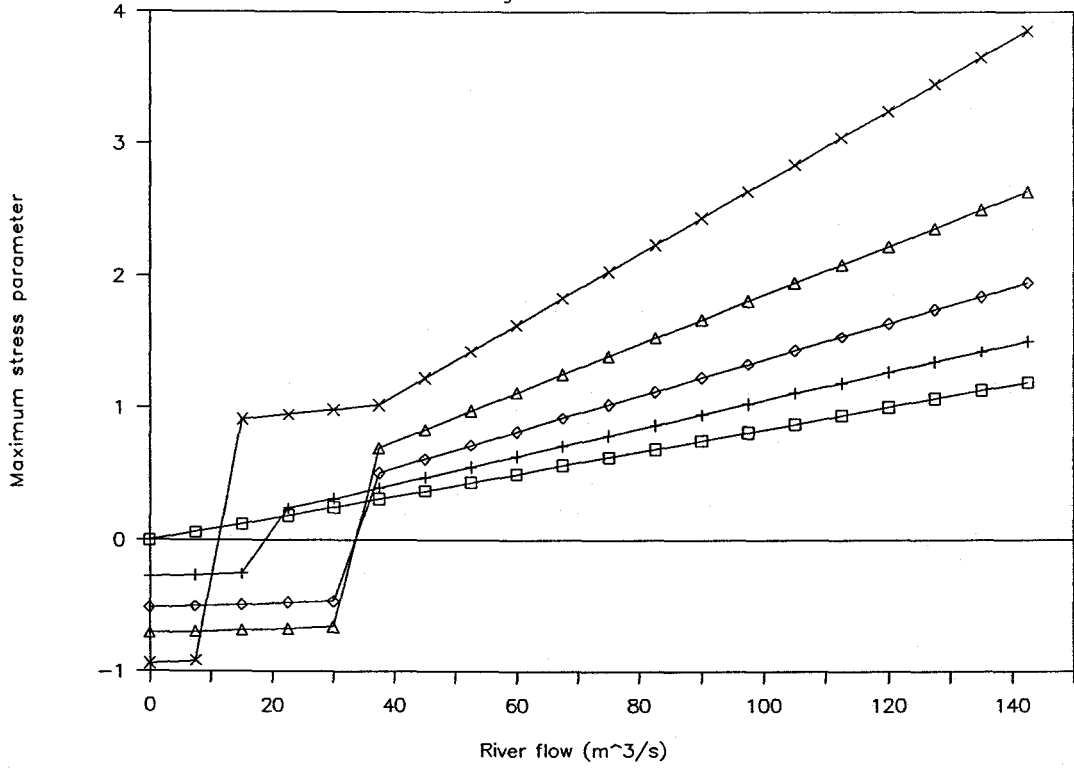


Fig 16 Maximum stress parameter for increasing river flow

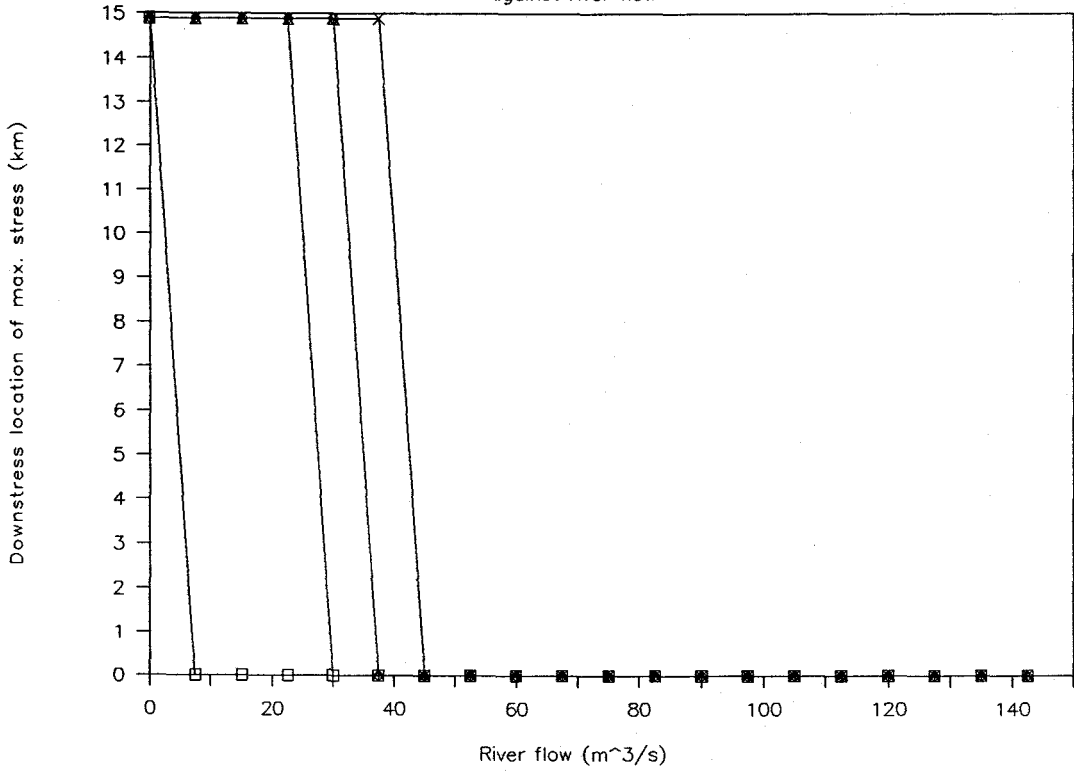
Maximum stress along Thames

against river flow



Location of max. stress along Thames

against river flow



□ tidescale 0.26 ◇ tidescale 0.52 △ tidescale 0.78 × tidescale 1.04

Fig 17 Maximum stress parameter for different tidal ranges

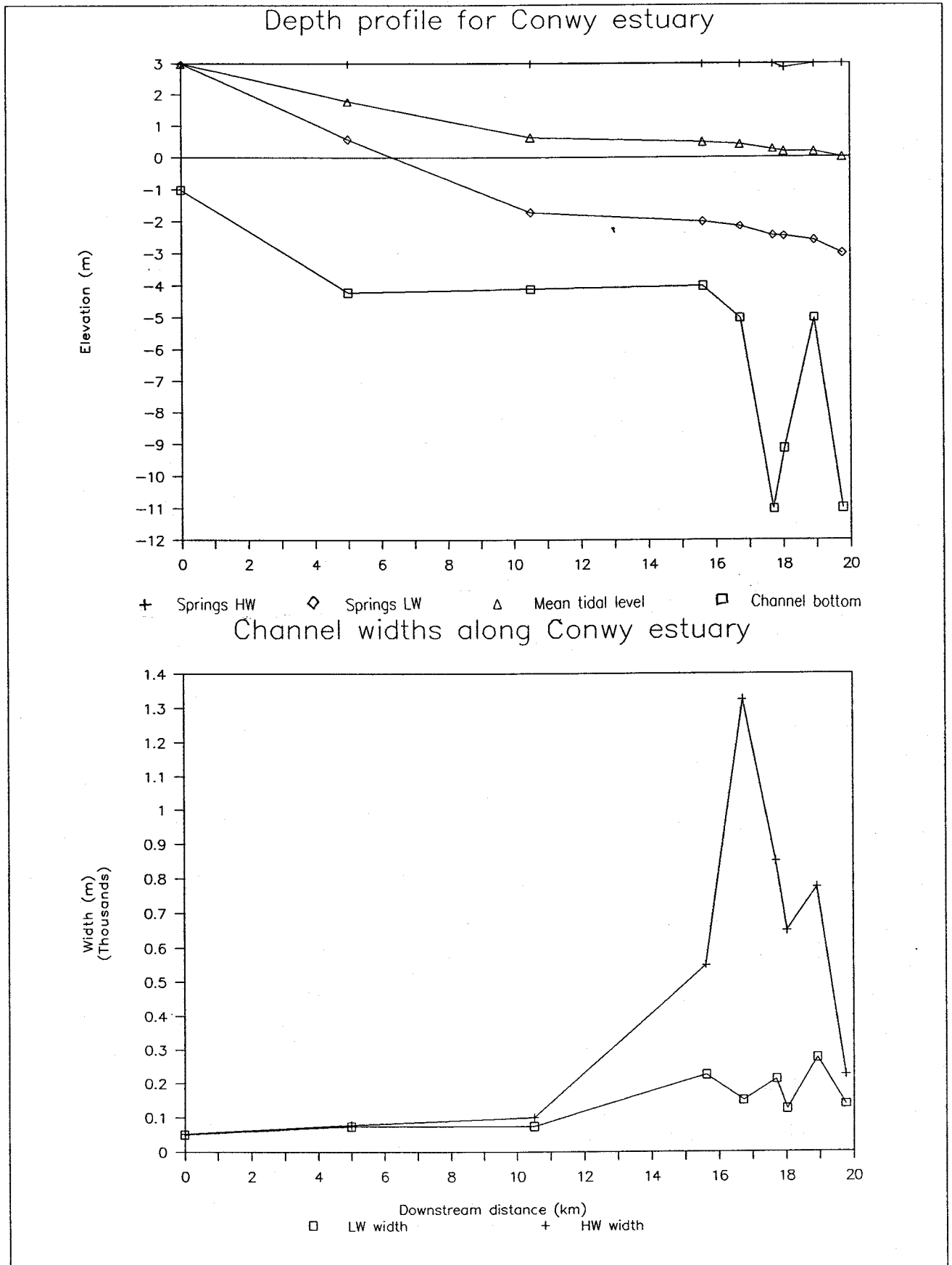


Fig 18 Longitudinal profile and channel widths for Conwy Estuary

Max & Min bottom stress parameter

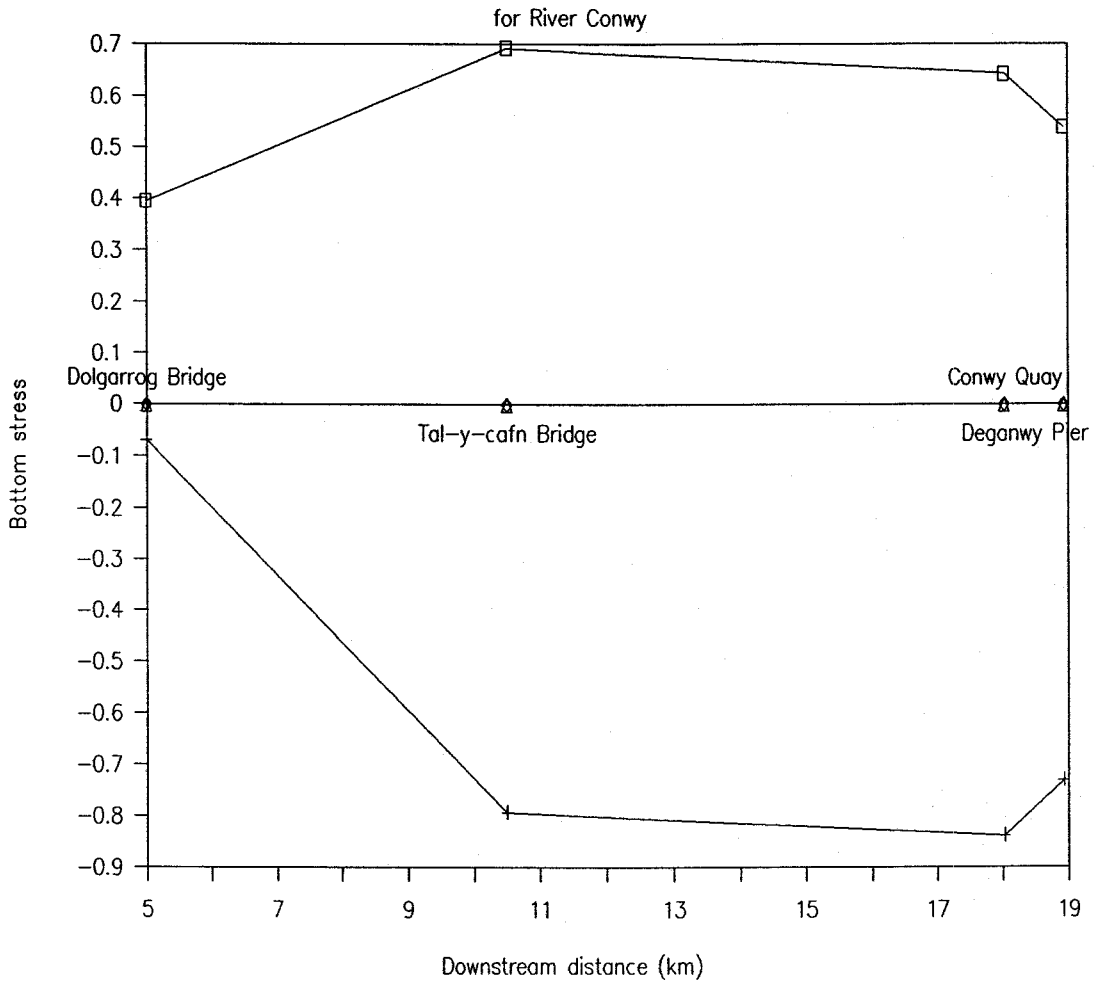


Fig 19 Maximum stress parameter

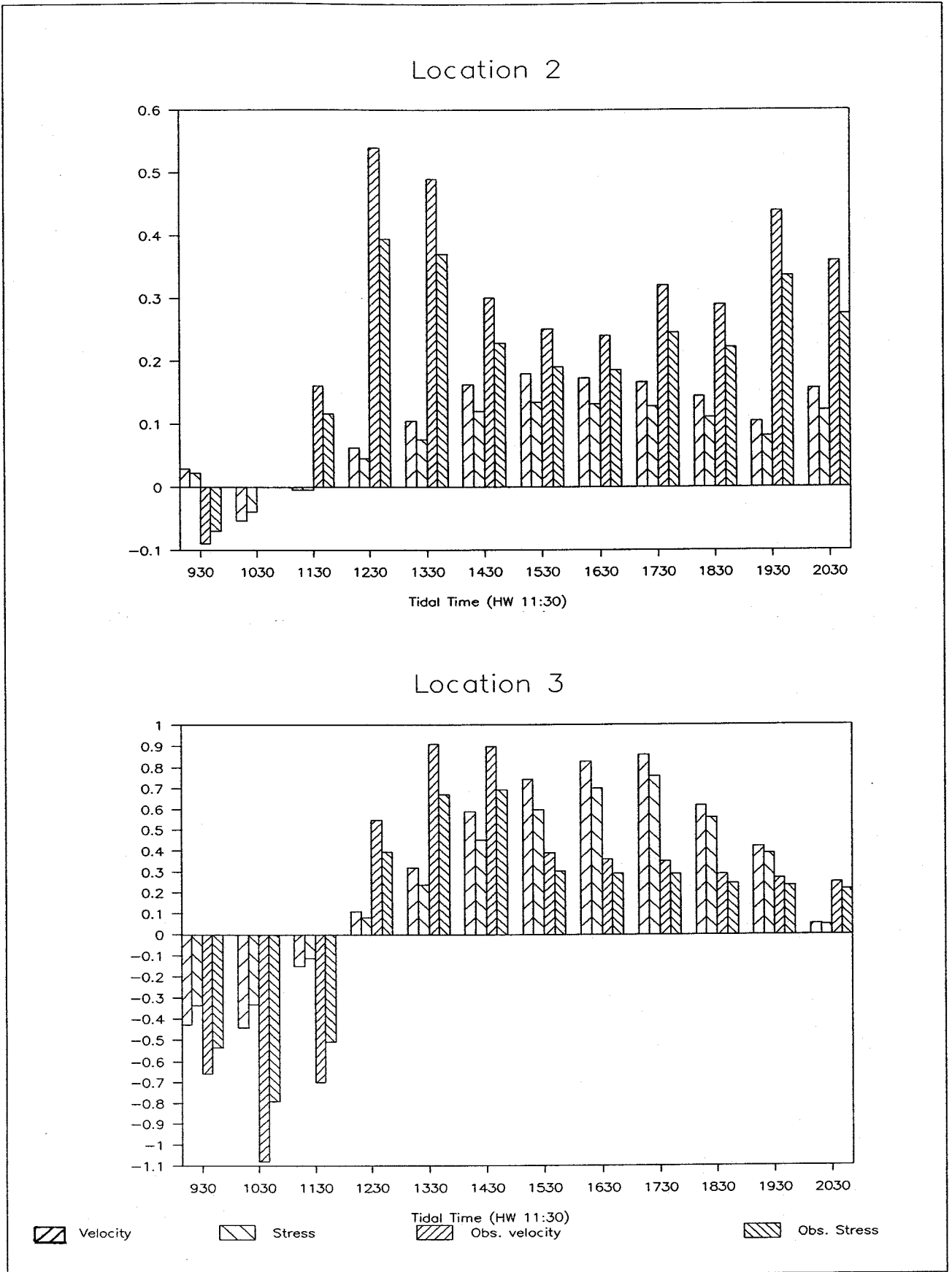
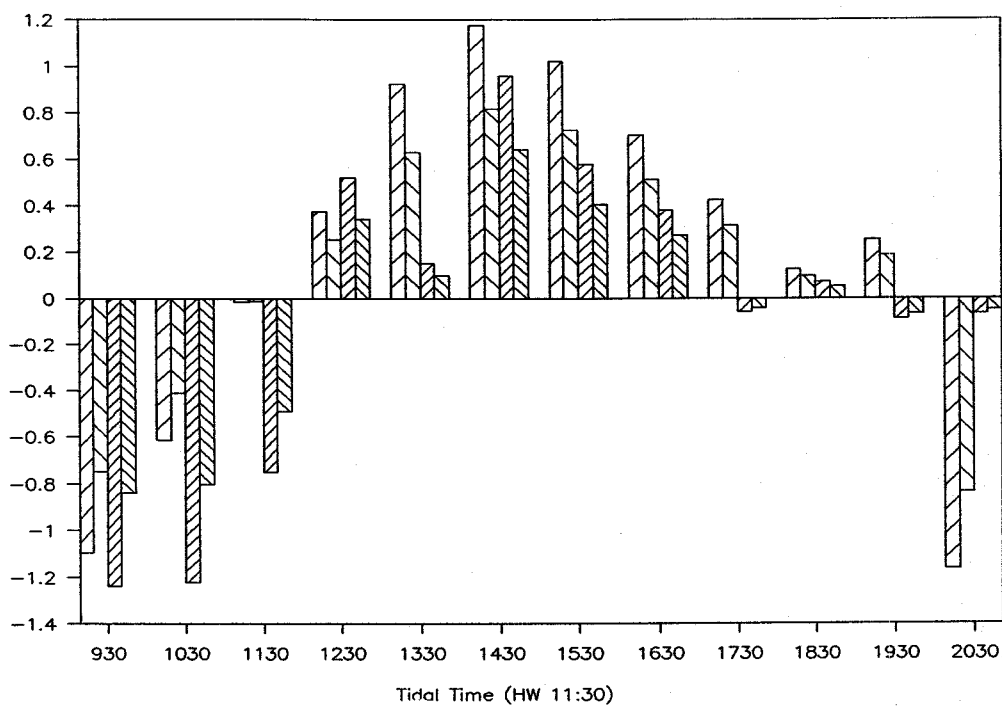
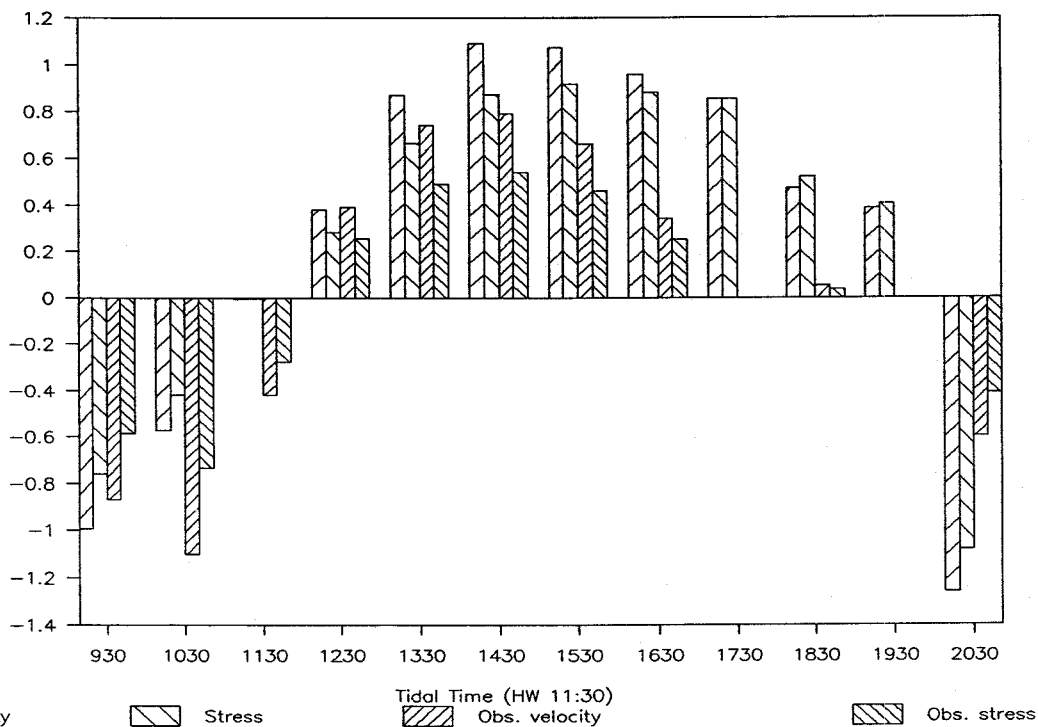


Fig 20 Conwy – comparison of model results with observations

Location 7



Location 8



Legend: Velocity (diagonal hatching), Stress (white fill), Obs. velocity (cross-hatch), Obs. stress (diagonal hatching)

Fig 21 Conwy – comparison of model results with observations

Maximum stress parameter for increasing

river flow along the Conwy

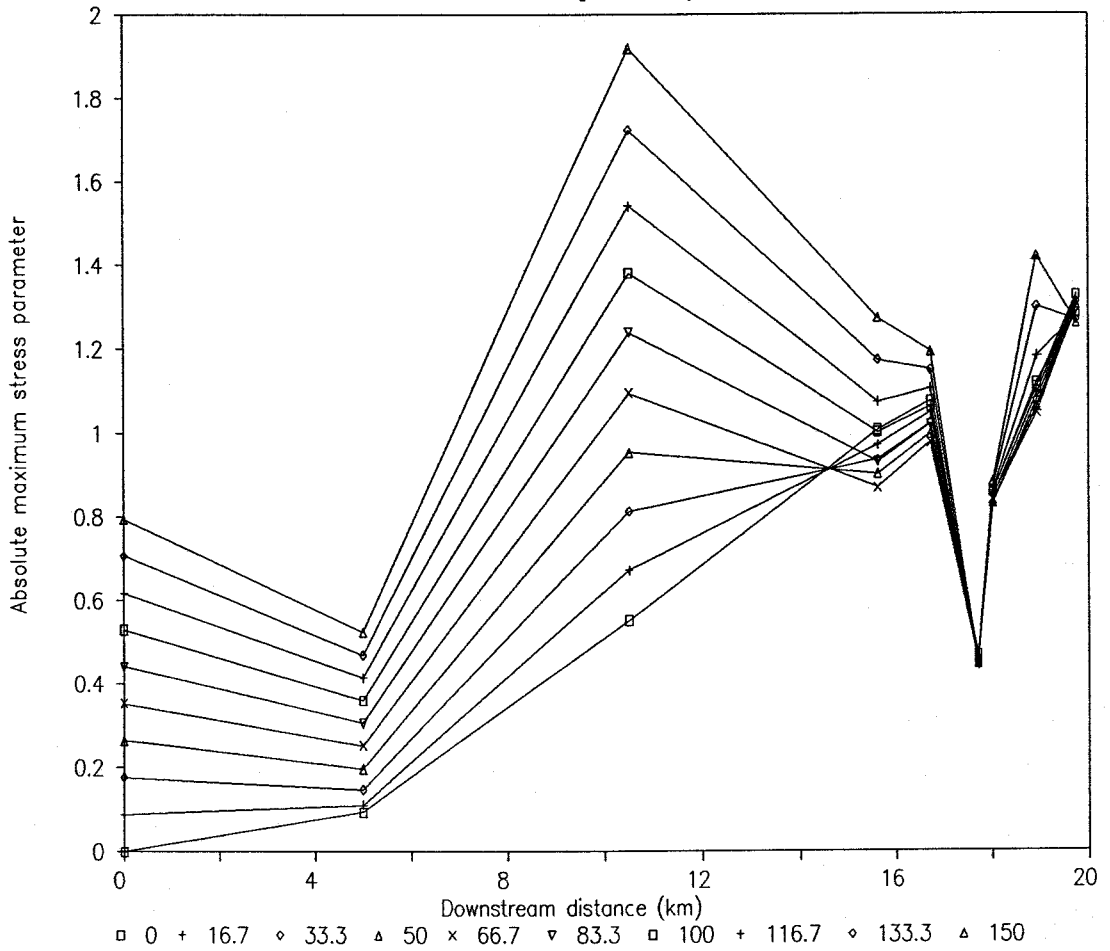
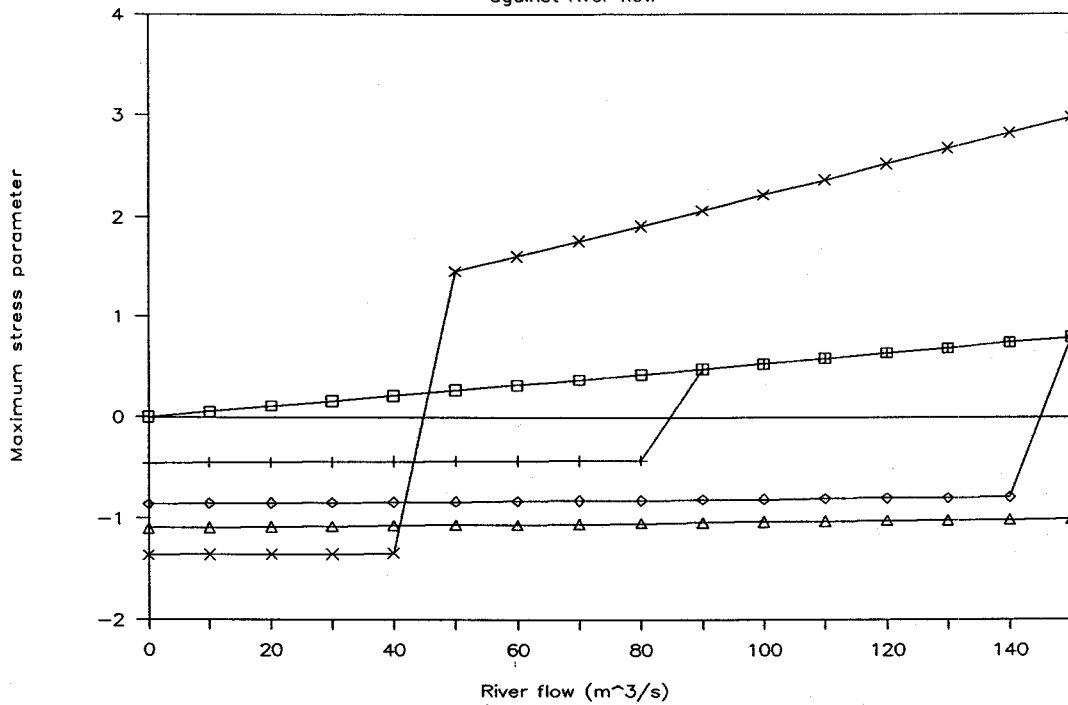


Fig 22 Maximum stress parameter for increasing river flow

Maximum stress along Conwy against river flow



Location of max. stress along Conwy against river flow

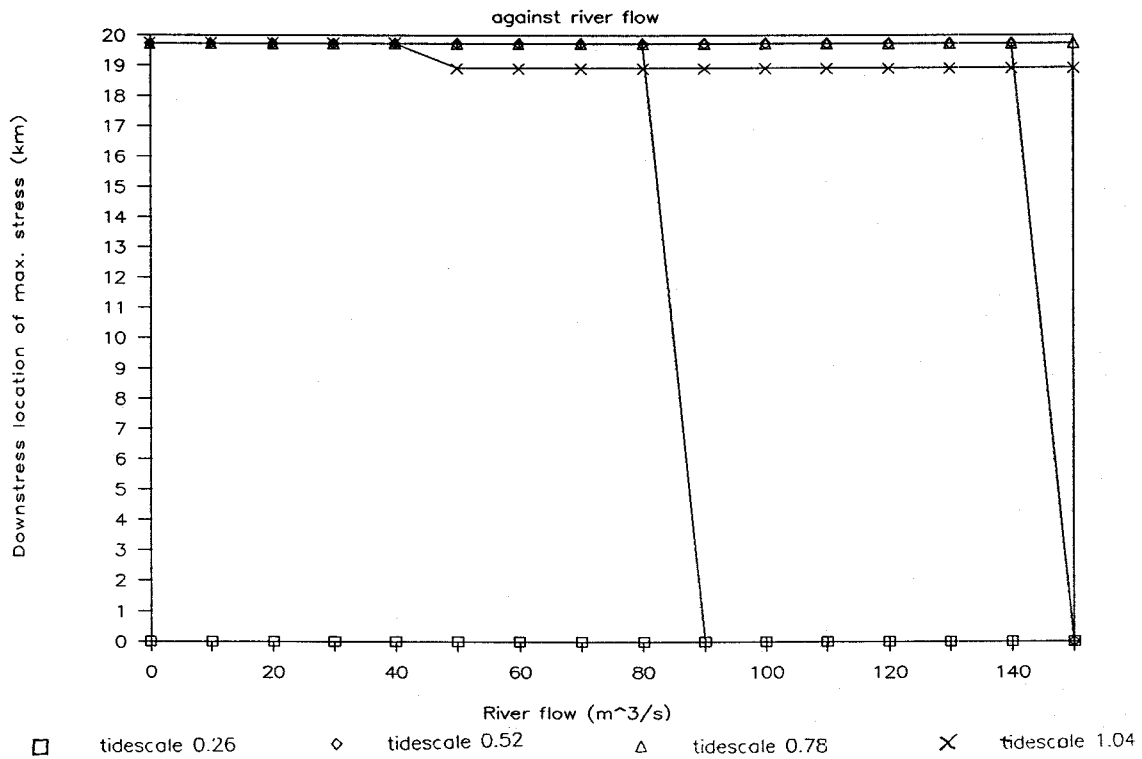


Fig 23 Maximum stress parameter for different tidal ranges

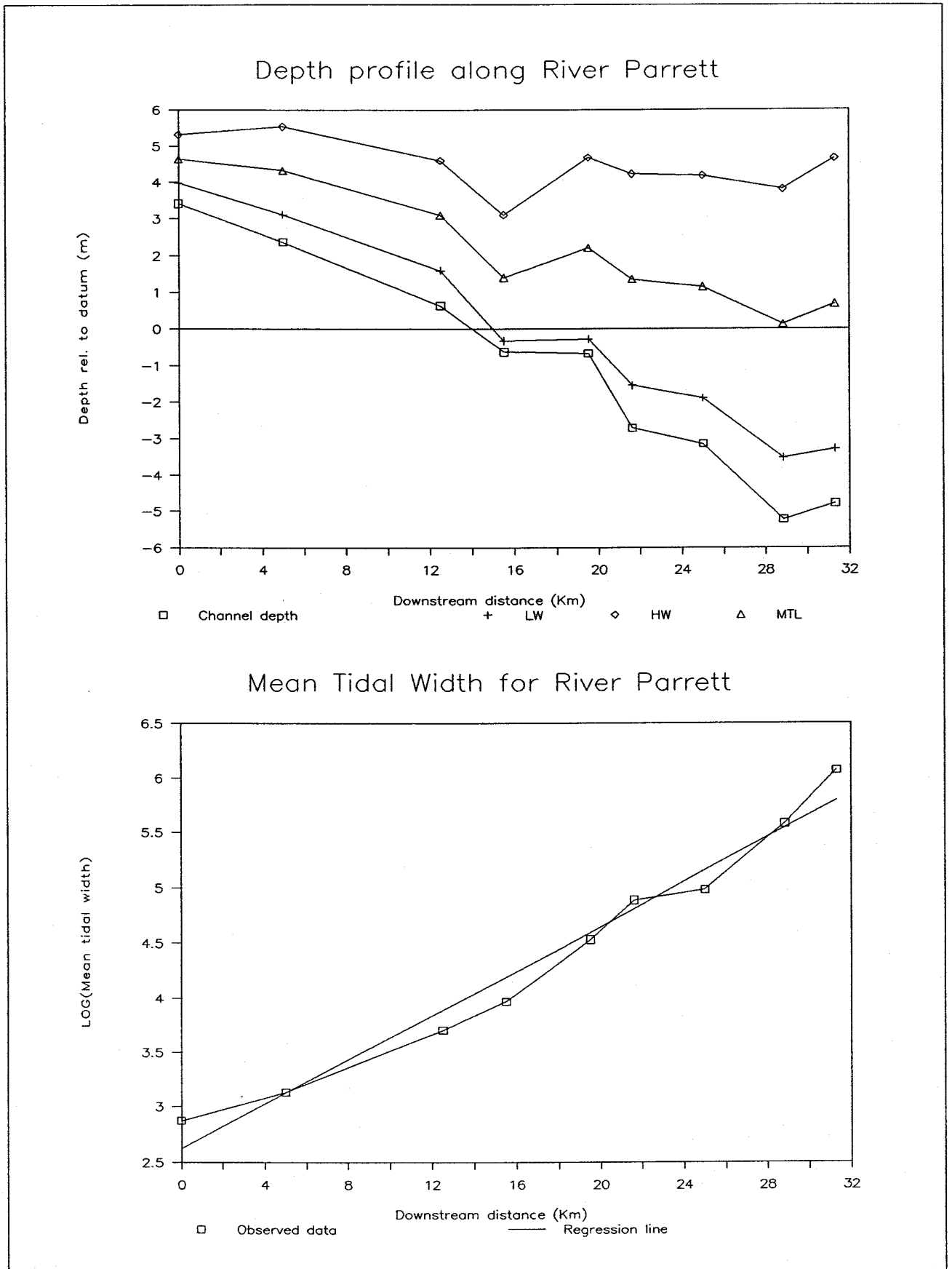


Fig 24 Longitudinal profile and mean tidal width for River Parrett

Max & Min bottom stress parameter

for River Parrett

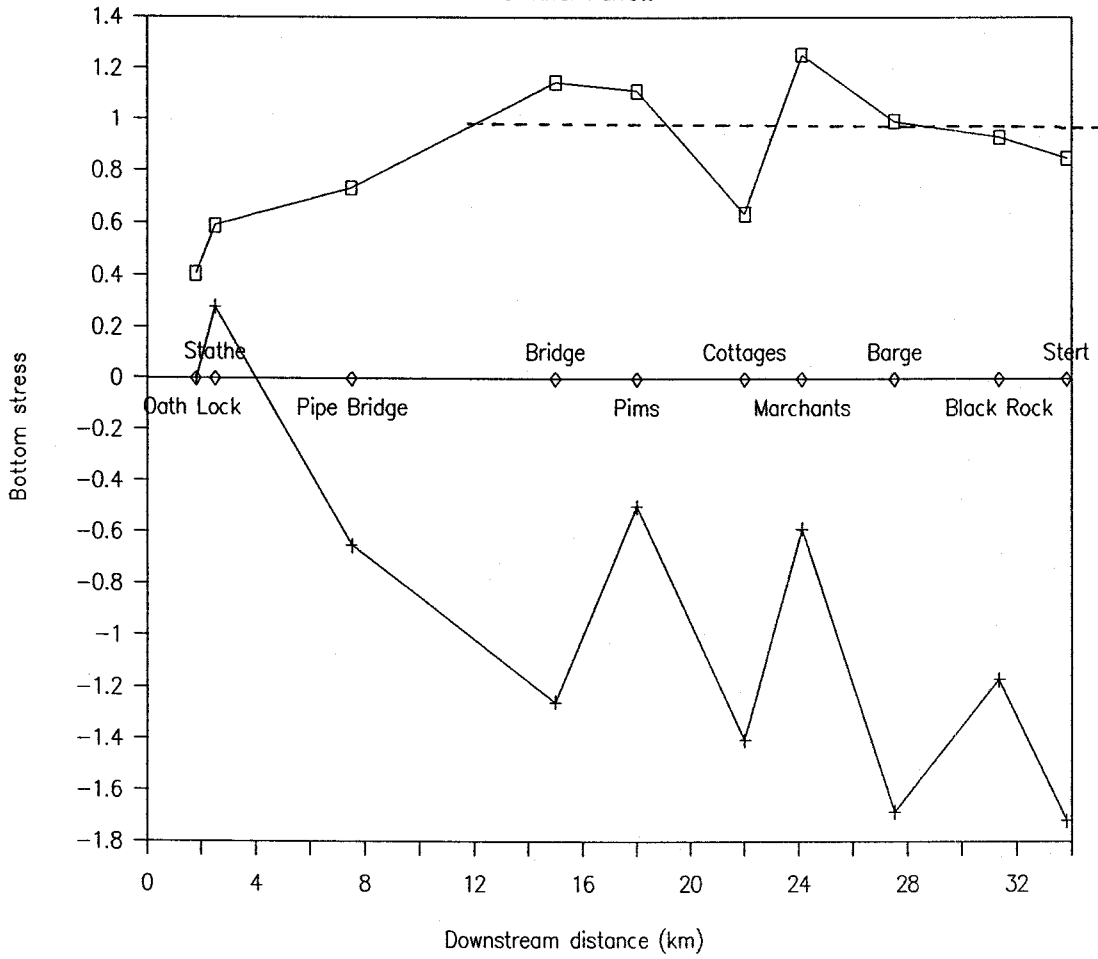
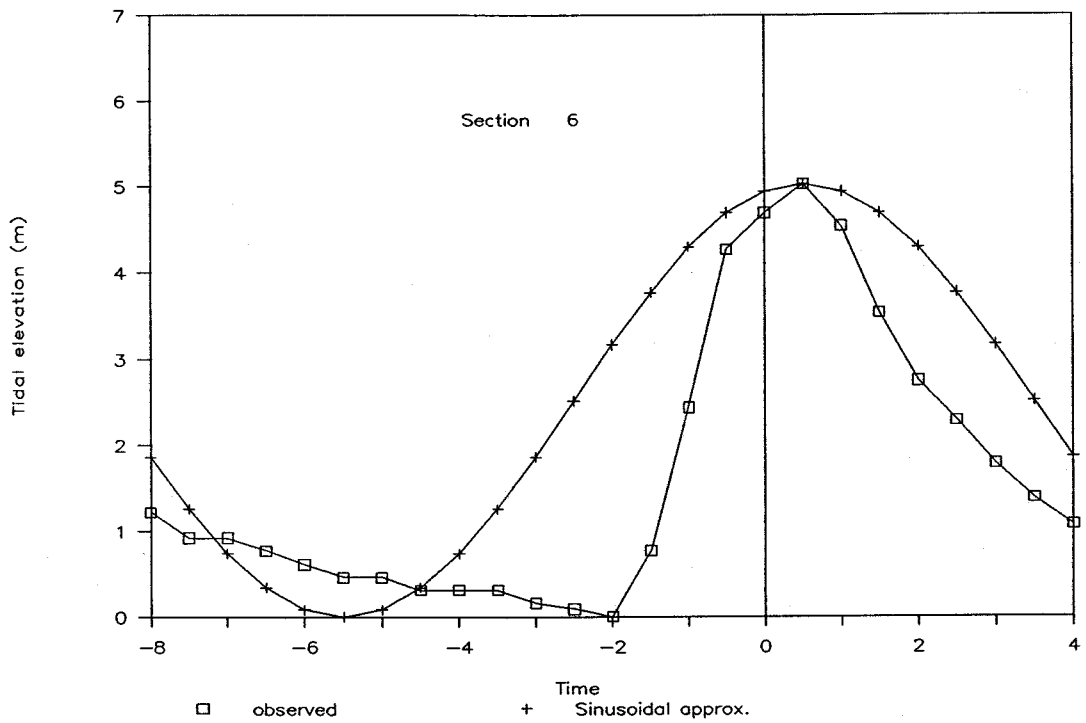


Fig 25 Parrett – Maximum and minimum stress parameter

Tidal curves for River Parrett



Tidal curves for River Parrett

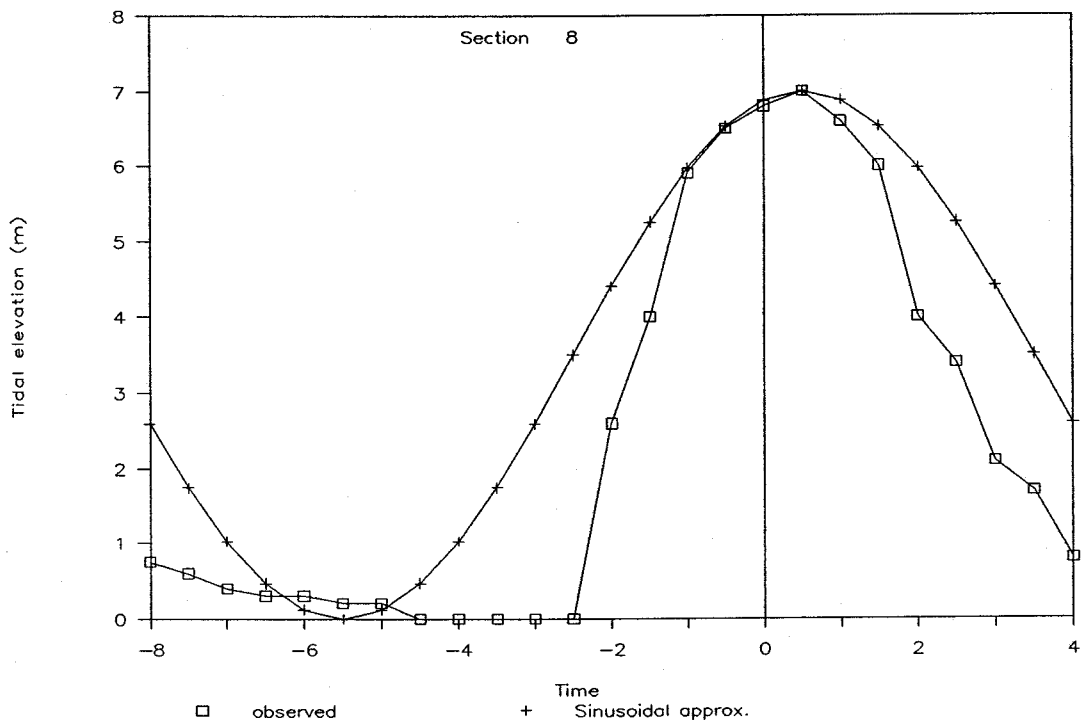
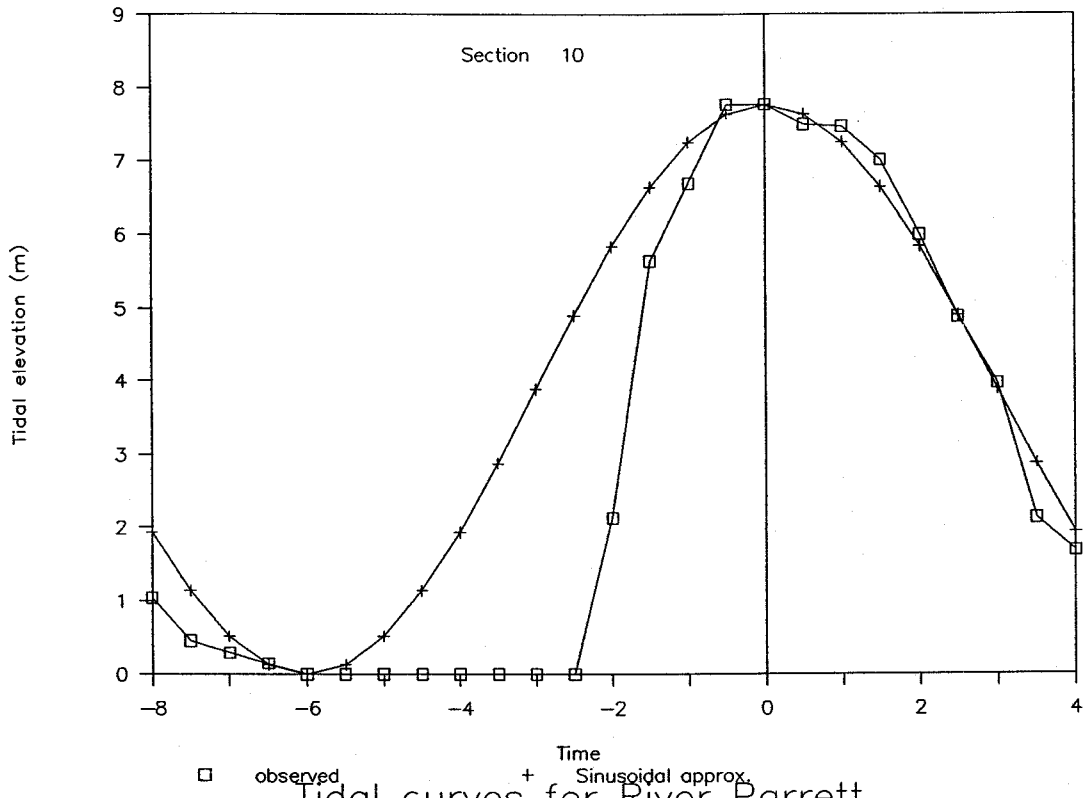


Fig 26 Tidal curves for River Parrett

Tidal curves for River Parrett



Tidal curves for River Parrett

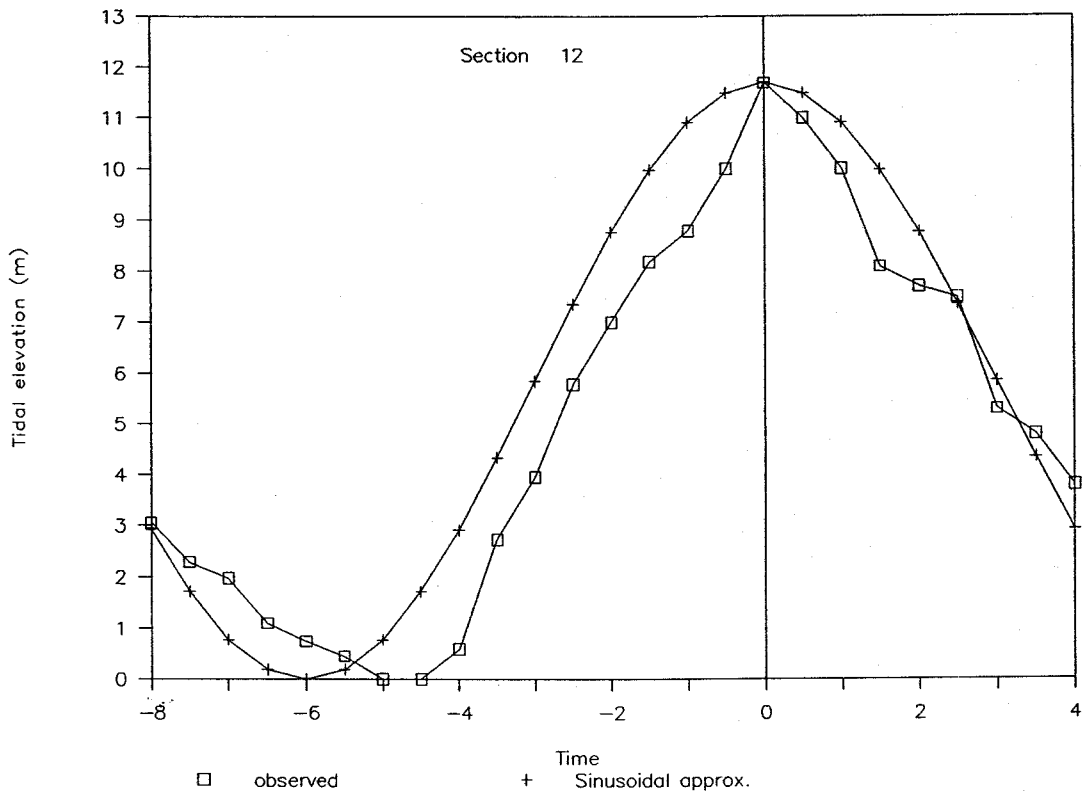


Fig 27 Tidal curves for River Parrett

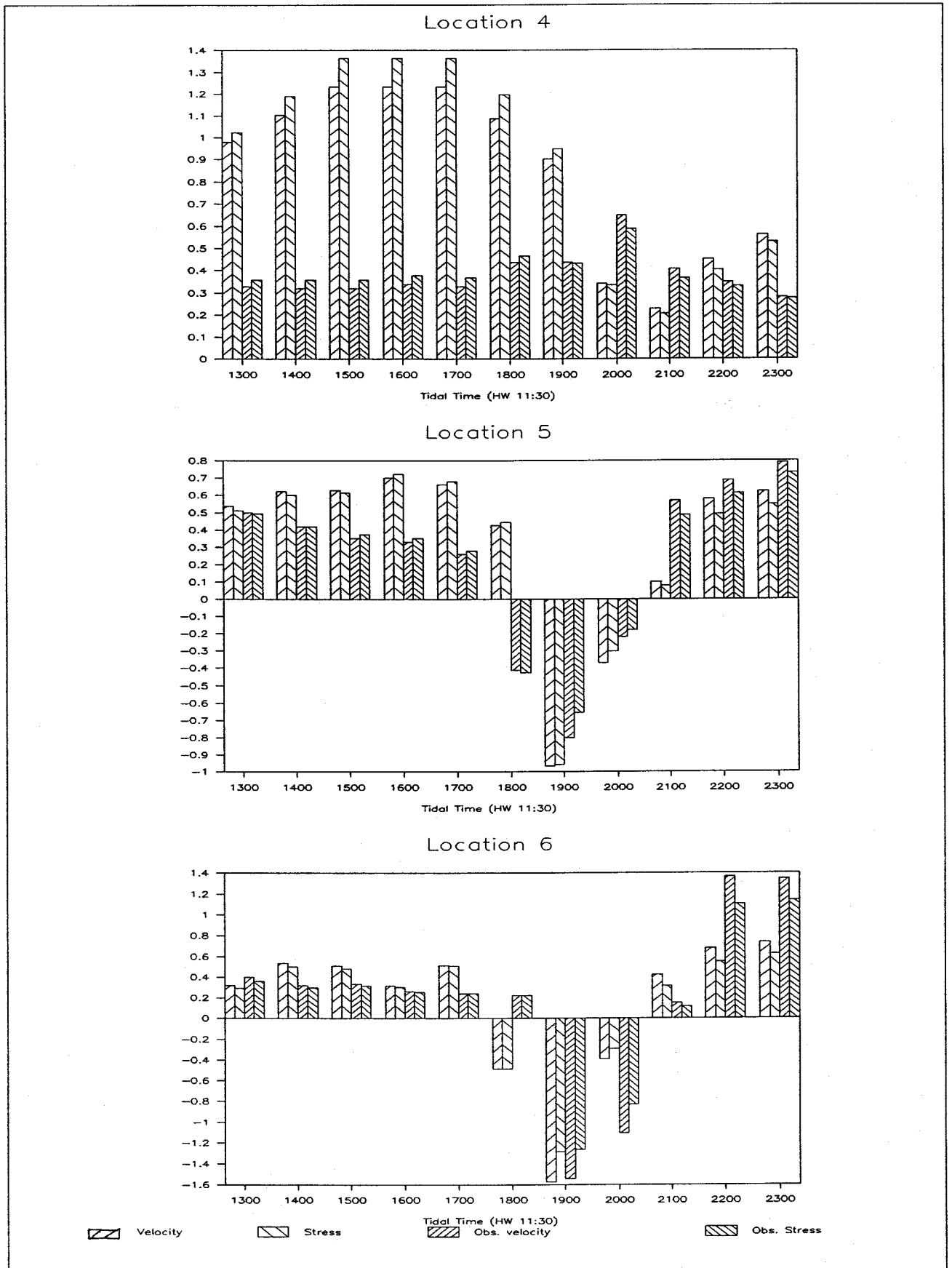
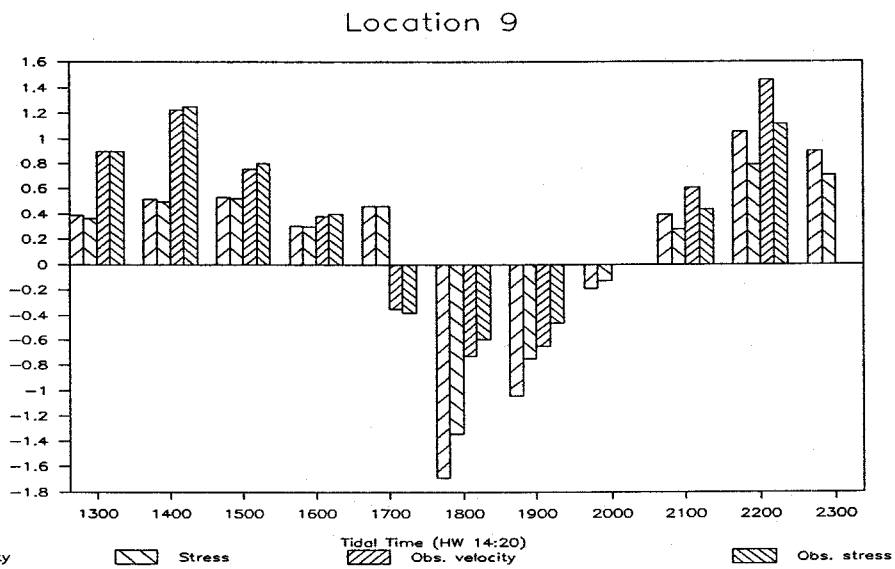
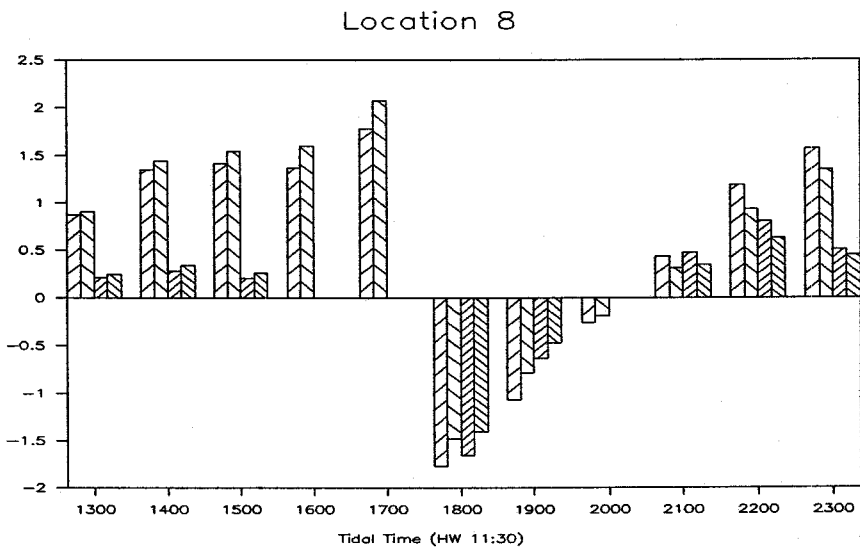
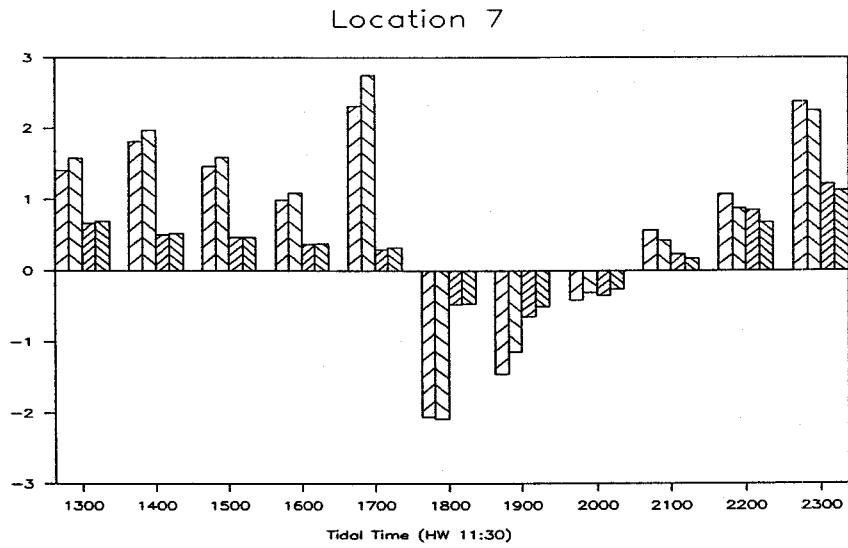


Fig 28 Parrett – Comparison of model results with observations



Velocity
 Stress
 Obs. velocity
 Obs. stress

Fig 29 Parrett – Comparison of model results with observations

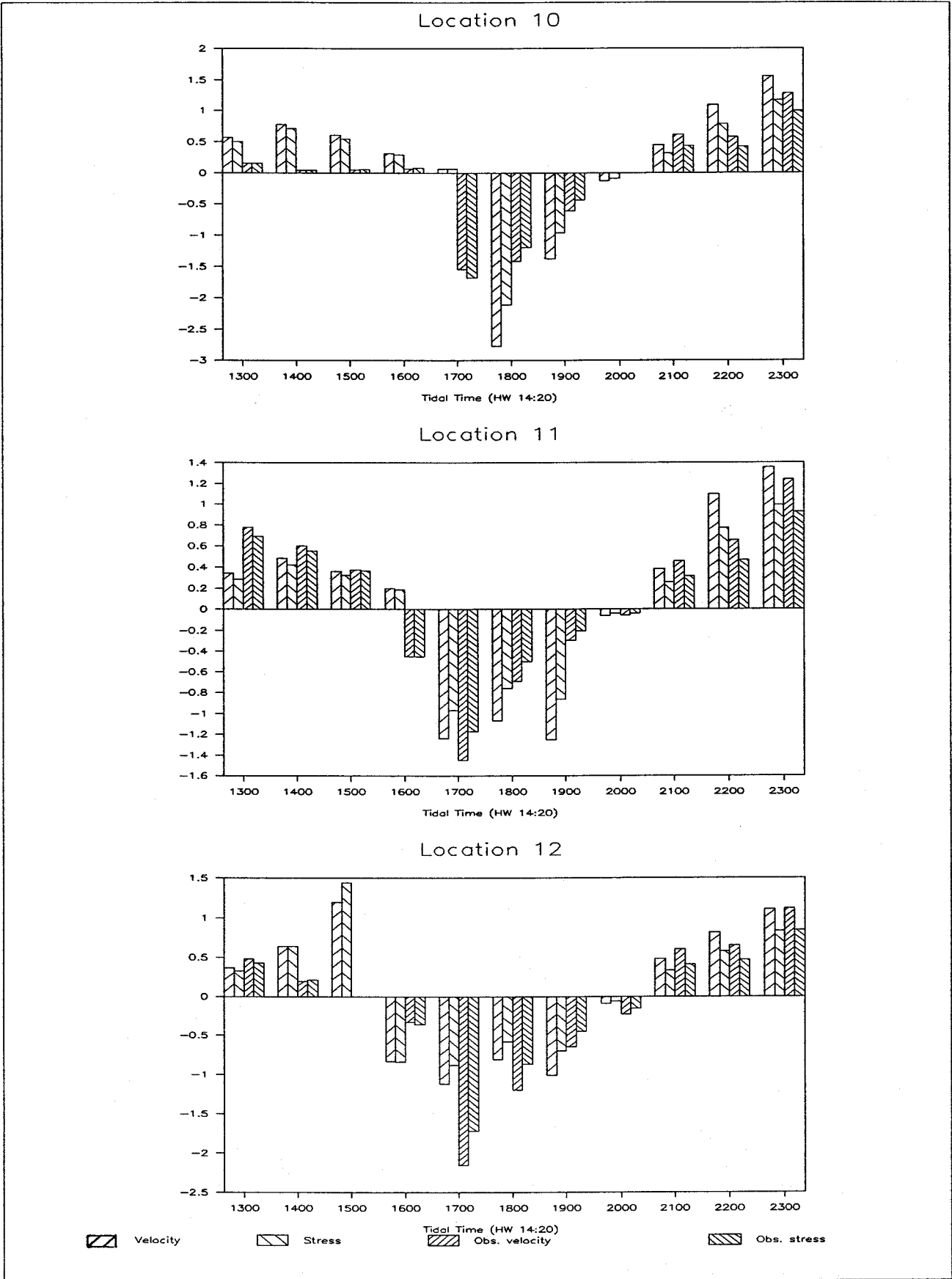
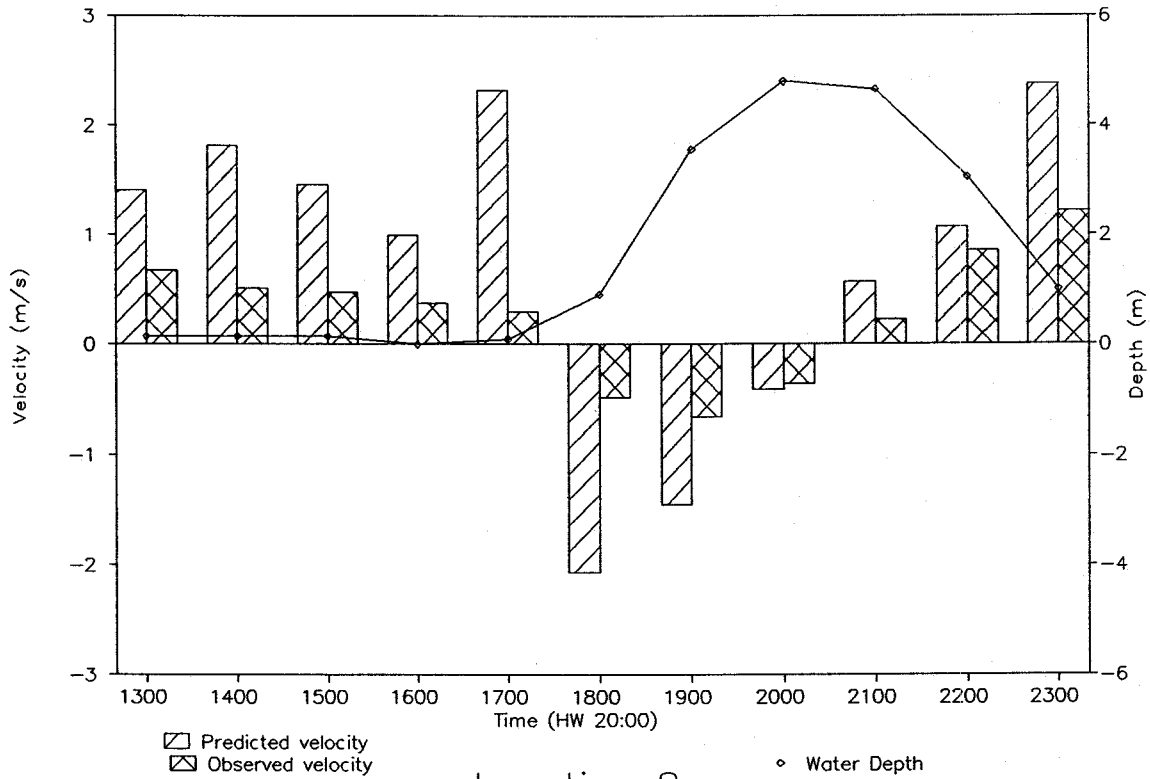


Fig 30 Parrett – Comparison of model results with observations

Location 7



Location 8

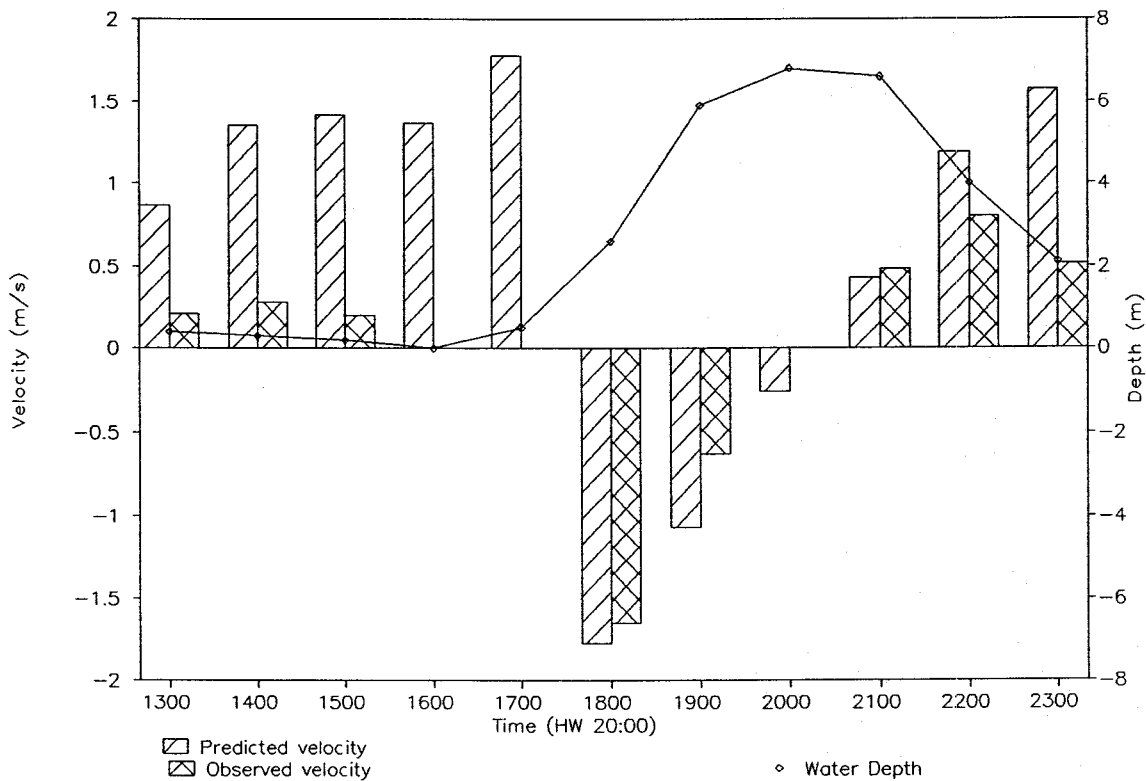


Fig 31 Comparison of velocity results overlaid with total water depth

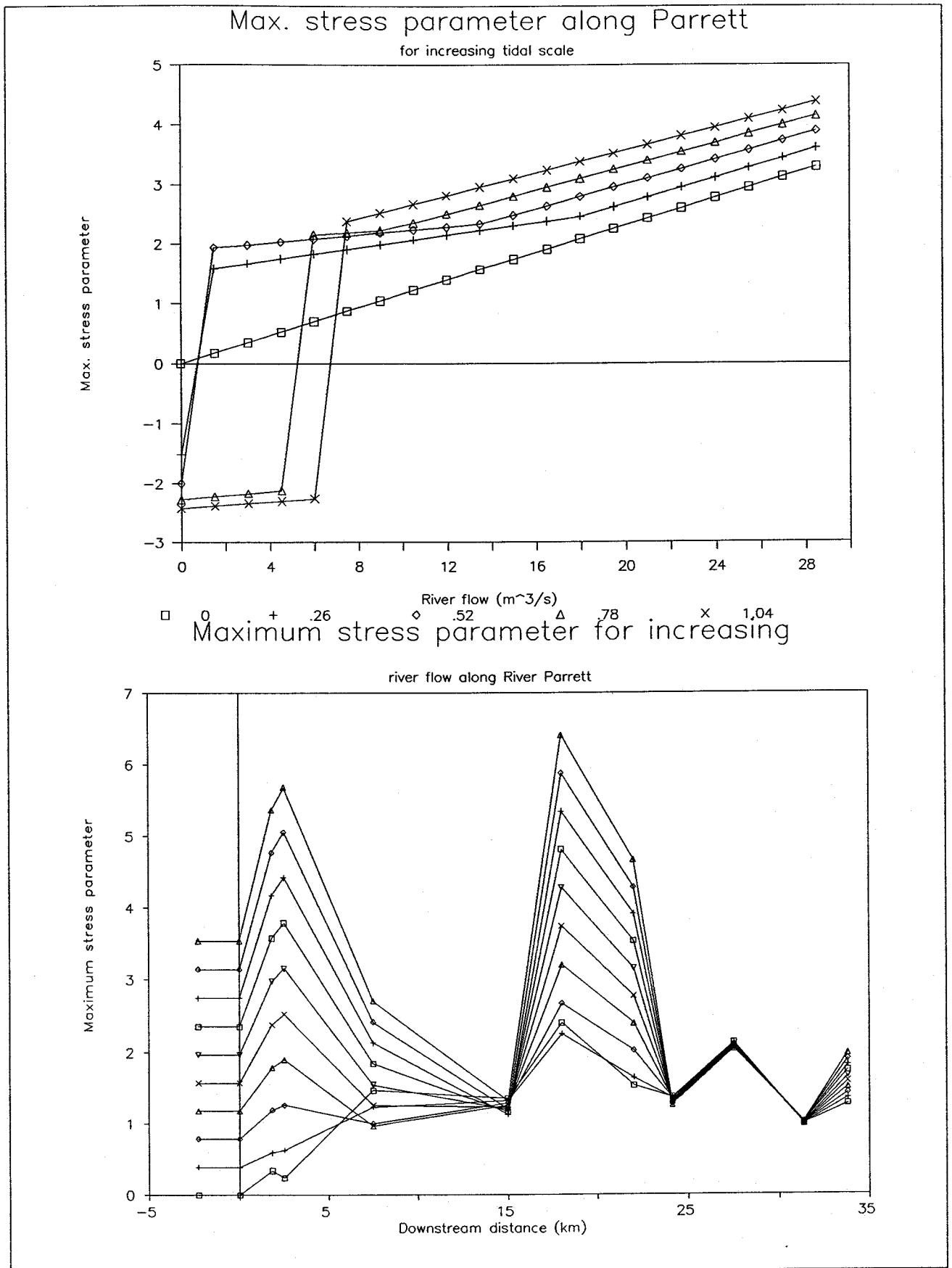
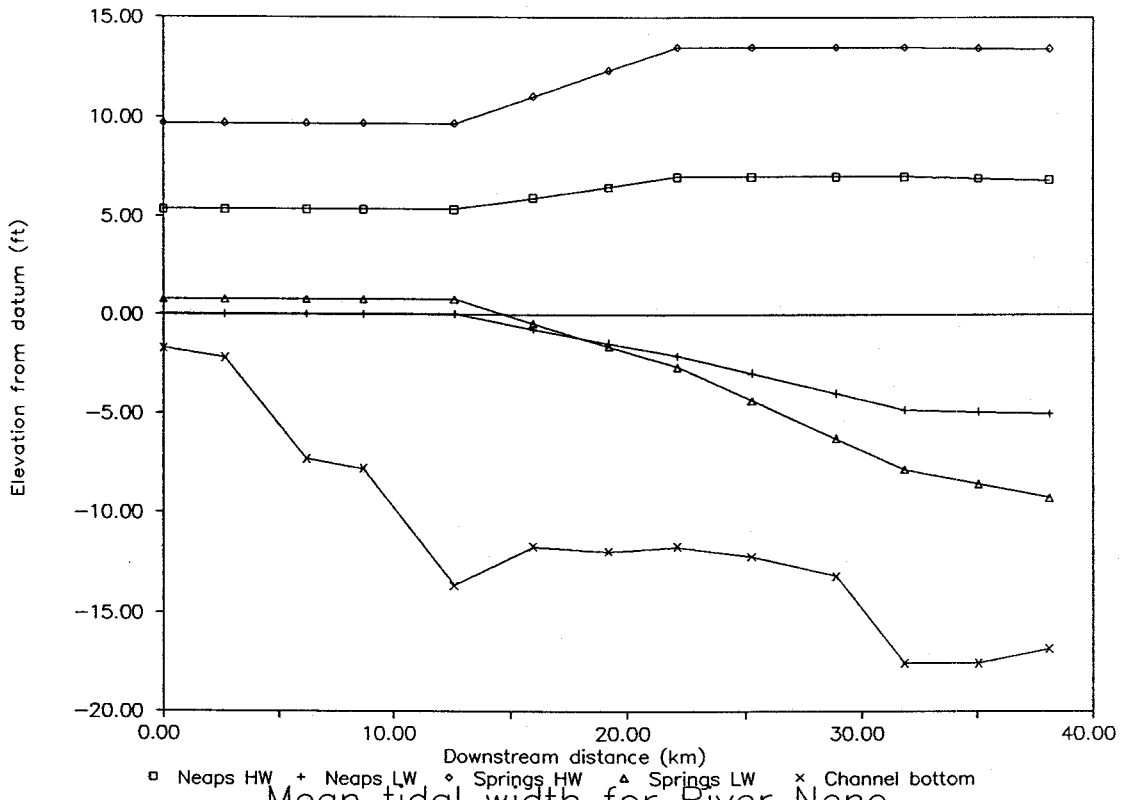


Fig 32 Maximum stress parameter for different tidal ranges and increasing river flow

Longitudinal profile of River Nene



Mean tidal width for River Nene

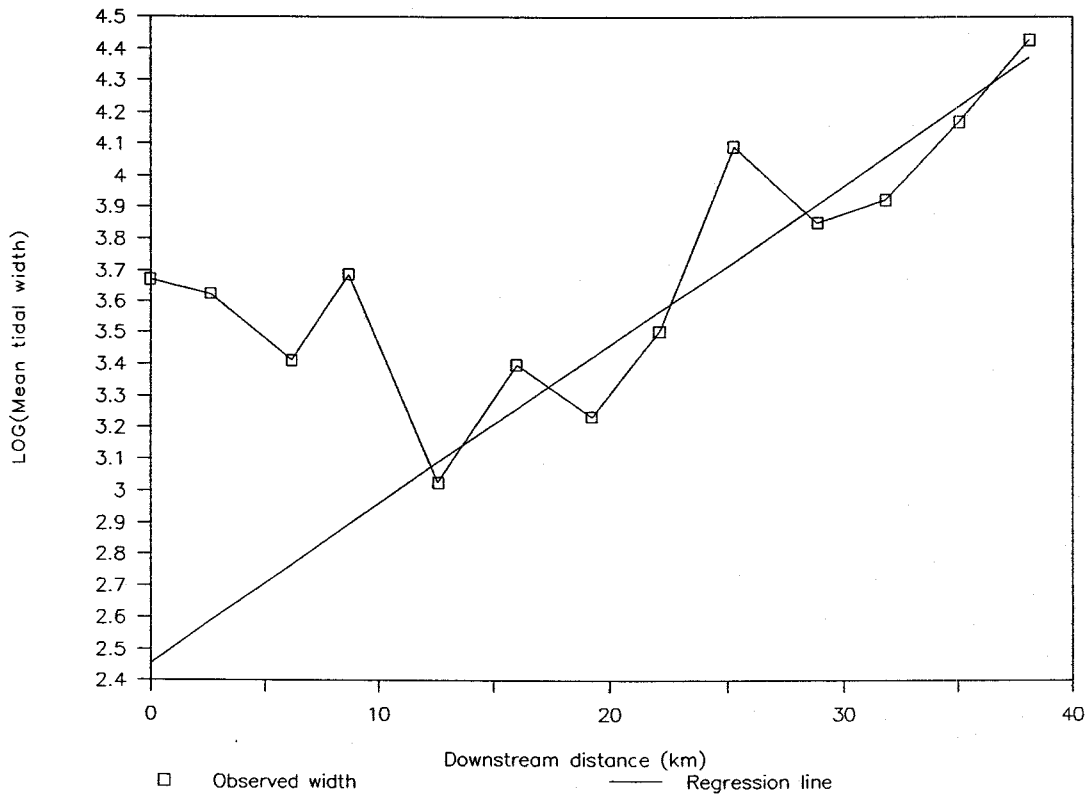


Fig 33 Longitudinal profile and mean tidal width for River Nene

Spring Tide on River Nene

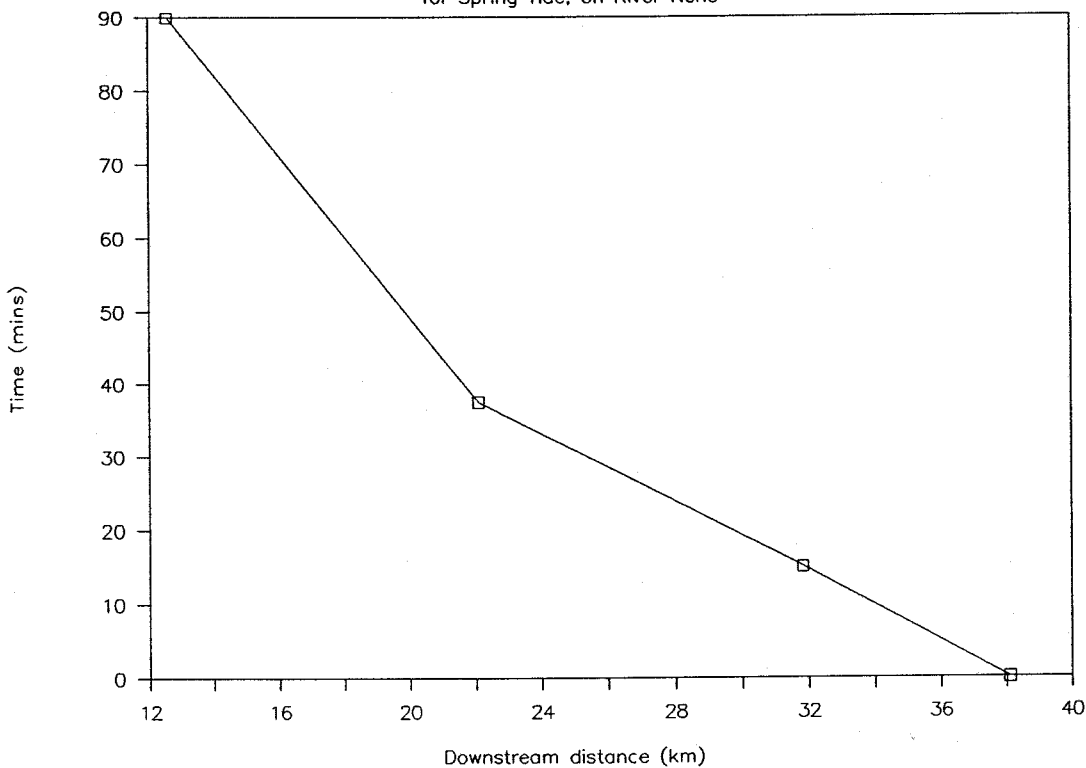
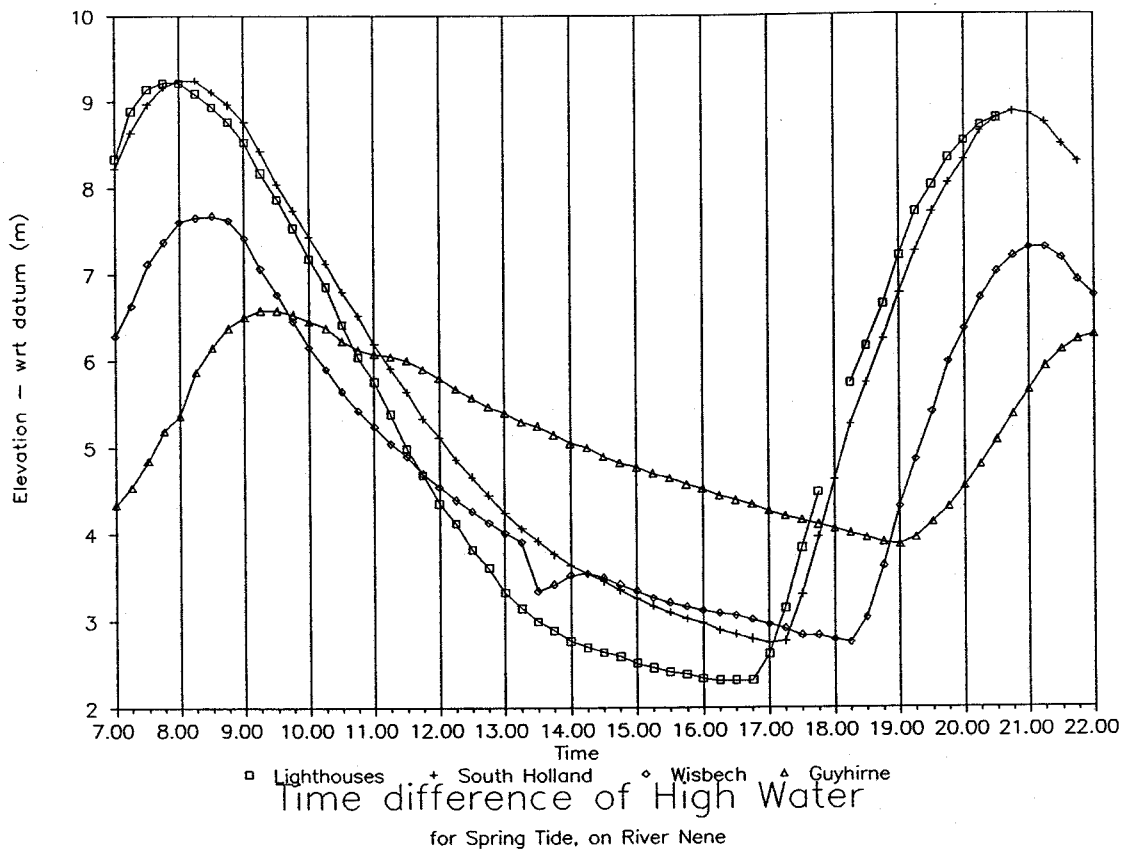


Fig 34 Spring tidal curves and phase differences for River Nene

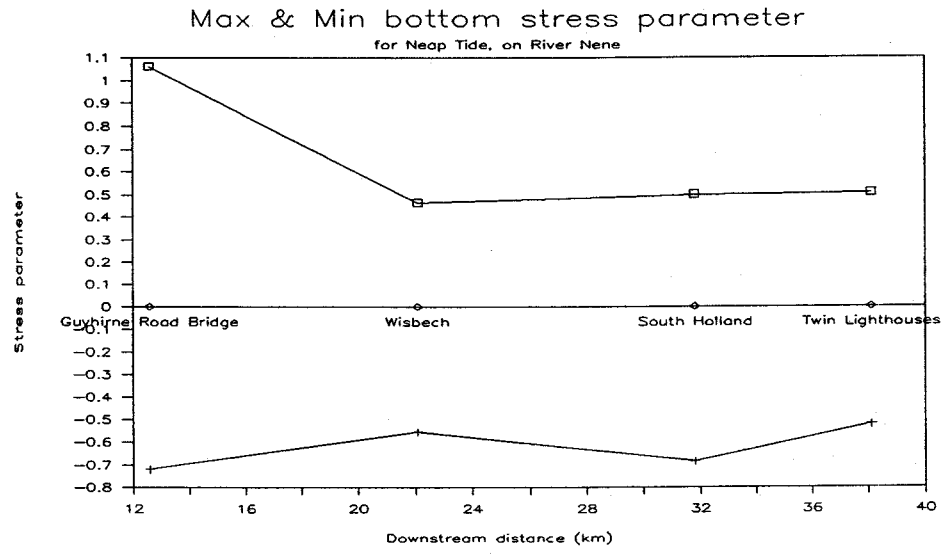
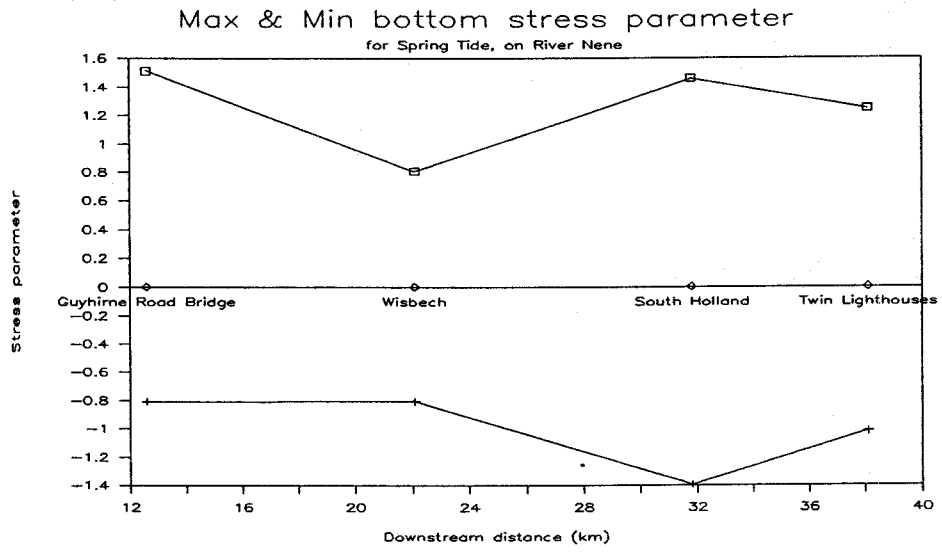
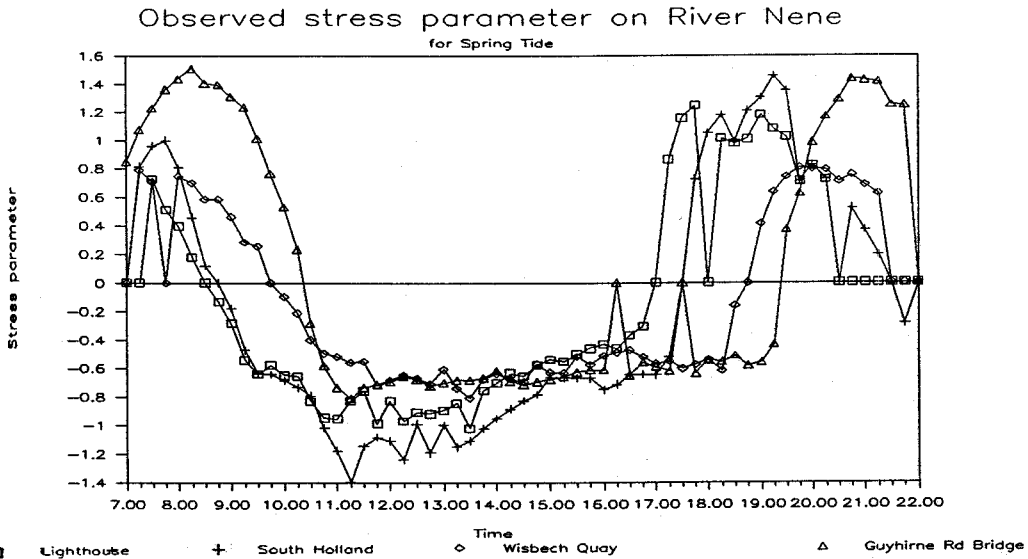


Fig 35 Stress parameter for River Nene; a) through tide, b) springs and c) neaps

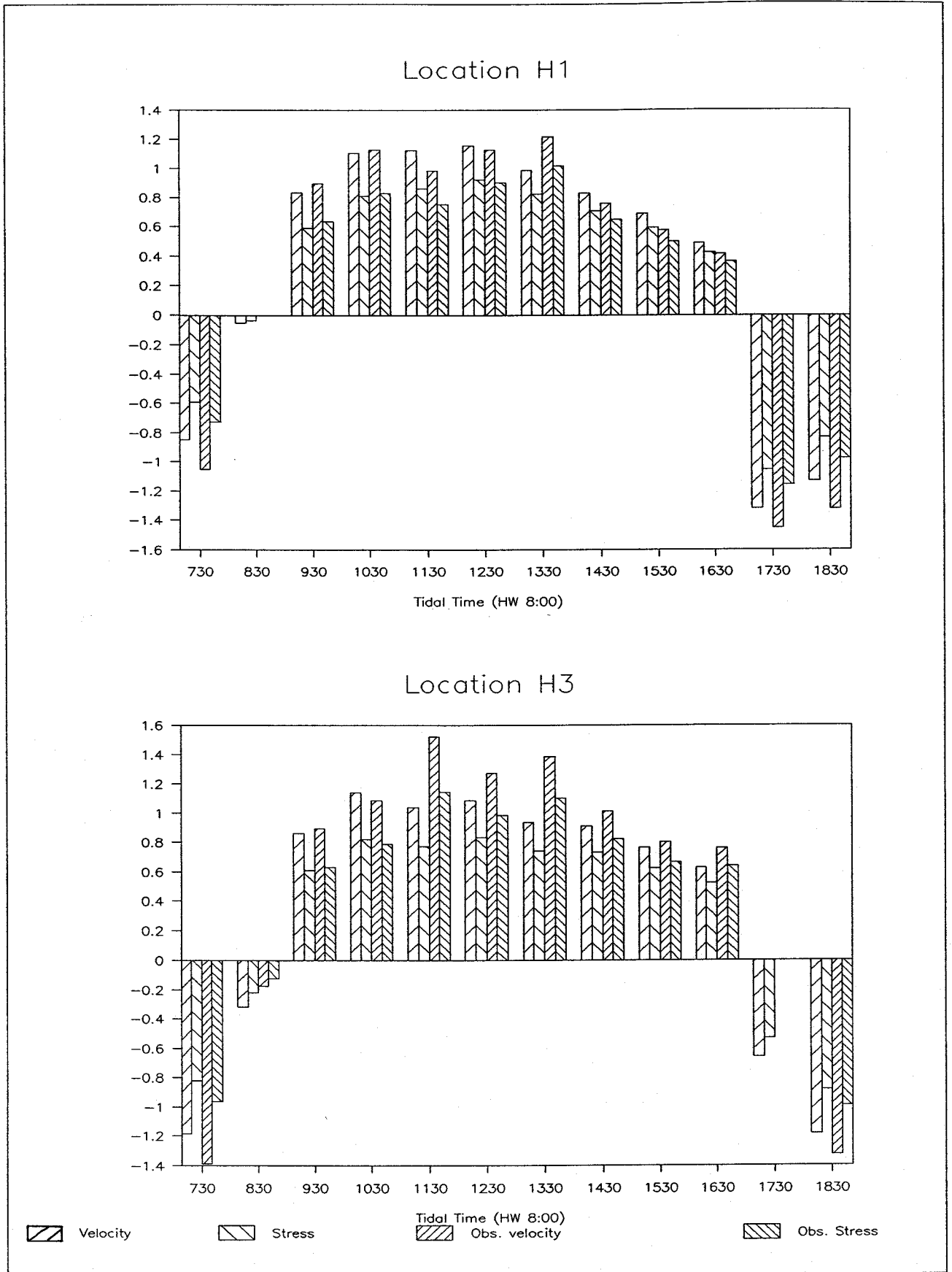
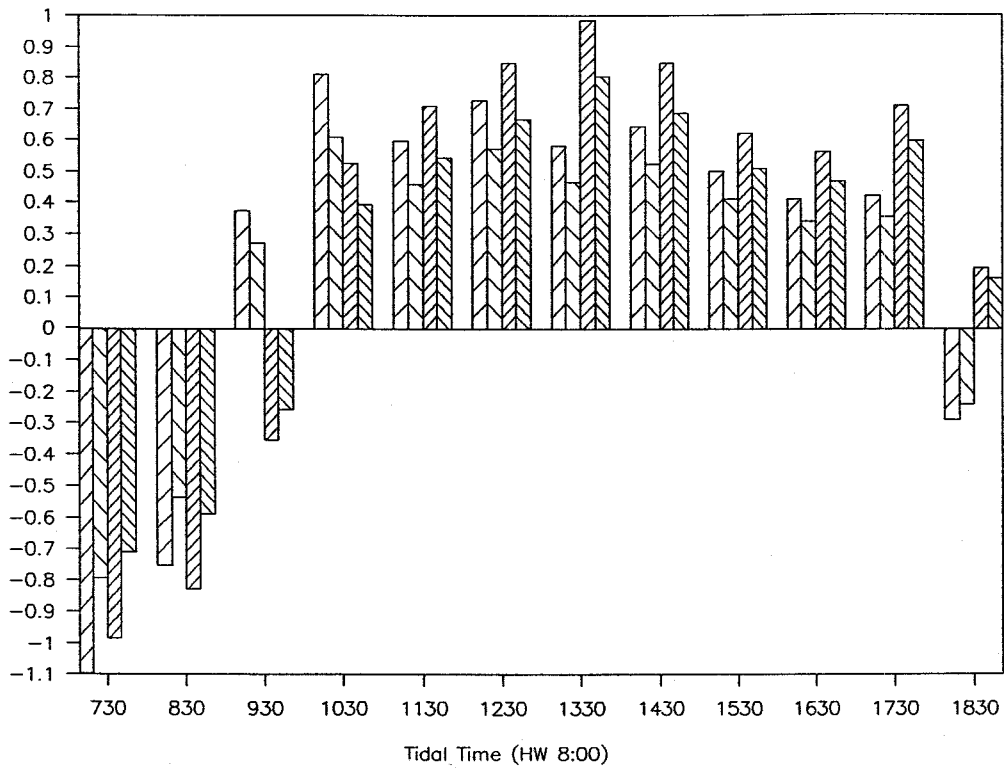
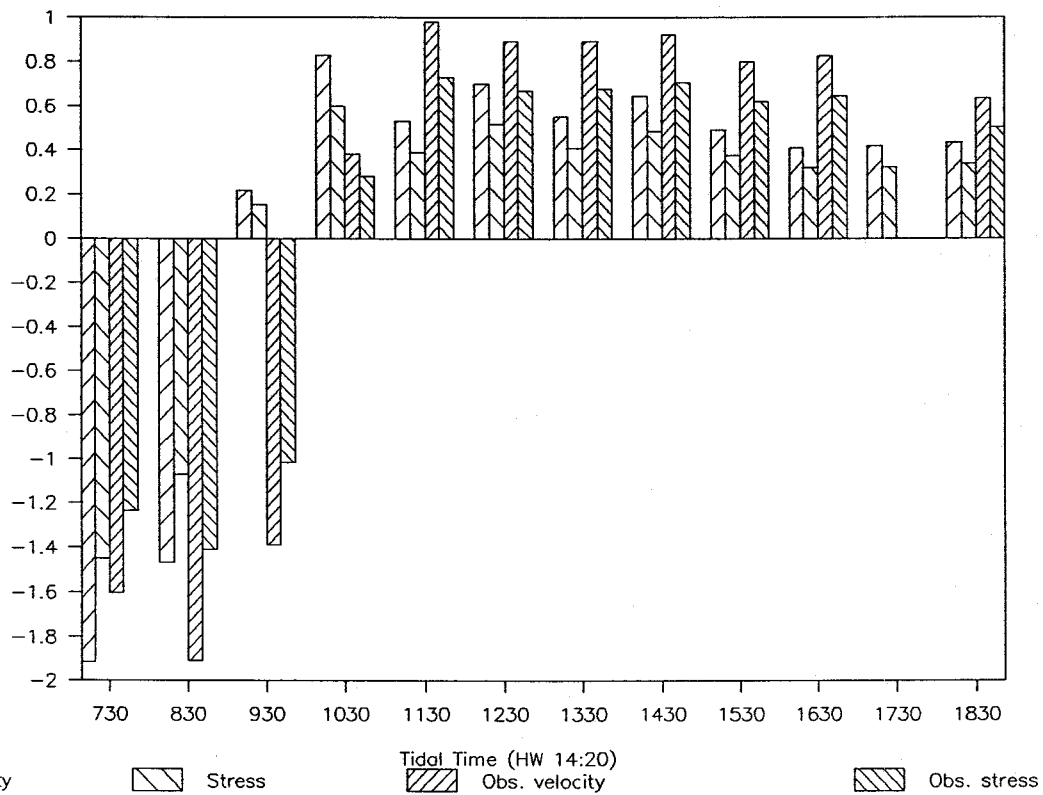


Fig 36 Nene – comparison of model results with observations

Location H6



Location 9



Legend: Velocity (diagonal hatching), Stress (cross-hatching), Obs. velocity (diagonal hatching), Obs. stress (diagonal hatching)

Fig 37 Nene – comparison of model results with observations

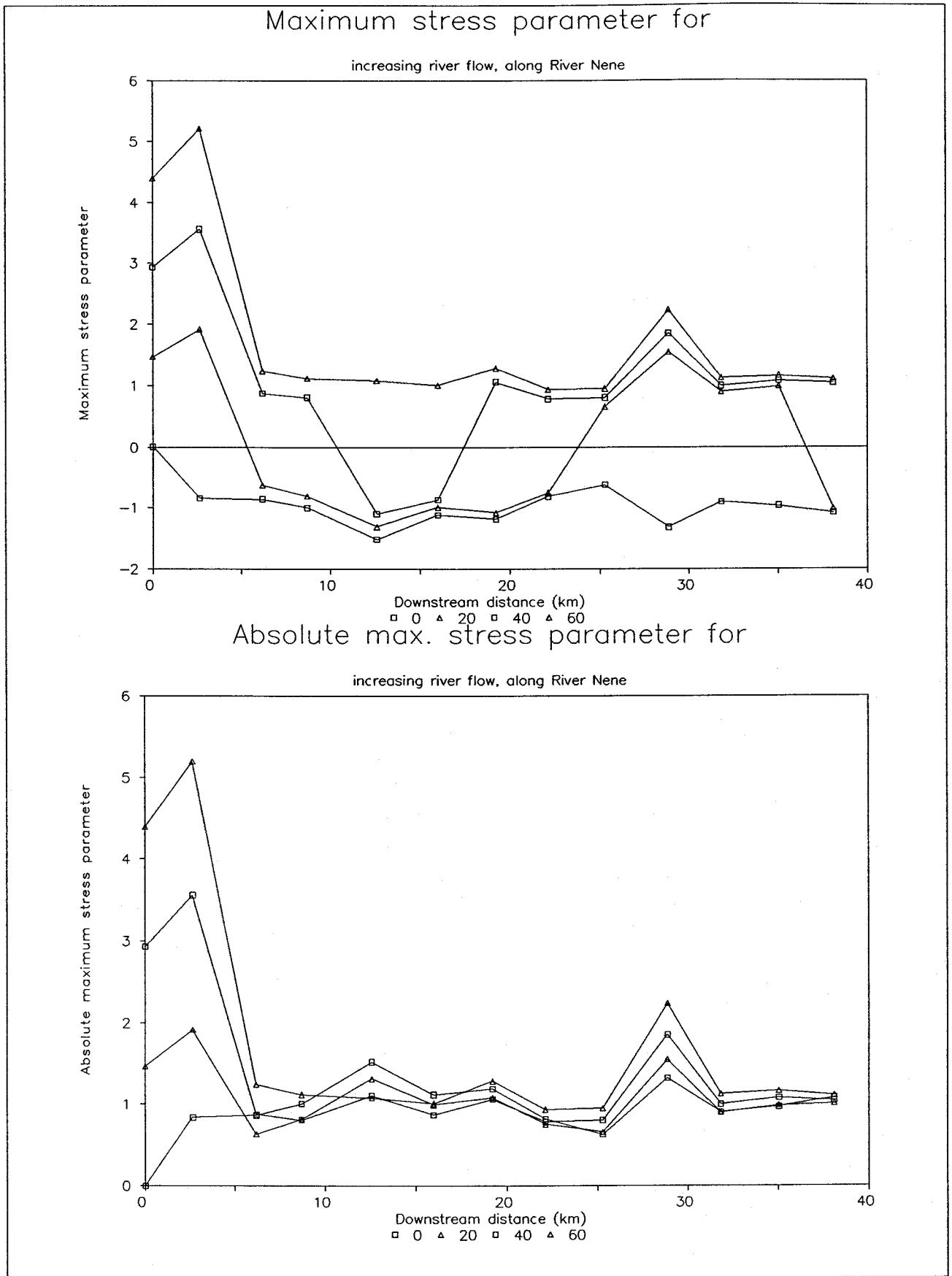
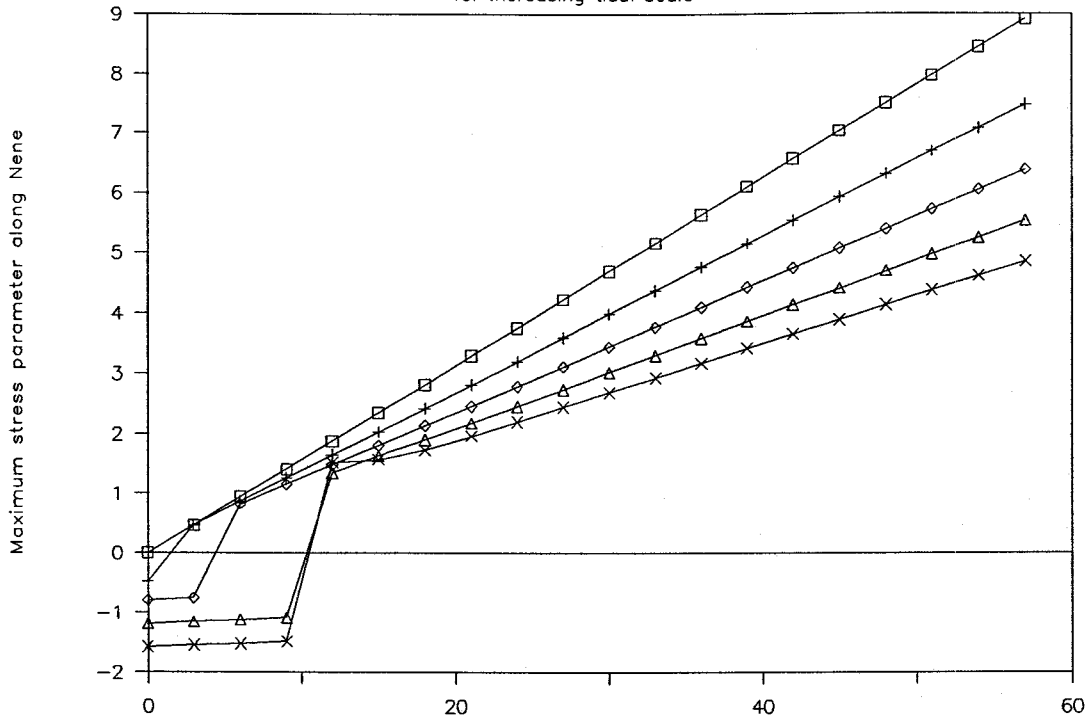


Fig 38 Maximum stress parameter for increasing river flow

Max. stress parameter along River Nene

for increasing tidal scale



Location of max stress along River Nene

for increasing tidal scale

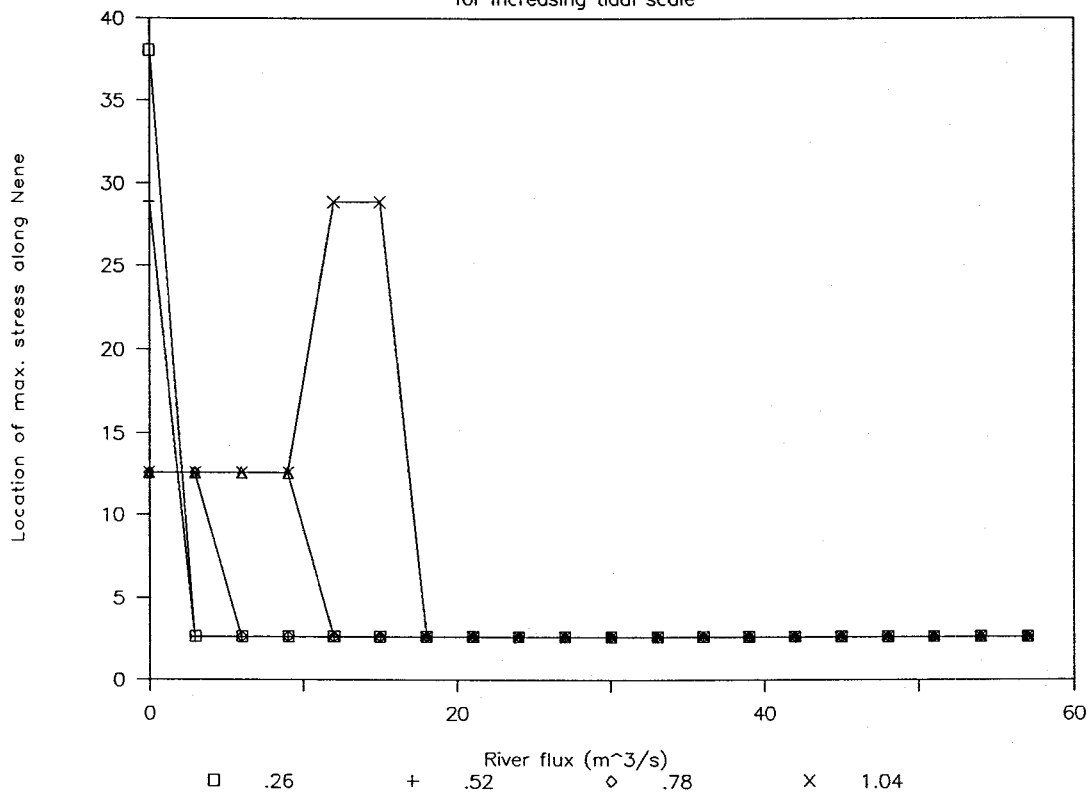
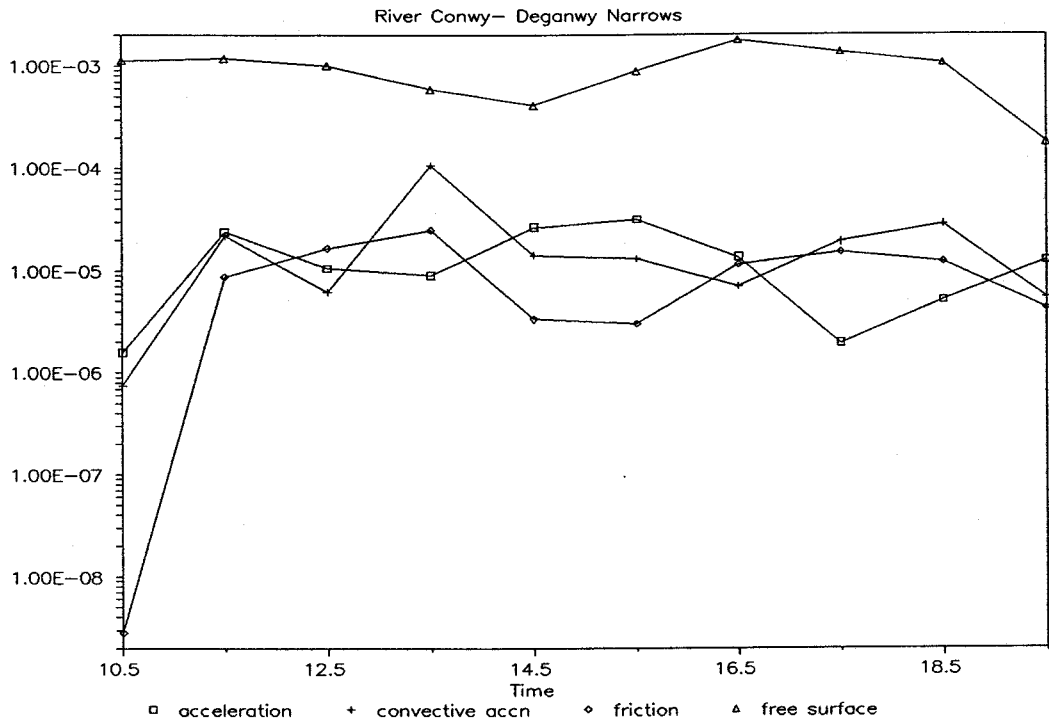


Fig 39 Maximum stress parameter for different tidal ranges

Magnitude of terms in the momentum eqn.



Magnitude of terms in the momentum eqn.

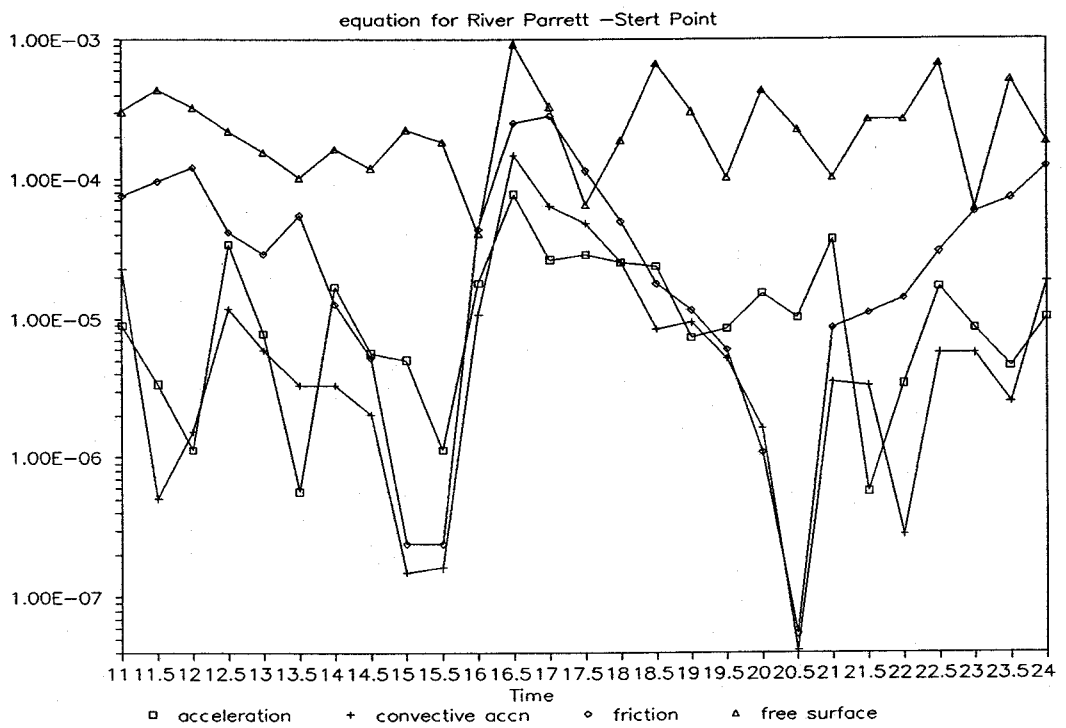
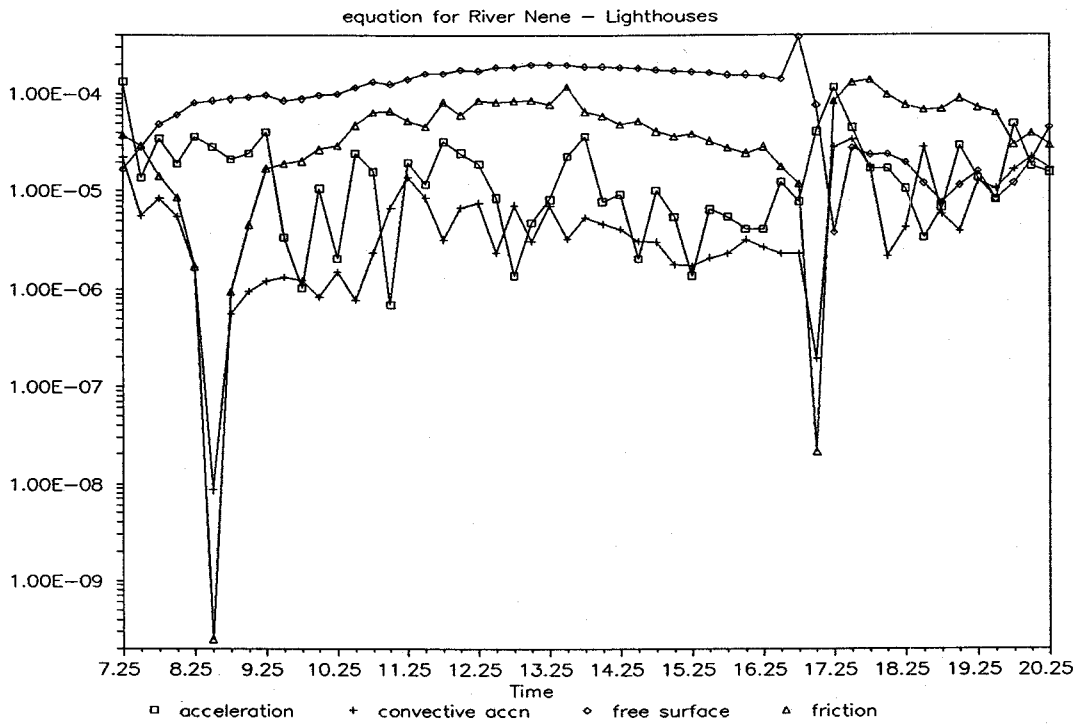


Fig 40 Magnitude of terms in the momentum eqn.
 a) Conwy and b) Parrett

Magnitude of terms in the momentum eqn.



Magnitude of terms in the momentum eqn.

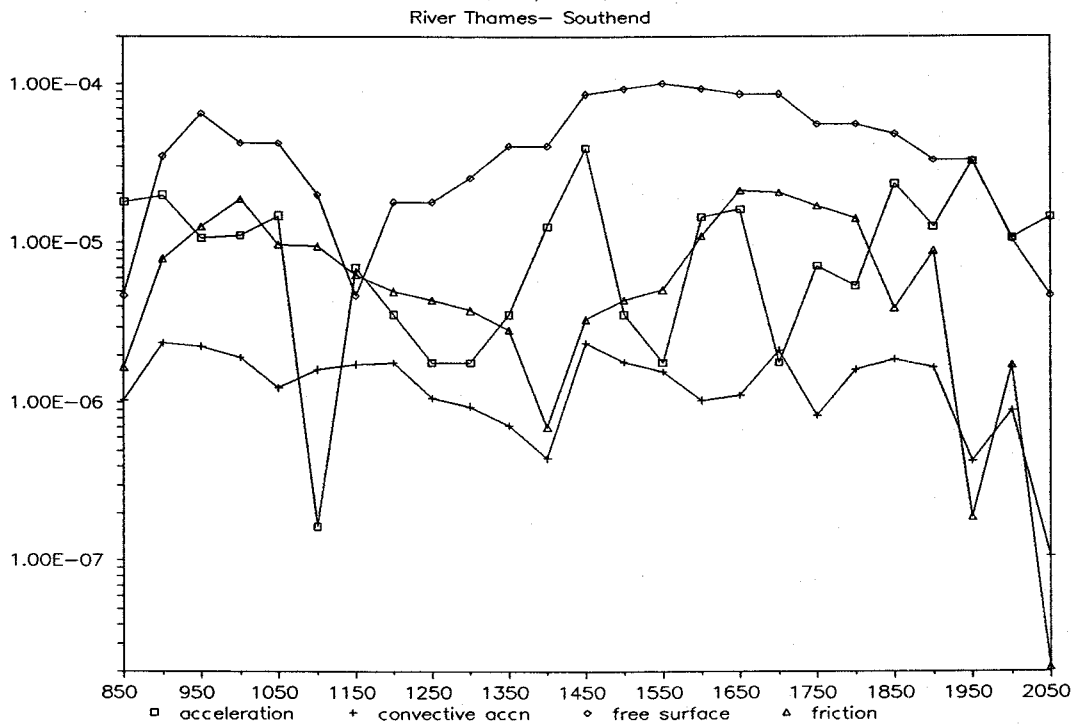


Fig 41 Magnitude of terms in the momentum eqn. 1
c) Nene and d) Thames

Comparison of actual and calculated

Mean Tide Depths for River Thames

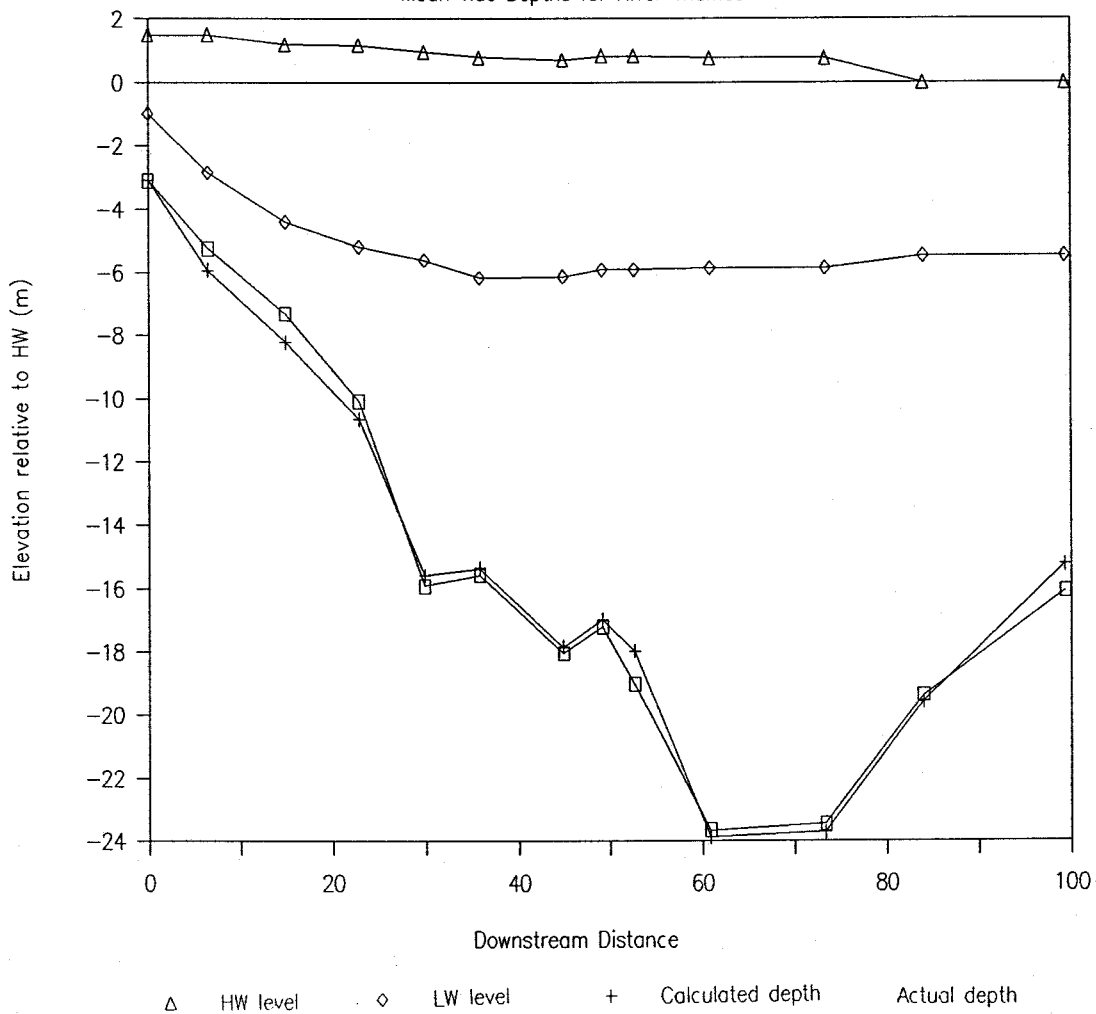
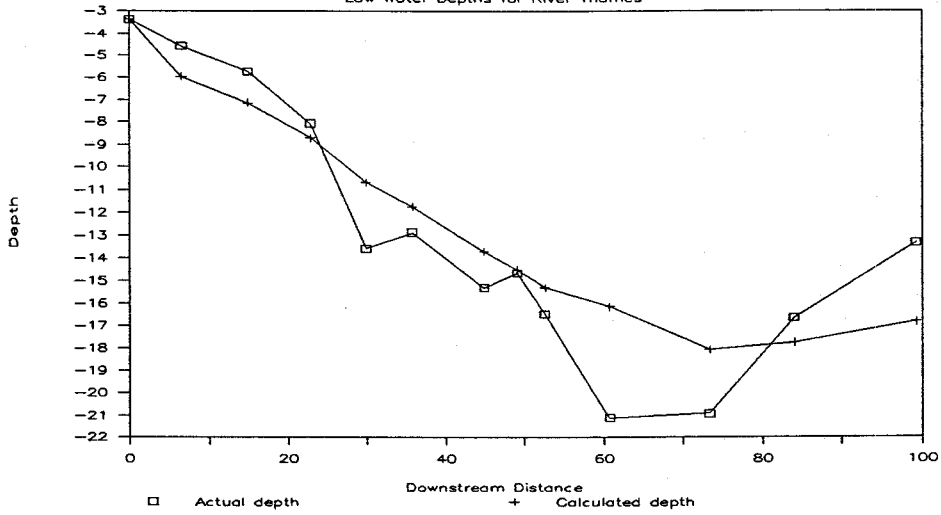


Fig 42 Stage I model prediction results

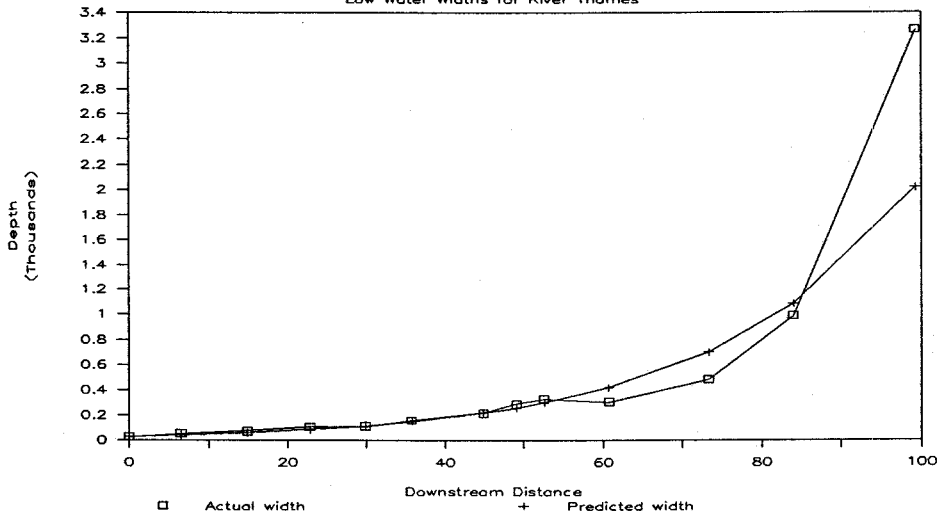
Comparison of actual and calculated

Low Water Depths for River Thames



Comparison of actual and predicted

Low Water Widths for River Thames



Comparison of actual and predicted

Low Water Widths for River Thames

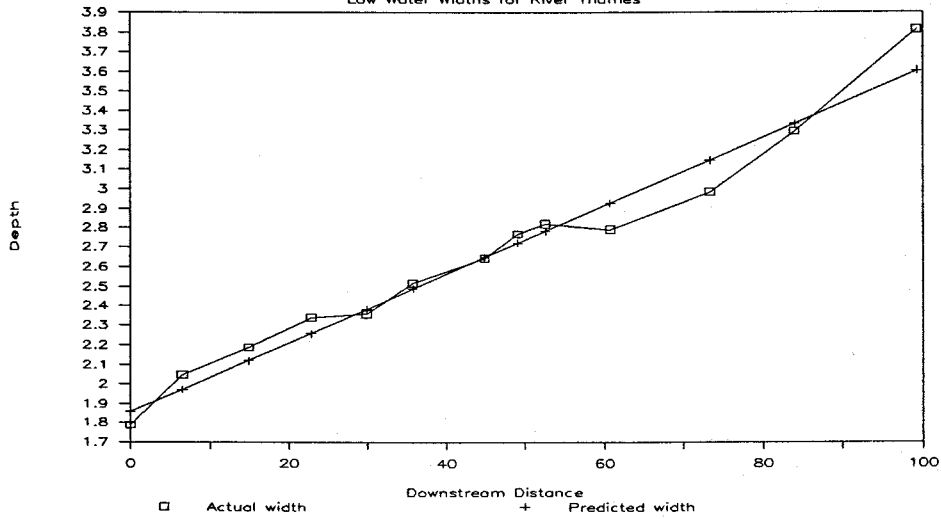


Fig 43 Stage II model prediction results

Comparison of actual and calculated

Low Water Depths for River Thames

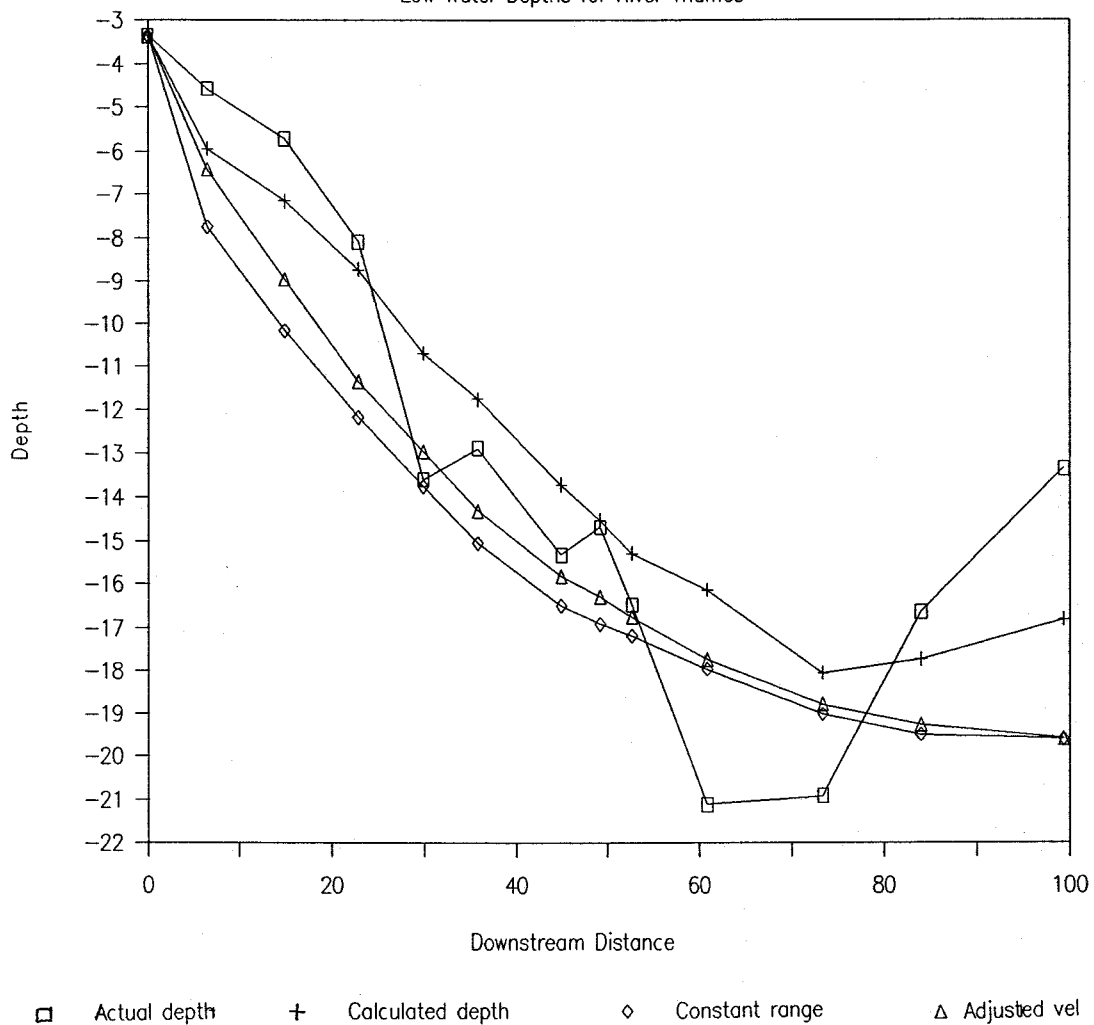


Fig 44 Stage III model prediction results